



2013

Biophysical Characterization of Tryptophan Locales, Mg²⁺ Binding and Protein Folding in G α Subunits

Matthew Najor
Loyola University Chicago

Follow this and additional works at: https://ecommons.luc.edu/luc_diss

 Part of the [Biochemistry Commons](#)

Recommended Citation

Najor, Matthew, "Biophysical Characterization of Tryptophan Locales, Mg²⁺ Binding and Protein Folding in G α Subunits" (2013). *Dissertations*. 730.
https://ecommons.luc.edu/luc_diss/730

This Dissertation is brought to you for free and open access by the Theses and Dissertations at Loyola eCommons. It has been accepted for inclusion in Dissertations by an authorized administrator of Loyola eCommons. For more information, please contact ecommons@luc.edu.



This work is licensed under a [Creative Commons Attribution-NonCommercial-No Derivative Works 3.0 License](#).
Copyright © 2013 Matthew Najor

LOYOLA UNIVERSITY CHICAGO

BIOPHYSICAL CHARACTERIZATION OF TRYPTOPHAN LOCALES, Mg^{2+}

BINDING AND PROTEIN FOLDING IN G_{α} SUBUNITS

A DISSERTATION SUBMITTED

TO THE FACULTY OF THE GRADUATE SCHOOL

IN CANDIDACY FOR THE DEGREE OF

DOCTOR OF PHILOSOPHY

PROGRAM IN CHEMISTRY

BY

MATTHEW S. NAJOR

CHICAGO, ILLINOIS

DECEMBER 2013

Copyright by Matthew S. Najor, 2013
All rights reserved.

ACKNOWLEDGMENTS

I would like to acknowledge all the people who made the completion of this dissertation possible. First and foremost, I would like to thank my graduate advisor, Dr. Duarte Mota de Freitas, for teaching me how to think critically and how to write scientifically. You are a terrific mentor and an even better friend.

I would also like to thank my dissertation committee, Dr. Miguel Ballicora, Dr. Paul Chiarelli and Dr. Ken Olsen for their guidance and valuable insight into my project. Other faculty members who have assisted me in my graduate education at Loyola University Chicago include Dr. Daniel Graham who helped me with data analysis. I would like to thank Dr. David French for his assistance in my NMR studies.

Graduate student colleagues who have made brightened my graduate tenure include Matt Bartucci, Dan Kissel, and Natalie Gumataotao. I would like to thank the undergraduate researchers who have contributed to the overall goal of the project: Steve Chukwulebe, Sean Keil, Iva Golemi, and Colin Senfelds. I also would like to acknowledge my lab mates Brian Levenson and Jessie Goosens. In addition, I would also like to thank former lab mate Dr. Guoyan Wang for teaching me the techniques of PCR and G protein cultures. Dr. Chris Malarkey deserves special thanks not only for his guidance and lab training in my first year of graduate school, but for his friendship as well.

My friends and family have been a continuous source of calm and inspiration during this time. My brothers Marc and Nicholas, my sister Courtney, and my Mom and Dad have never doubted and always believed in me now and forever. My grandmother Lyla and grandfather George, for always supporting me and encouragement in my dreams. Finally, I would like to thank my wife Lindsay for her unwavering love, patience and overall belief in me during my time in graduate school.

To my parents for all their undying love, encouragement and continuous support

TABLE OF CONTENTS

ACKNOWLEDGMENTS	iii
LIST OF TABLES	viii
LIST OF FIGURES	ix
LIST OF ABBREVIATIONS	xii
CHAPTER ONE: INTRODUCTION	1
CHAPTER TWO: CONTRIBUTIONS OF EACH TRP RESIDUE TOWARDS THE INTRINSIC FLUORESCENCE OF THE G _{iα1} PROTEIN	13
Introduction	13
Materials and Methods	15
Expression and Protein Purification	15
Fluorescence Measurements	15
Trypsin Digestion Analyzed by SDS-PAGE	16
Modeling	16
Results	17
AMF and GTPγS Activation of WT G _{iα1} and its Trp Mutants	17
Shifts in the Emission Spectrum of Activated G _{iα1} Proteins	26
Trypsin Digestion of G _{iα1} Proteins	30
Discussion	30
CHAPTER THREE: FOLDING OF G _α SUBUNITS: CHANGES IN THE ENVIRONMENTS OF TRP AND TYR RESIDUES AND ON THE SECONDARY STRUCTURE	41
Introduction	41
Materials and Methods	45
Expression and Protein Purification	45
Fluorescence Measurements	46
Tyrosine Assay	46
Determination of Secondary Structure	47
Refolding of G _α Subunits	47
Results	48
AMF and GTPγS Activation of G _{iα1}	48
Fluorescence Emission Spectra of G _α Proteins	50
Tyrosine Assays	54
Temperature–Dependence of Secondary Structure G _{iα1}	58
Discussion	64
CHAPTER FOUR: Mg ²⁺ DEPENDENCE OF THE FOLDING OF G _α SUBUNITS	75
Introduction	75

Materials and Methods	78
Expression and Protein Purification	78
Calculation of $[Mg^{2+}]_f$ in the Presence of EDTA	78
Fluorescence Measurements	79
Determination of Secondary Structure	79
Results	80
Effect of Mg^{2+} on the Intrinsic Fluorescence of G_α subunits	80
Changes in the secondary structure of $G_{i\alpha 1}$ and $G_{s\alpha}$	85
Discussion	91
APPENDIX A: EFFECT OF DTT ON WT $G_{i\alpha 1}$ ACTIVATION	95
APPENDIX B: Li^+ INHIBITION OF $GTP\gamma S$ BINDING AND GTP HYDROLYSIS	101
REFERENCES	108
VITA	114

LIST OF TABLES

Table 1. Kinetic Parameters for Activation of WT and W Mutants	21
Table 2. Solvent Exposure of W residues in WT and W Mutants	25
Table 3. Observed and Calculated Distances and λ_{\max} shifts in WT and W Mutants	29
Table 4. Interaction Energies between R208 and W211	36
Table 5. Computational Calculations for Solvent Exposure of R208 in the Molecular Models	39
Table 6. T_m 's Estimated for all G_α Proteins Using Three Spectroscopic Methods	53
Table 7. Composition of WT $G_{i\alpha 1}$ Secondary Structure at Various Temperatures	61
Table 8. Composition of WT $G_{s\alpha}$ Secondary Structure at Various Temperatures	69

LIST OF FIGURES

Figure 1. G – protein signaling cascade	3
Figure 2. Crystal structure of WT $G_{i\alpha 1}\cdot\text{GDP}\cdot\text{Mg}^{2+}$	5
Figure 3. Solvent effects on ANS	8
Figure 4. Model of WT $G_{i\alpha 1}$ depicting its carbon backbone	18
Figure 5. Intrinsic Tryptophan fluorescence of WT $G_{i\alpha 1}$ and its W131F, W258F and W211F mutants after activation with AlF_4^-	20
Figure 6. Intrinsic Tryptophan fluorescence after $\text{GDP}\rightarrow\text{GTP}\gamma\text{S}$ exchange	22
Figure 7. Emission spectra of WT $G_{i\alpha 1}$ and its three Trp mutants in the GDP conformation	23
Figure 8. Intrinsic tryptophan fluorescence of $G_{i\alpha 1}$ proteins	27
Figure 9. Depiction of red shifts undergone by WT and W mutants upon addition of AlF_4^- or $\text{GTP}\gamma\text{S}$	28
Figure 10. Trypsin digests of wild-type and various tryptophan mutants of $G_{i\alpha 1}$	31
Figure 11. Molecular dynamic calculations of R208 solvent exposure in WT and its three Trp mutants in all conformations	40
Figure 12. WT $G_{i\alpha 1}\cdot\text{GDP}\cdot\text{Mg}^{2+}$ displaying its three tryptophan residues, Arg208 and Mg^{2+}	43
Figure 12. WT $G_{i\alpha 1}\cdot\text{GTP}\gamma\text{S}$ depicting the same residues as Fig. 12 except the bound nucleotide is $\text{GTP}\gamma\text{S}$	44
Figure 13. Temperature dependence of AlF_4^- activation of WT $G_{i\alpha 1}\cdot\text{GDP}\cdot\text{Mg}^{2+}$	49

Figure 14. Temperature dependence of GTP γ S Activation of WT G $_{i\alpha 1}$ •GDP•Mg $^{2+}$	51
Figure 15. Fluorescence emission spectra of WT G $_{i\alpha 1}$ •GDP•Mg $^{2+}$ as a function of temperature	52
Figure 16. Refolding of WT G $_{i\alpha 1}$ •GTP γ S	55
Figure 17. Refolding of WT G $_{i\alpha 1}$ in all three conformations as monitored by fluorescence	56
Figure 18. WT G $_{i\alpha 1}$ •GDP depicting its 13 Tyr residues	57
Figure 19. Unfolding of WT G $_{i\alpha 1}$ as monitored through Tyr movement	59
Figure 20. Unfolding of WT G $_{i\alpha 1}$ •GDP•Mg $^{2+}$ secondary structure	60
Figure 21. Unfolding of WT G $_{s\alpha}$ •GDP•Mg $^{2+}$ secondary structure	63
Figure 22. Denaturation and refolding of WT G $_{i\alpha 1}$ •GDP	65
Figure 23. Unfolding of WT G $_{i\alpha 1}$ •GDP in the presence of guanidinium HCl	71
Figure 24. Mg $^{2+}$ dependence of AlF $_4^-$ activation of WT G $_{i\alpha 1}$	81
Figure 25. Mg $^{2+}$ dependence of AlF $_4^-$ activation of WT G $_{s\alpha}$	82
Figure 26. GTP γ S activation of WT G $_{i\alpha 1}$ dependent on Mg $^{2+}$	83
Figure 27. GTP γ S activation of WT G $_{s\alpha}$ dependent on Mg $^{2+}$	84
Figure 28. Shift resulting from AlF $_4^-$ activation of WT G $_{i\alpha 1}$ and G $_{s\alpha}$ at various [Mg $^{2+}$] $_F$	86
Figure 29. Shift resulting from GTP γ S activation of WT G $_{i\alpha 1}$ and G $_{s\alpha}$ at various [Mg $^{2+}$] $_F$	87
Figure 30. Secondary structure of WT G $_{i\alpha 1}$ •AMF at various Mg $^{2+}$ concentrations	88

Figure 31. Mg^{2+} dependent activation of $G_{i\alpha 1}$ and $G_{s\alpha}$ with AlF_4^- or $GTP\gamma S$	89
Figure 32. Mg^{2+} dependent activation of $G_{i\alpha 1}$ and $G_{s\alpha}$ with AlF_4^- or $GTP\gamma S$	90
Figure 33. WT $G_{i\alpha 1}\cdot GDP\cdot Mg^{2+}$ activation with AlF_4^- at various DTT concentrations	98
Figure 34. Visualization of WT $G_{i\alpha 1}\cdot GDP$ polymerization with SDS – PAGE	99
Figure 35. Effect of Li^+ on $GTP\gamma S$ binding to WT $G_{s\alpha}$	105
Figure 36. Effect of Li^+ on GTP Hydrolysis of WT $G_{s\alpha}$	106

LIST OF ABBREVIATIONS

2YT	2 x yeast extract tryptone
α	Alpha helices
AC	Adenylyl Cyclase
ADP	Adenosine 5' –diphosphate
$AlCl_3$	Aluminum chloride
AlF_4^-	Aluminum fluoride
AMF	Aluminum magnesium fluoride
ANS	8-Anilinonaphthalene-1-sulfonic acid
ATP	Adenosine 5' –triphosphate
β	Beta sheets
cAMP	3',5' -cyclic adenosine monophosphate
CD	Circular dichroism
ϵ	Extinction coefficient
Δ	Change in solvent exposure
Δ_E	Change in the total interaction energies between GDP and either AMF or GTP γ S
$\Delta\lambda_{max}$	Change in λ_{max} between GDP and either AMF or GTP γ S
DTT	Dithiothreitol
EDTA	Ethylenediaminetetraacetic acid
EGTA	Ethylene glycol – bis (β – aminoethylether) – N,N,N',N' – tetra acetic acid
Elec (E)	Electrostatic interaction

F_{\max}	Maximum fluorescence intensity
G	Guanine nucleotide binding
GDP	Guanosine 5'-diphosphate
$\text{GDP}\cdot\text{AlF}_4^-$	Guanosine 5'-diphosphate tetrafluoroaluminate complex
G_i	Inhibitory G protein of cAMP
$G_{i\alpha}$	α subunit of the inhibitory G protein of cAMP
G_s	Stimulatory G protein of cAMP
$G_{s\alpha}$	α subunit of the stimulatory G protein of cAMP
GSK – 3 β	Glycogen synthase kinase – 3 beta
G_t	Transducin G protein
GTP	Guanosine 5'-triphosphate
GTP γ S	Guanosine 5'-[γ -thio] triphosphate
FPLC	Fast protein liquid chromatography
HCl	Hydrochloric acid
His ₆ - $G_{s\alpha}$	N – terminus hexahistidine tagged $G_{s\alpha}$ protein
λ_{\max}	Wavelength of maximum fluorescence
kDa	Kilo dalton
Li ⁺	Lithium ion
Mg ²⁺	Magnesium ion
MgCl ₂	Magnesium chloride
MgSO ₄	Magnesium Sulfate
NaCl	Sodium chloride
NaF	Sodium fluoride
NaH ₂ PO ₄	Sodium dihydrogenphosphate
NaOH	Sodium hydroxide

PDB	Protein data bank
RC	Random coil
SDS	Sodium dodecyl sulfate
SDS – PAGE	Sodium dodecyl sulfate polyacrylamide gel electrophoresis
T	Turns
Tris – Cl	Tris(hydroxymethyl)amino methane
UV – Vis	Ultraviolet visible spectrophotometry
VdW	Van der Waals interaction
W	Tryptophan

CHAPTER ONE

INTRODUCTION

Many proteins, peptides, lipids, ions and small molecules are responsible for cellular signaling. Hormones and neurotransmitters are known to transmit cellular signals, by binding to a receptor which then transduces the signal to the inside of the cell and activates kinases, phosphatases, proteases, and nucleotide binding proteins. Many of these proteins switch between an “on” and “off” phase, varying the intensity and duration of the transmitted signal. Guanine nucleotide binding proteins, G – proteins, are among the most prevalent found signal - transducing proteins (1).

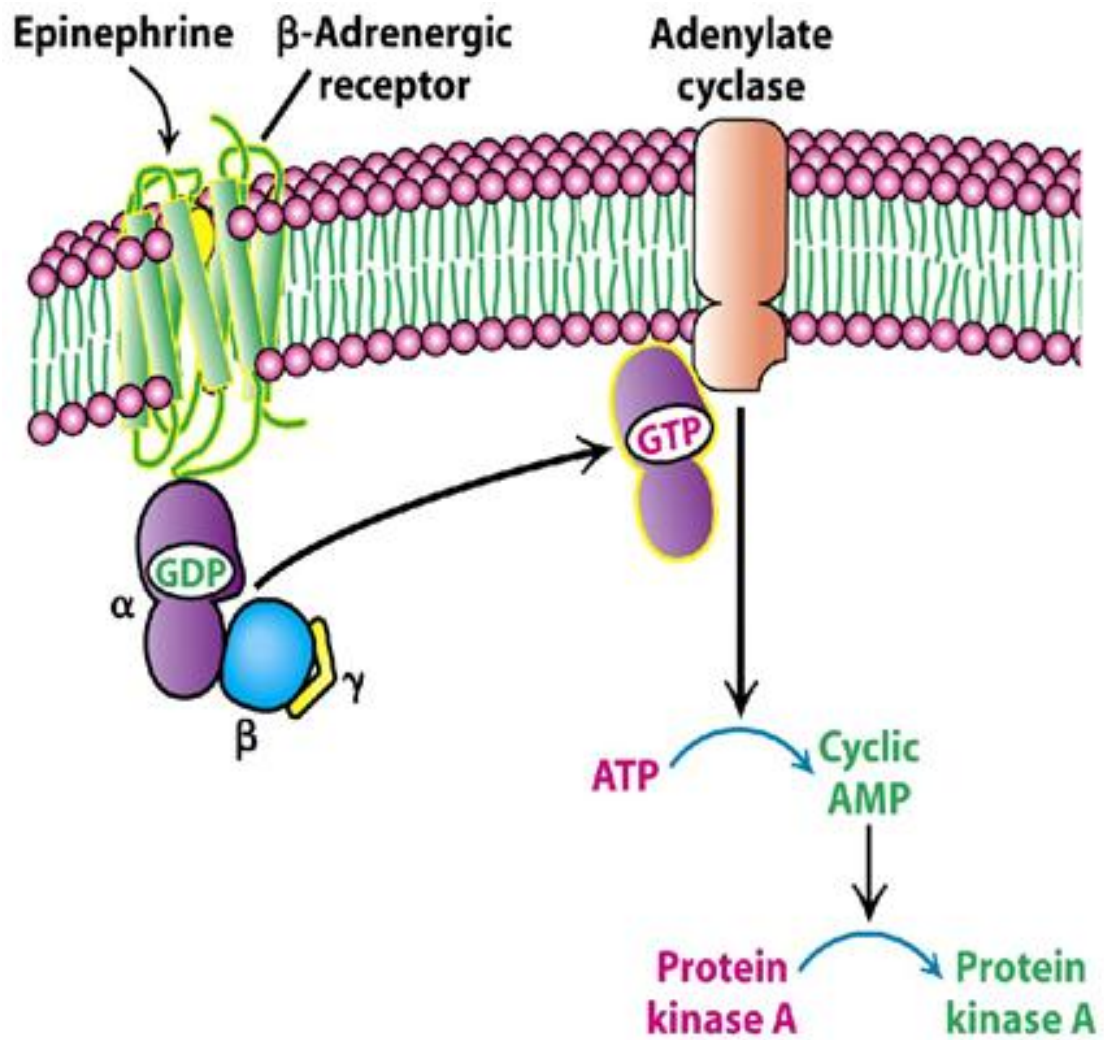
Alfred Gilman and Martin Rodbell were awarded the 1994 Nobel Prize in physiology or medicine for their work and discovery of G – proteins. There are two major classes of G – proteins: large heterotrimeric membrane bound proteins and small monomeric proteins, such as Ras (1, 2).

Heterotrimeric G – proteins are associated with many hepta - helical serpentine transmembrane domain receptors, which are more commonly known as G – protein coupled receptors (GPCRs), and they regulate intracellular signaling cascades in response to GPCR activation. G – proteins are bound to the inside surface of the transmembrane where they act as molecular switches between intracellular receptors and effectors. Heterotrimeric G – proteins consist of α , β , and γ subunits (3). The α – subunit contains the guanine nucleotide (GDP/GTP) binding site in the GTPase domain. Upon activation of the extracellular receptor, the G protein exchanges GDP for GTP in the α subunit.

The binding of GTP induces a conformational change in the α subunit and promotes dissociation of the α subunit from the $\beta\gamma$ complex. The now active α – GTP subunit and the $\beta\gamma$ complex interact with downstream effectors. Activation is terminated by hydrolysis of GTP which produces inorganic phosphate (P_i) and returns the G – protein back to its GDP conformation. Deactivation signals re-association of the α – subunit and the $\beta\gamma$ complex to form the heterotrimer. The α – subunit consists of two domains: the GTPase domain, involved in the binding and hydrolysis of GTP, and a highly concentrated α – helical domain that buries the GTP within the core of the protein (4). The α - subunits interact with various effector molecules, such as adenylyl cyclase, and induce different physiological and biological responses. Activated G – proteins bind to adenylyl cyclase affect the production of cAMP from ATP (Fig. 1).

There are 23 known G_α proteins encoded from 16 G_α genes in the human genome. These genes translate to proteins in the 39 – 45 kD molecular weight range, and, based on sequence conservation, can be divided into 4 subclasses of the G_α family: $G_{\alpha(s/olf)}$, $G_{\alpha(i1/i2/i3/o/t-rod/t-cone/gust/z)}$, $G_{\alpha(q/11/14/16)}$, and $G_{\alpha(12/13)}$ (1). $G_{olf\alpha}$ is expressed in the olfactory sensory neurons. $G_{s\alpha}$ consists of four variant splice forms, two short ($G_{s\alpha} - S$) and two long ($G_{s\alpha} - L$). Structurally they are similar and functionally indistinguishable. $G_{s\alpha}$ is ubiquitously expressed and known to elevate levels of cAMP. The $G_{i\alpha}$ family is known to inhibit various types of adenylyl cyclase and lowers the intracellular levels of cAMP. $G_{o\alpha}$ is abundantly found in the nervous system where it has been found to activate Ca^{2+} and K^+ channels (5). $G_{z\alpha}$ is expressed in the adrenal medulla of the brain,

Figure 1. G – protein signaling cascade

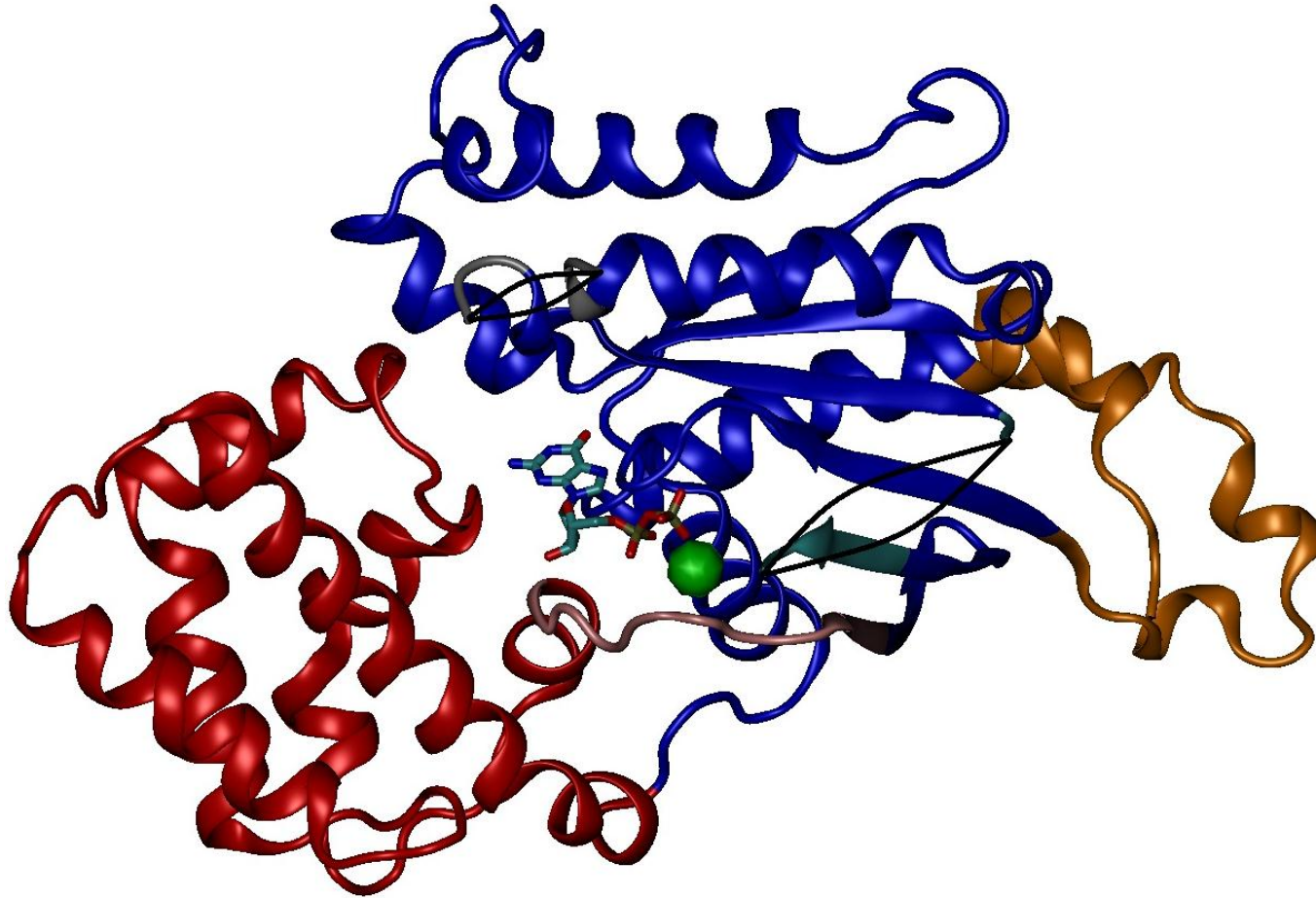


neuronal cells, and platelets (6). Like $G_{i\alpha}$, $G_{z\alpha}$ inhibits adenylyl cyclases, although it displays slower kinetics in GTP hydrolysis compared to other G_{α} subunits (7). $G_{t\alpha}$, which includes rod and cone transducins, and gustducin are involved in sensory functions (6). Subunits of the $G_{q\alpha}$ family, including isoforms G_{11} , G_{14} and G_{16} , directly activate phospholipase C β - isozymes. Activation of phospholipase C produces inositol phosphate (IP_3), which in turn triggers the release of Ca^{2+} ions from Ca^{2+} storage in cells and diacylglycerol (DAG) (8, 9). G - proteins $G_{12\alpha}$ and $G_{13\alpha}$ are expressed ubiquitously and stimulate a multitude of downstream effectors, such as PLC A_2 , and the Na^+/H^+ exchanger (10). In addition to secondary messengers, it has been demonstrated that they are directly involved with the activation of Rho GTPases (11).

The α subunit of G proteins is composed of two domains, an α - helical and GTPase domain, which contains the active site (12). GTPase domain is composed of six-stranded β -sheets surrounded by five α -helices. The active site contains the guanine nucleotide and the binding sites for the $G_{\beta\gamma}$ dimer, membrane receptors and downstream effectors. There are five conserved sequences in the GTPase domain, the diphosphate binding loop (P - loop) (GXGESGKS), the Mg^{2+} -binding loops (RXXTXGI and DXXG), and the guanine ring-binding motifs (NKXD and TCAT) (Fig. 2). There are three flexible loops known as switches I, II and III near the γ - phosphate in the active site. The switch regions are ordered and held in place by contacts with the γ - phosphate of GTP (12). In contrast, switch regions II and III are unordered in the GDP-bound conformation of $G_{i\alpha1}$, but not in $G_{t\alpha}$ (13). The α - helical domain is composed of six α -helices that form a lid over the nucleotide-binding site in the GTPase domain.

Figure 2. Crystal structure of WT $G_{i\alpha 1}$ •GDP• Mg^{2+} (1BOF, (13)).

Displaying the GTPase domain (blue), α – helical domain (red), helical micro domain (orange), switch I (pink), switch II (cyan), switch III (silver), guanine nucleotide, GDP, and Mg^{2+} ion (green sphere). The black brackets connecting the switch II and III regions indicate unordered structure.



This domain may also play a significant role in coupling specific G proteins to specific effectors (14). Both the amino (N) and carboxyl (C) termini of the α subunits are key determinants of receptor-binding specificity and play a critical role in G-protein activation, but their structures are not clear because they were disordered in the crystals. The N-terminus forms an α -helix that is ordered by its interaction with G_{β} in the heterotrimeric structure of G proteins, however, its structure in the active conformation of the G_{α} subunits remains unknown (15, 16).

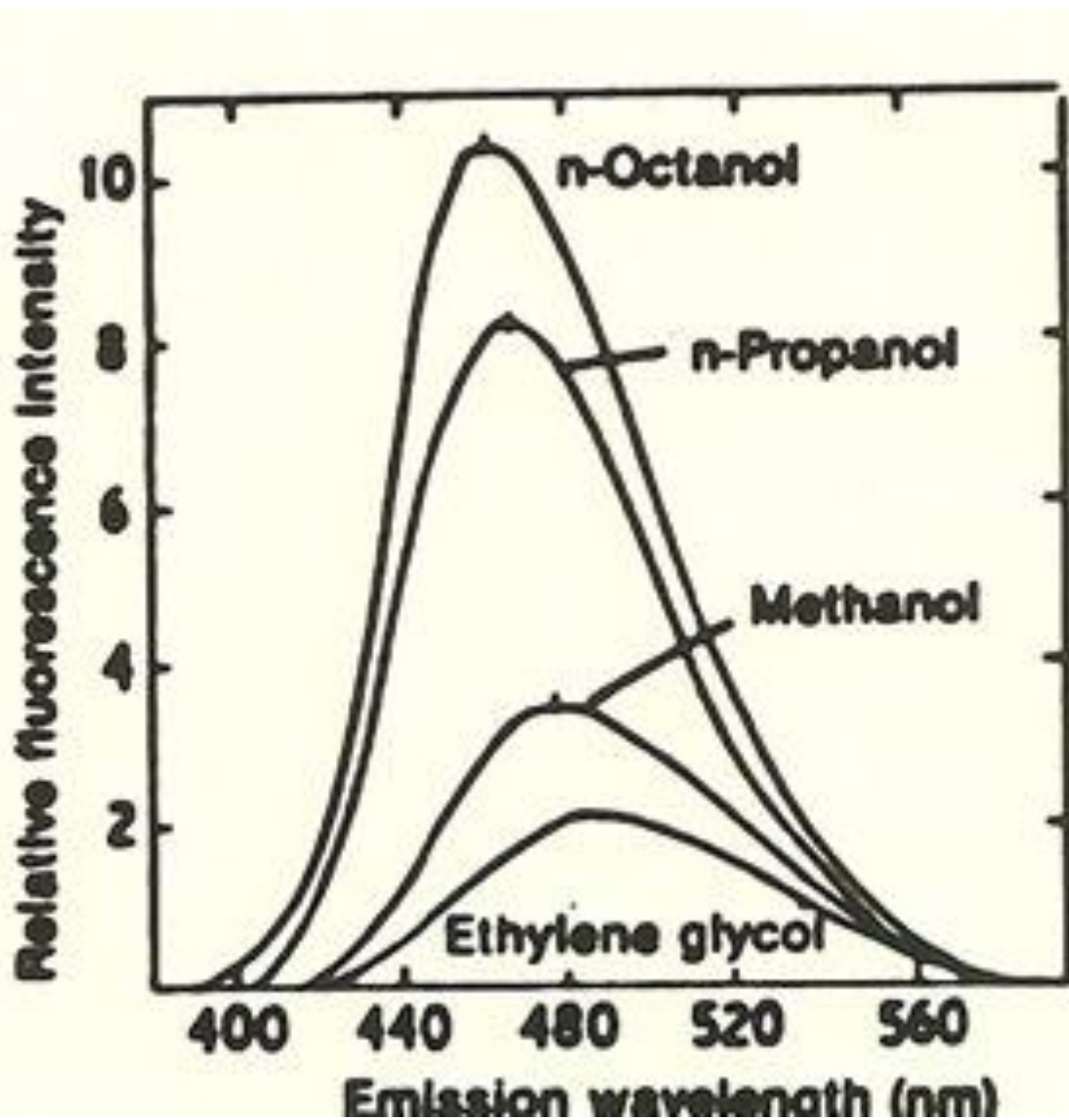
Unique to $G_{i\alpha 1}$ and $G_{s\alpha}$ is the fact that they contain three and four tryptophan residues, respectively. W131 in $G_{i\alpha 1}$ and W154 in $G_{s\alpha}$ are located in the α – helical domain, W211 in $G_{i\alpha 1}$ and W234 in $G_{s\alpha}$ are contained in the switch II region within the GTPase domain, and W258 in $G_{i\alpha 1}$ and W277 and W281 in $G_{s\alpha}$ are found in the GTPase domain (12, 17, 18). The W211 and W258 residues appear in close proximity as depicted in the crystal structure of $G_{i\alpha 1}$. The presence of tryptophan residues in most proteins is scarce and they typically provide a role of stability (19). G_{α} subunits are unique in that the conformational changes that occur upon activation can be monitored through the change in the Trp residues environment. Addition of AlF_4^- or $GTP\gamma S$ to $G_{\alpha}\cdot GDP$ results in a conformational change, which can be detected through the intrinsic tryptophan fluorescence of the protein. An increase in fluorescence is observed when the Trp residues move from a solvent exposed environment to one that is hydrophobic (20).

Weber and Laurence worked with numerous polycyclic aromatic compounds and found that when in water they were non fluorescent. However, upon binding to serum albumin they were highly fluorescent (21). One of the aromatic compounds

studied was 8-Anilino-naphthalene-1-sulfonic acid (ANS), a known extrinsic fluorophore used today to probe the environment of biological molecules through changes in its hydrophobic regions (20, 22). Decreasing the polarity of ANS results in a shift of the λ_{\max} to lower wavelengths (blue shift) and an increase in fluorescence intensity in the emission spectrum (20) (Fig. 3). The blue shifts are best explained through the Planck relation: $E = h\nu$, which displays a direct relationship between energy (E) and frequency (ν). Since the speed of light (c), ν and wavelength (λ) are related by $\lambda\nu=c$, the equation can also be expressed as $E = \frac{hc}{\lambda}$. Excited states have an electron density that is more distorted than in the ground states. Thus, excited molecules are more inclined to interact with a polar environment so as to align the solvent dipoles and cause the emission spectrum to shift toward a higher λ_{\max} (red shift). The quantum yield or fluorescence intensity increases as the polarity of the environment decreases because the rate of intersystem crossing is reduced in nonpolar environments. The effects observed with ANS also occur with intrinsic chromophores such as tryptophan.

Gilman and co-workers (23) established this technique as an indirect method to investigate G-protein activity. Chabre worked with the α -subunit of G_t and was able to determine that the increase in fluorescence observed from activation was from a major contribution of W207, which is equivalent to W211 in $G_{i\alpha 1}$ (24). $G_{t\alpha}$ contains

Figure 3. Solvent effects on ANS



two tryptophan residues, therefore, investigation of the mutant W207F would lead to findings that W207 was or was not the major contributor to the observed fluorescence. Because $G_{i\alpha 1}$ has three Trp residues, the question of contribution is much more complex.

In addition to the increased fluorescence observed in $G_{i\alpha} \cdot \text{AMF}$ and $G_{i\alpha} \cdot \text{GTP}\gamma\text{S}$, Chabre found a shift of the λ_{max} to higher wavelengths (red shift) in the emission spectra (24). Hamm and co-workers (25) followed up on Chabre's work and found evidence for a red shift in WT $G_{i\alpha 1} \cdot \text{AMF}$. A comparison between the crystal structures of $G_{i\alpha} \cdot \text{GDP}$ and $G_{i\alpha} \cdot \text{AMF}$ revealed a change in the distances between R204 and W207 to be 8.0 Å and 5.8 Å, respectively (25). Through the use of Trp mutants, W211C and W258F, Hamm – and co-workers (25) were able to determine that the cause of the shift was due to the close proximity of R208 and W211 in $G_{i\alpha 1} \cdot \text{AMF}$, the equivalent Arg and Trp in the active site of $G_{i\alpha}$. However, they neglected to study the effects of the shift in the $\text{GTP}\gamma\text{S}$ conformation and the contribution from W131.

Another indirect method for exploring the R208 – W211 bridge formation is through trypsin digestion in combination with SDS – PAGE. Trypsin cleaves on the carboxyl end of arginine and lysine residues. SDS – PAGE of WT $G_{i\alpha 1} \cdot \text{GDP}$ displays a band at a molecular weight near 41kDa. In the presence of trypsin the single band at 41 kDa is no longer observed, but two new bands appear at 21 kDa and 17 kDa. The two fragments correspond to digestion at R208. In contrast, WT $G_{i\alpha 1} \cdot \text{AMF}$ and $\text{GTP}\gamma\text{S}$ in the presence of trypsin continue to show a band at 41 kDa (26). Therefore,

$G_{i\alpha 1}$ is protected from tryptic digestion while activated and vulnerable to proteolysis in its GDP conformation (26).

Converting each Trp residue to a phenylalanine (F) via site direct mutagenesis produced three independent mutants, which were used to explore the contribution of each Trp residue towards the overall change in intrinsic tryptophan fluorescence for the AMF and GTP γ S conformations. In addition, we used the mutants to examine how the formation of the R208 – W211 bridge affects the red shift in the emission spectra of $G_{i\alpha 1}$.

The crystal structures of $G_{i\alpha 1}$ •GDP (1GDD and 1BOF), AMF (1GFI), and GTP γ S (1GIA) conformations are available (12, 13, 17). The $G_{i\alpha 1}$ •GDP displays unordered structure in the switch I and II regions, whereas both active structures show ordering of those two regions. Mg^{2+} has octahedral geometry in the active site near the guanine nucleotide of both AMF and GTP γ S forms. In the GTP γ S form, Mg^{2+} is bound to four equatorial ligands, the oxygen atoms of the hydroxyl groups in Thr181 and Ser47, and the oxygen atoms in the β – and γ – phosphate groups of GTP γ S, and two water ligands occupy the axial positions. In the AMF conformation, the Mg^{2+} coordination is identical to that of the GTP γ S form with the exception that one fluoride ion from AlF_4^- is bound to the equatorial position once occupied by the γ – phosphate. It is known that Mg^{2+} is required for the formation of the AMF complex and for the hydrolysis of GTP. We hope to better understand the extent to which Mg^{2+} contributes to the conformational states in which GTP γ S, AlF_4^- or GDP are bound to G_α subunits.

We plan to investigate, through circular dichroism, the secondary structure upon activation with GTP γ S and AMF. In addition, we plan to gain insight into the role of Mg²⁺ in the folding of G_{i α 1} and G_{s α} in the AMF and GTP γ S forms.

The structure of a protein is essential to its biological function. Occurrences of mutations in DNA manifest in changes in the amino acid sequence that can lead to a plethora of problems, such as misfolding, interference of effector sites, unwanted translational modifications, etc. Ultimately this can produce incorrect function that leads to disease. Mutations in the GNAS and GNAI1 genes that encode for G_{s α} and G_{i α 1} have been implicated in numerous tumors found in the human body (27). Hot spot mutations at Q227 and R201 in GNAS have led to cancers, 10.6% and 88.1% of the time, in the biliary tract, pituitary gland, and small intestine (27). GNAI1, albeit to a much lower degree than GNAS, is associated with mutations at R208 leading to carcinomas in the large intestine (27).

Misfolding of proteins is another major contributor to detrimental neurological disorders and the occurrence of certain types of cancers (27, 28). For example, Alzheimer's and Parkinson's diseases arise from aggregation of a prion protein, known as β – amyloid. It is a protein comprised of a multitude of β – sheets and upon accumulation begins to aggregate and form particulate on the brain leading to neurological dysfunction (28).

We aim to examine the folding mechanism of G_{i α 1} and G_{s α} , through spectroscopic techniques that include fluorescence, circular dichroism, and UV - Vis. Fluorescence spectroscopy can give us local insight by monitoring the change in the tryptophan environment. CD will provide information on alterations in the secondary

structure. Lastly, $G_{i\alpha 1}$ and $G_{s\alpha}$ are comprised of numerous tyrosines at their surface.

We also intend to gain knowledge on protein folding of the tertiary structure through UV – vis spectroscopy.

In conclusion, we hope to add important knowledge on the structural and functional aspects of G_{α} proteins, which may lead to the development of better therapeutics for the treatment of G_{α} subunit related - illnesses.

CHAPTER TWO
CONTRIBUTIONS OF EACH TRP RESIDUE TOWARDS THE INTRINSIC
FLUORESCENCE OF THE $G_{i\alpha 1}$ PROTEIN

Introduction

G proteins are membrane-bound guanine-nucleotide binding proteins. Heterotrimeric G proteins consist of three subunits (α , β , and γ) that mediate transduction of extracellular signals to various intracellular effectors (29). Once a receptor protein binds to an extracellular hormone or neurotransmitter, it triggers the activation of the corresponding G protein. The activation of a G protein is accompanied by a conformational change in which GDP bound to the α subunit exchanges for GTP and the $\beta\gamma$ dimer dissociates. The activated G protein returns to its resting, GDP-bound inactive state via hydrolysis of bound GTP and release of inorganic phosphate. GTP binding impacts the structures of three flexible loop segments located near the γ -phosphate, which are named switches I, II, and II. In the GTP-bound state, these switch regions are held in place by the γ -phosphate whereas in the GDP-bound state they are less ordered (29). $G_{i\alpha 1}$ and $G_{s\alpha}$ are, respectively, the inhibitory and stimulatory α -subunits that are responsible for the decreased or increased production of the secondary messenger adenosine-3',5'-monophosphate (cAMP) (30). This study focuses on the environment of tryptophan (W) residues in $G_{i\alpha 1}$. W211 is located in the conformational-dependent switch II region. $G_{i\alpha 1}$ also contains two other tryptophans, W131 and W258, that are located in

the alpha helical and GTPase domains, respectively. X-ray crystallographic studies have provided a wealth of structural information on the different conformations of G proteins (12, 13, 18, 31-34). These static structural studies have been complemented with dynamic investigations in solution.

Radiolabeling of guanosine nucleotides with either ^{32}P and ^{35}S is a common method used for probing activation of G proteins by exploring the cycle of GTP→GDP exchange and hydrolysis (35). However, unlike electron paramagnetic studies using cysteine-anchored spin labeled G proteins (36, 37), radioactive assays do not give insight into the movements of the segments within G_α subunits. An indirect method of measuring protein activation in G proteins is through intrinsic tryptophan fluorescence, a tool that was pioneered by Gilman and co-workers (38). As observed for other proteins (39), when tryptophan residues move into less-solvent exposed environments the fluorescence intensity increases. Enhancements of fluorescence intensity were observed when either the active conformation was formed upon the exchange of GDP with GTP γ S (non-hydrolyzable analog) or the transition state conformation was attained via addition of AlF_4^- to $G_{i\alpha 1} \cdot \text{GDP}$ (38). Chabre et al. (24) found that for transducin (G_t), the change in fluorescence intensity upon activation was dependent on the presence of W207. (W207 in G_t is the sequence counterpart of W211 in $G_{i\alpha 1}$) When mutated to a phenylalanine, the W207F mutant of G_t displayed a decrease in fluorescence (24, 40). The polarity of the environment also affects the λ_{max} values of W residues by shifting them to lower wavelengths, i.e., λ_{max} undergoes a *blue* shift (20). However, Hamm and co-workers (25) found evidence for a π -cation interaction between arginine (R208) and

W211 in $G_{i\alpha 1}$ based on the observed *red* shifts (to higher wavelengths) in the λ_{\max} of the emission spectra of the activated forms of $G_{i\alpha 1}$ (25).

The purpose of this investigation is to build on the foundation set by these previous studies and explore how each W contributes to the overall intrinsic fluorescence and to the R208-W211 electrostatic interaction in $G_{i\alpha 1}$.

Materials and Methods

Expression and Protein Purification

$G_{\alpha 1}$ was obtained and purified as described previously (41). W131F, W211F, and W258F mutants were prepared by site-directed mutagenesis using a kit provided by Stratagene (La Jolla, CA). Proteins were dialyzed overnight at 4 °C in 20 mM Tris pH 8.0 buffer containing 10% (v/v) glycerol, and 1 mM DTT and then stored at -80 °C. Protein purity was greater than 95% as estimated by SDS – PAGE.

Fluorescence Measurements

Experiments were performed using a PTI QuantaMaster fluorimeter (Photon Technologies, Inc., Mirmingham, NJ). Time-based assays were conducted with excitation and emission wavelengths set at 280 nm and 340 nm, respectively. Assays were initiated after 60 sec by addition of either AlF_4^- as a premixed solution (50 μ M $AlCl_3$ and 10 mM NaF) or 20 μ M GTPyS to pre-incubated 500 $G_{\alpha 1}$ nM protein samples in buffer containing 50 mM Tris, pH 7.5, 1 mM DTT and 5 mM $MgCl_2$. Time-based assays were normalized to zero at 60 sec. Graphpad Prizm 3.0 was used for analyzing the time-dependent curves. The W211-R208 bridge formation was probed using emission spectra recorded over a wavelength range of 300-400 nm with excitation wavelength set at 280 nm. Signal integration time was 1 sec, and the bandpass for both excitation and

emission was 5 nm. In emission spectra, the maximal fluorescence intensities before and after activation with either AlF_4^- or $\text{GTP}\gamma\text{S}$ were normalized to 1.0.

Rates for biphasic activation of AMF were calculated by fitting the data to the equation:

$$Y = Y_0 \left[\frac{k_2 e^{-k_1 t} - k_1 e^{-k_2 t}}{k_1 - k_2} \right]$$

Rates for monophasic activation with $\text{GTP}\gamma\text{S}$ were calculated by fitting the data to the equation:

$$Y = Y_{max}(1 - e^{-k_1 x})$$

Trypsin Digestion Analyzed by SDS-PAGE

WT or mutant $\text{G}_{\alpha 1}$ proteins at 15 μM were incubated for 60 min at 30 °C in 50 mM Tris, pH 8.0, 5 mM MgSO_4 , 5mM DTT with either 100 μM GDP or $\text{GTP}\gamma\text{S}$ or 50 μM AlCl_3 and 10 mM NaF (26). Where indicated, trypsin (26 $\mu\text{g}/\text{ml}$) was added and incubated for an additional 10 min at 30 °C. SDS-containing buffer was added and samples were incubated for 10 min at 100 °C. Proteins were separated in a SDS 12.5 % polyacrylamide gel.

Modeling

The coordinates of GDP (1BOF, (13)), GDP- AlF_4^- (1GFI, (12)) and $\text{GTP}\gamma\text{S}$ (1GIA, (12)) derivatives of $\text{G}\alpha 1$ were downloaded from the Protein Data Bank (PDB, (42)). Missing loops in these structures were modeled using the corresponding transducin structures (1TAG, (33), 1TAD, (34) and 1TND, (32)) and Swiss Model. Each simulation box, containing one subunit, GDP or GTP, Mg^{2+} , a TIP3 water box extending at least 10 Å beyond the protein in all directions and 0.1 M NaCl adjusted to neutralize

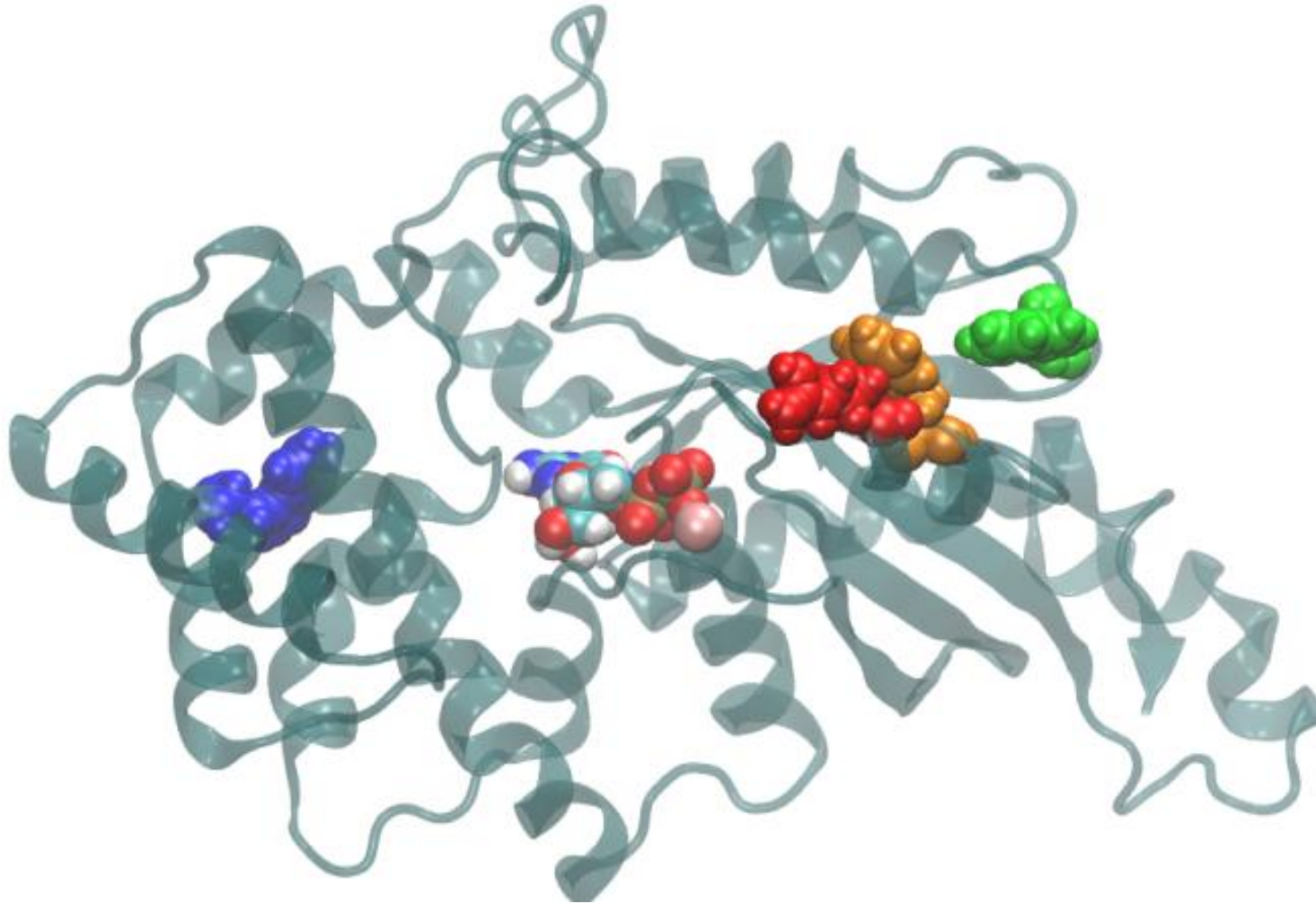
the charge in the water box, was assembled using the molecular graphics program VMD. The simulation box was then brought to equilibrium using the molecular dynamics program NAMD. The equilibration procedure involved energy minimization with and without restraints on the protein coordinates (3000 steps each), slow heating from 10 to 310 K (30,000 steps), and then pressure and temperature equilibration using a Langevin piston (10,000 steps). Finally, unrestrained dynamics for 100,000 steps was done before data was acquired. Periodic boundary conditions were used. The cutoffs for non-bonding (van der Waals and electrostatic) interactions were 12 Å. The switch distance was 10 Å, and 1.0 1-4 scaling factor was used. All calculations were done using CHARMM 27 parameters. The initial tryptophan point mutation models were generated using VMD and then subjected to the same equilibration procedure as the wild type structures. All molecular graphics diagrams were generated using VMD.

Results

AMF and GTP γ S Activation of WT G $_{i\alpha 1}$ and its Trp Mutants

G $_{i\alpha 1}$ contains three trp residues: W131 is located in the helical domain; W211 is in the switch II region and W258 in the GTPase domain (Fig. 4). Intrinsic tryptophan fluorescence is a common method used for detecting G $_{\alpha}$ protein activity that has been well documented (38). To understand the contributions of each tryptophan towards the overall fluorescence of the protein, three mutants were prepared in which the tryptophan residues were mutated to phenylalanine (W131F, W211F, and W258F). Phenylalanine

Figure 4. Model of WT $G_{i\alpha 1}$ depicting its carbon backbone.
GDP nucleotide, three Trp residues, W131 (blue), W211 (orange), and W258 (green), and R208 (red).



was chosen as a replacement for tryptophan because of similar structure and size characteristics, and low quantum yield and distinct λ_{\max} value (43).

Upon addition of AlF_4^- , the fluorescence intensity of WT $\text{G}_{\text{ia1}} \text{GDP} \cdot \text{AMF}$ reached a maximum of $40.3 \pm 0.04 \%$ ($n \geq 3$) after 2 min (Fig. 5, curve C). This increase in fluorescence intensity is characteristic of an activated WT $\text{G}_{\text{ia1}} \text{GDP} \cdot \text{AMF}$ protein (38). AMF activation of W131F (Fig. 5, curve A) displayed the highest fluorescence intensity (F_{\max}), followed by W258F (Fig. 5, curve B), which exhibited a slight, but significantly larger fluorescence intensity than WT (Table 1). In contrast, W211F $\text{G}_{\text{ia1}} \cdot \text{GDP} \cdot \text{Mg}^{2+}$ displayed an initial decrease in fluorescence upon addition of AlF_4^- (data not shown). As binding of AlF_4^- progressed, there was a gradual increase in fluorescence intensity that was too small to be viewed in figure 5, and indicated that, unlike the three other proteins, sample dilution was not offset by the large increases in fluorescence intensity associated with AMF activation. Addition of $\text{GTP}\gamma\text{S}$ to WT, W131F and W258F mutants also resulted in increases in fluorescence intensity similar to the $\text{GDP} \cdot \text{AMF}$ counterparts (Fig. 6). As in activation with AlF_4^- , full exchange of GDP for $\text{GTP}\gamma\text{S}$, followed the same order of plateaus for WT and W131F and W258F mutants, and W211F exhibited no change in fluorescence intensity.

Despite the fact that W211F does not display an increase in fluorescence upon activation, the GDP conformation did exhibit significant fluorescence in its emission spectra similar to WT and W258F (Fig. 7). Interestingly, the emission of the W131F mutant in the GDP conformation was significantly smaller than in the other proteins (Fig. 7). In addition to its GDP conformation, W211F also exhibited similar fluorescence in its

Figure 5. Intrinsic Tryptophan fluorescence of WT $G_{i\alpha 1}$ (C) and its W131F (A), W258F (B) and W211F (D) mutants after activation with AlF_4^- .

Fluorescence (%) = $((F_o - F_i)/F_i) * 100$, where F_i and F_o are the fluorescence intensities in arbitrary units at the start of the activation and at time t

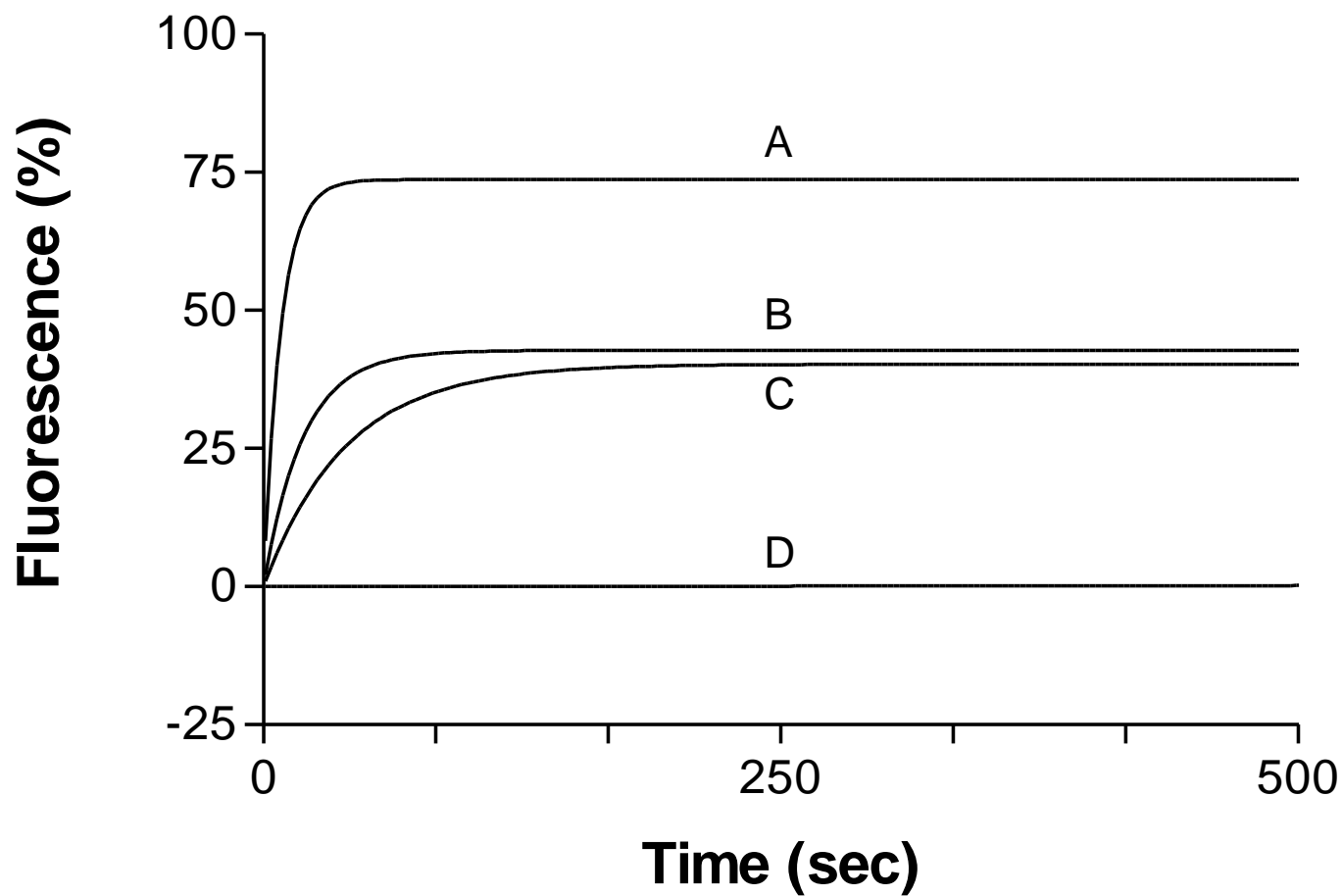


Table 1. Kinetic Parameters for Activation of WT and W Mutants

Protein	AMF Activation		GTP γ S Activation	
	Initial Rate Constant (k) ^{1,3} (sec ⁻¹)	F _{max} ^{2,3} (%)	Rate Constant (k) ^{1,3} (sec ⁻¹)	F _{max} ^{2,3} (%)
WT G_{1α1}	0.03	40.3	0.94 x 10 ⁻³	41.8
W131F	0.2	73.7	0.13 x 10 ⁻²	63.0
W211F	N/A	N/A	N/A	N/A
W258F	0.06	42.8	0.11 x 10 ⁻²	55.5

- 1 Error reported is less than 0.5%
- 2 Error reported is less than 0.5%
- 3 Average data from n ≥ 3 experiments

Figure 6. Intrinsic Tryptophan fluorescence after GDP→ GTPγS exchange.
The curves are labeled as in Fig. 5. Fluorescence % is calculated in the same manner as in Fig. 5.

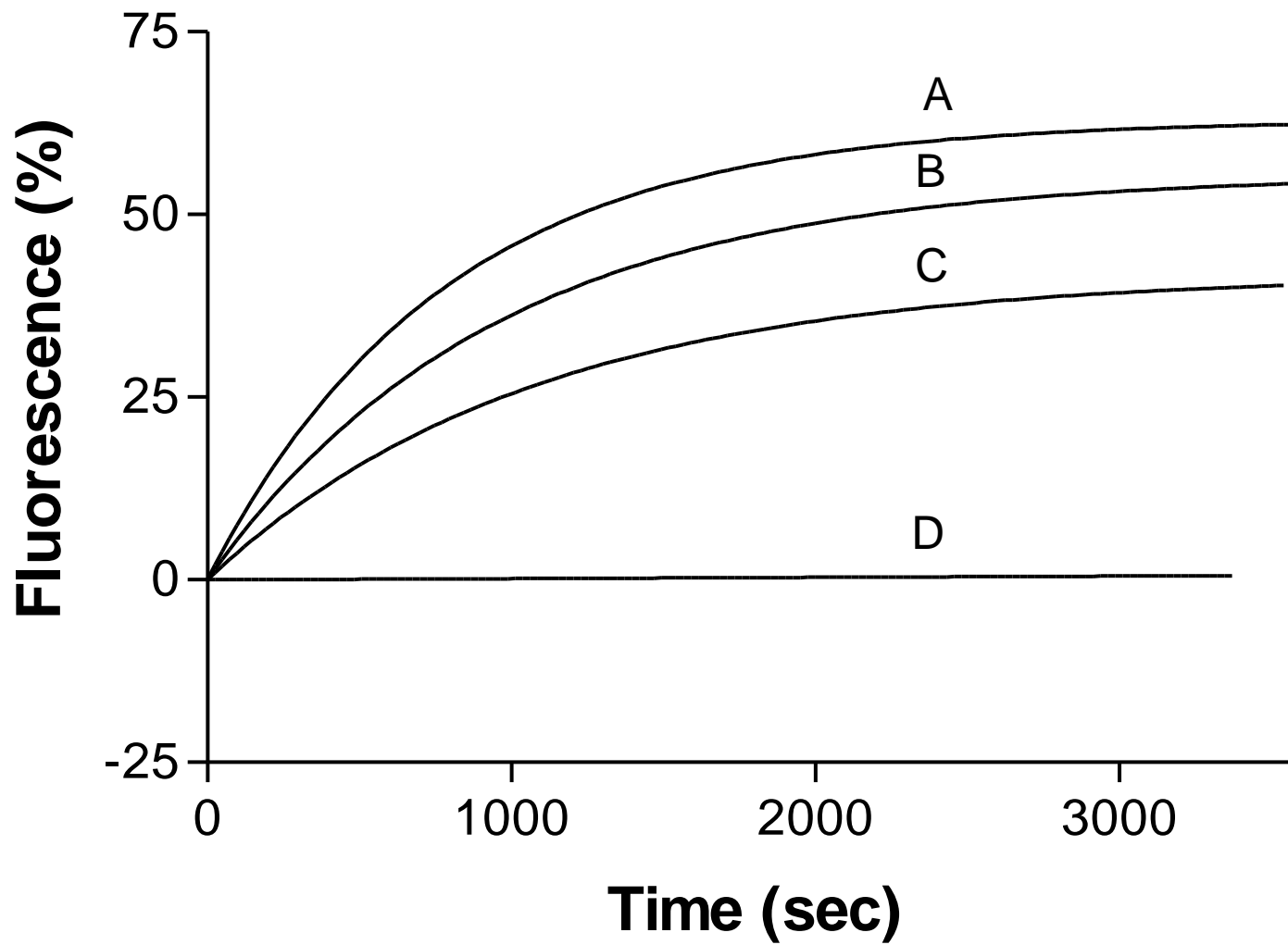
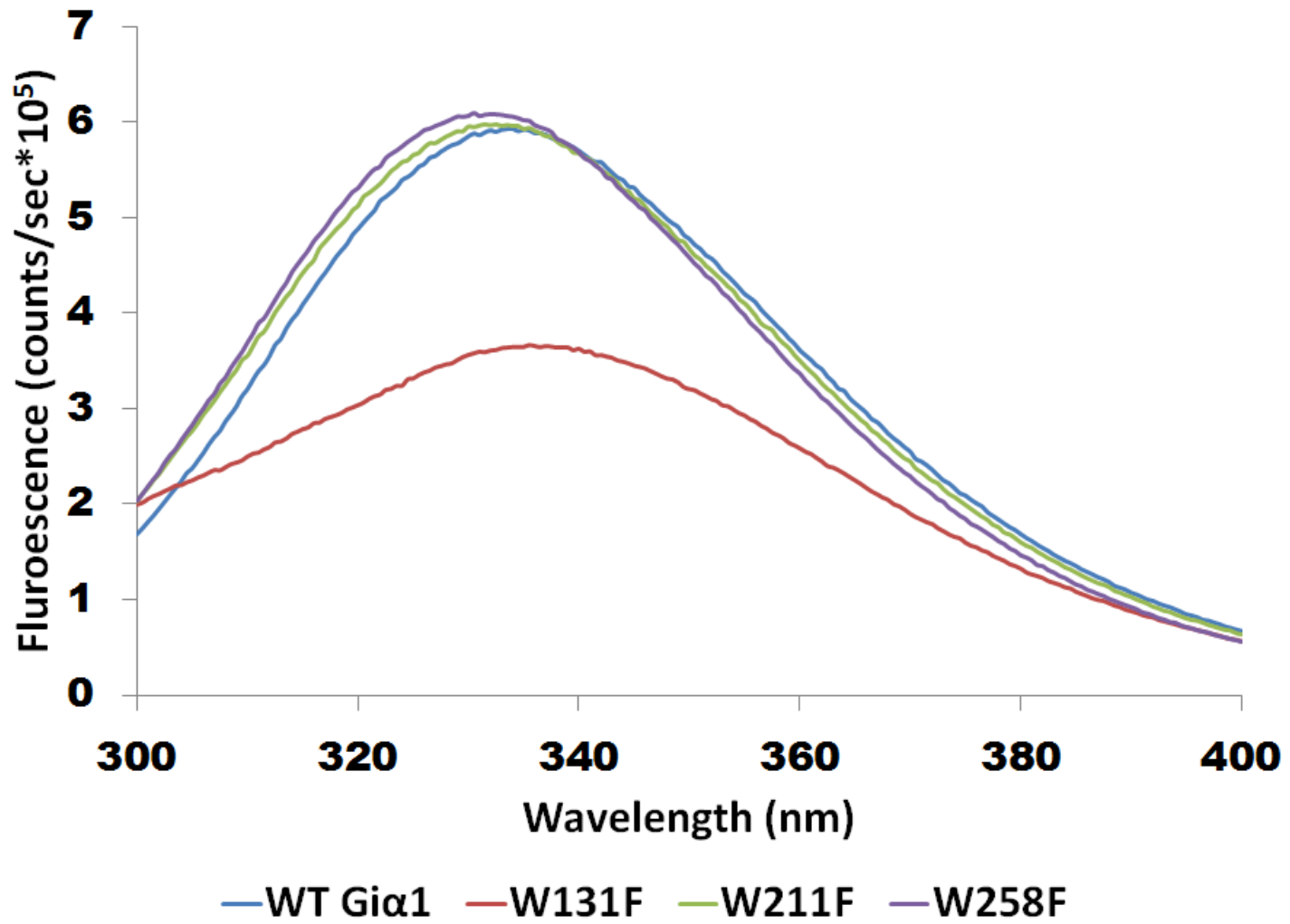


Figure 7. Emission spectra of WT $G_{i\alpha 1}$ and its three Trp mutants in the GDP conformation



AMF and GTP γ S conformations and activation of WT, W131F, and W258F G $_{i\alpha 1}$ also showed substantial increases in their emission spectra. However, for the active conformations, the emission of the W258F mutant was larger than in the other proteins (data not shown). AMF activation of WT, W131F, and W258F was biphasic with the initial k_1 rates differing by less than one order of magnitude (Table 1). However, the rates for the second step were approximately four orders of magnitude larger (data not shown). In contrast, GTP γ S activation of WT, W131F and W258F was monophasic with rates that were of the same order of magnitude, but smaller than the initial k_1 rates observed for AMF activation (Table 1).

The crystal structures of WT G $_{i\alpha 1}$ GDP (1BOF), AMF (1GFI) and GTP γ S (1GIA) are known (12, 13). However, in all three conformations many crucial amino acids are missing, including R208 and W211, which lie in the switch II region. The missing residues of WT G $_{i\alpha 1}$ were built in using homology modeling of the WT transducin (G $_t$) crystal structures (33, 34, 44). Structures of W131F, W211F, and W258F mutants in all three conformations were generated from the WT G $_{i\alpha 1}$ models. In an attempt to rationalize the experimental findings in Figs. 5 and 6, we calculated for each tryptophan residue the change in solvent exposure (Δ) between the GDP and either the AMF or GTP γ S conformations (Table 2). For AMF activation, W131F displayed the largest overall value of Δ , followed by W258F, WT, and W211F. The same calculations were performed for GTP γ S activation and the same trend was observed (Table 2). For each of the three W mutants, predicted maximum fluorescence (F_{max}) values were calculated by using the total Δ for each mutant and by setting WT G $_{i\alpha 1}$ •GDP with AMF or GTP γ S

Table 2. Solvent Exposure of W residues in WT and W Mutants

Protein	Conformation and Solvent Exposure	W131	W211	W258	Total Δ^1	Estimated F_{\max}	Observed ² F_{\max}
WT	GDP	22	114	179	210*		
	AMF	32	8	161	134*		
	$\Delta_{\text{AMF-GDP}}$	10	-105	-18	-114	40	40.3 \pm 0.04
	GTP	51	7	157	143*		
W131F	$\Delta_{\text{GTP-GDP}}$	29	-107	-22	-100	40	41.8 \pm 0.07
	GDP	0	144	202	346		
	AMF	0	9	129	138		
	$\Delta_{\text{AMF-GDP}}$	0	-135	-73	-208	73	73.7 \pm 0.04
W211F	GTP	0	12	176	188		
	$\Delta_{\text{GTP-GDP}}$	0	-132	-26	-158	63	63.0 \pm 0.03
	GDP	21	0	166	187		
	AMF	20	0	165	185		
W258F	$\Delta_{\text{AMF-GDP}}$	-1	0	-1	-2	0.7	N/A
	GTP	15	0	165	180		
	$\Delta_{\text{GTP-GDP}}$	-6	0	-1	-7	3	N/A
	GDP	43	118	0	161		
	AMF	22	12	0	34		
	$\Delta_{\text{AMF-GDP}}$	-20	-106	0	-126	44	42.8 \pm 0.02
	GTP	20	13	0	33		
	$\Delta_{\text{GTP-GDP}}$	-23	-105	0	-128	51	55.5 \pm 0.02

¹ A negative indicates a decrease in solvent exposure of the tryptophan residue.

²Errors less than 0.5 % for $n \geq 3$

*(sum of the row) X ($\frac{2}{3}$) to normalize for contribution of two Trp residues

activation at the observed values of 40%. The obtained theoretical values were within 5 % of the actual experimental data (Table 2; last column).

Shifts in the Emission Spectrum of Activated $G_{i\alpha 1}$ Proteins

Fluorophores, such as (ANS), undergo an increase in fluorescence intensity as well as a blue shift as solvent polarity decreases (20). We therefore investigated whether the predicted blue shifts would be observed for WT and W mutants of $G_{i\alpha 1}$. The contribution of the shift in λ_{\max} was separated from the increase in fluorescence intensity by normalizing the relative fluorescence maximum of each spectrum to 1.0 (Fig. 8). In contrast to the predicted blue shifts, WT $G_{i\alpha 1}$ GDP•AMF displayed a red shift of 2.4 ± 0.1 nm when compared to its GDP bound counterpart (Fig. 8a). Both WT $G_{i\alpha 1}$ •GDP•AMF (Fig. 8a) and WT $G_{i\alpha 1}$ •GTP γ S (Fig. 8b) exhibited similar red shifts. Upon activation with AlF_4^- , W258F had the largest $\Delta\lambda_{\max}$ value of 3.2 ± 0.1 nm, followed by WT $G_{i\alpha 1}$, and W131F at 2.1 ± 0.1 nm; in contrast to the other proteins, W211F displayed the only negative $\Delta\lambda_{\max}$ value of -0.4 ± 0.4 nm (Fig. 9). Upon exchange with GTP γ S (Fig. 9), W131F $G_{i\alpha 1}$ had the largest $\Delta\lambda_{\max}$ value of 3.9 ± 0.5 nm, followed by W258F with 3.6 ± 0.1 nm and WT with 2.5 ± 0.2 nm; W211F again displayed a negative $\Delta\lambda_{\max}$ of -0.4 ± 0.2 nm.

π -cation interactions between lysines or arginines with the aromatic side chains of tryptophans, tyrosines and phenylalanines have been previously investigated (45, 46). Electrostatic interactions at distances less than 6 Å are found to be favorable with $E_{es} < -2$ kcal/mol (25, 45). Distances between the C atom in the guanidinium group of R208 and the geometric center of the indole ring of W211 in WT and mutant $G_{i\alpha 1}$ protein models were measured for all conformations (Table 3). In the GDP conformation,

Figure 8. Intrinsic tryptophan fluorescence of $G_{i\alpha 1}$ proteins. Emission of 0.5 μM WT $G_{i\alpha 1}$ before (blue trace) and after activation with either AlF_4^- (panel A; red trace) or $\text{GTP}\gamma\text{S}$ (panel B; red trace).

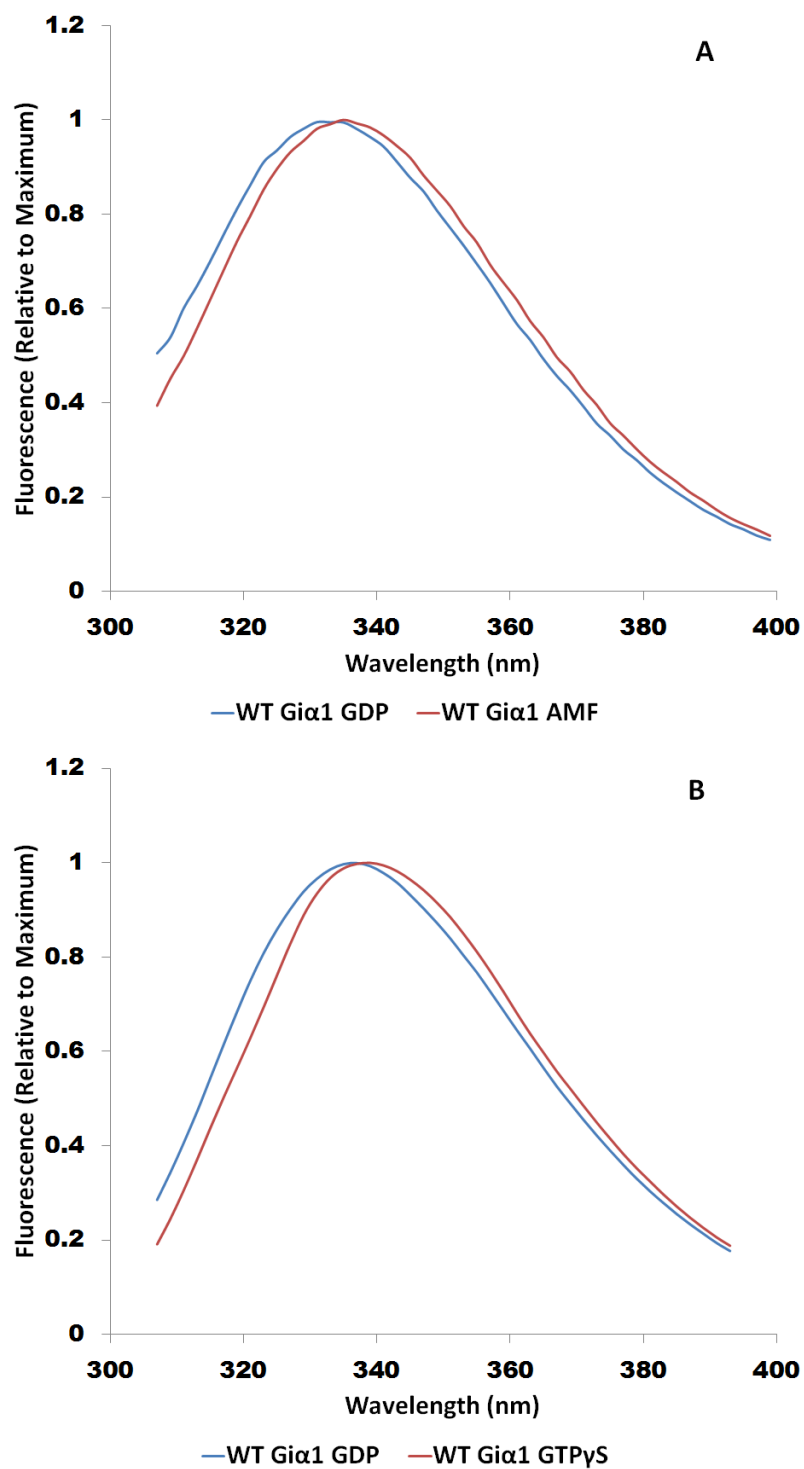


Figure 9. Depiction of red shifts undergone by WT and W mutants upon addition of AlF_4^- (left set of 4 bars) or $\text{GTP}\gamma\text{S}$ (right set of 4 bars).

The asterisks indicate statistically significant changes $n \geq 3 \pm \text{SEM}$. measurements at $p < 0.001$

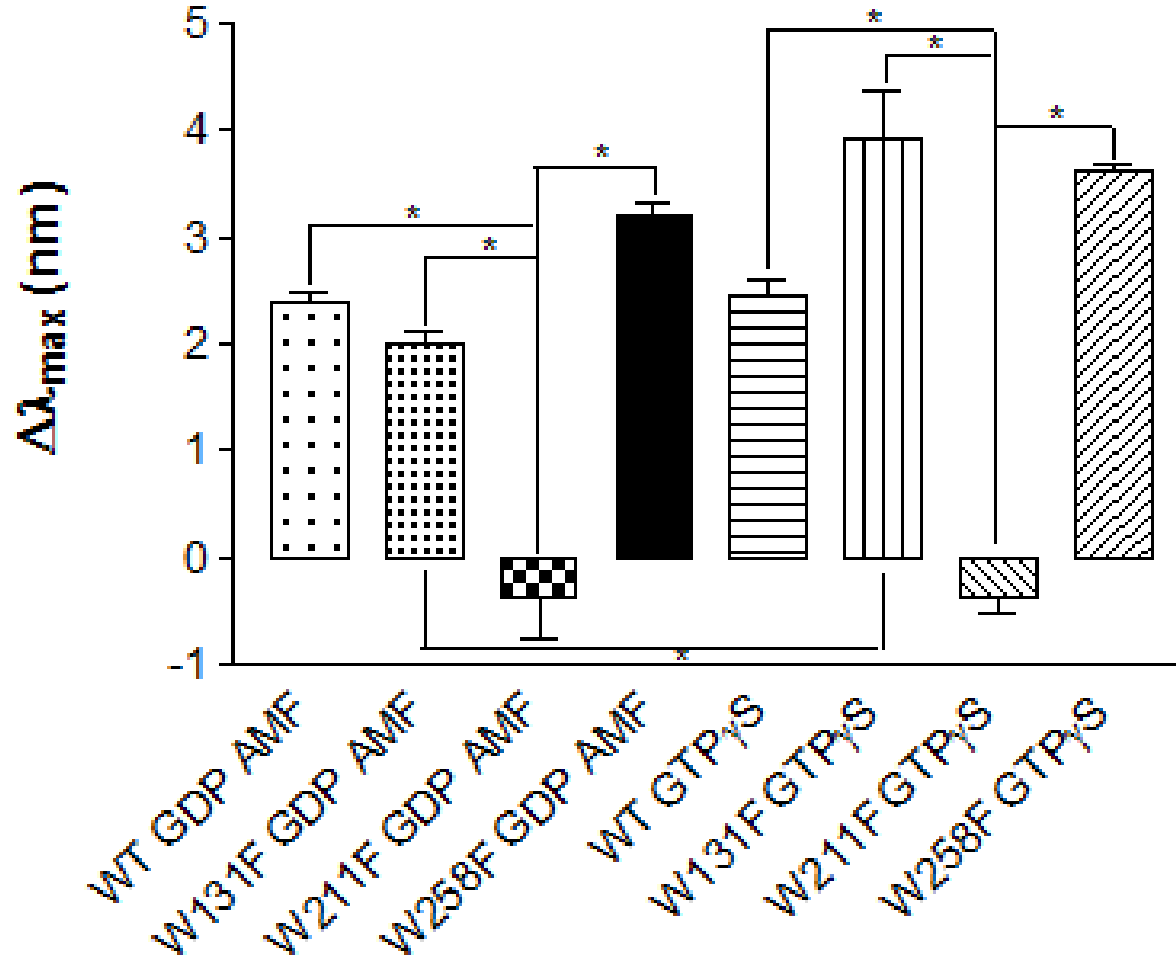


Table 3. Observed and Calculated Distances and λ_{\max} shifts in WT and W Mutants

	GDP	AMF Activation		GTPγS Activation	
	Model Distance (\AA) ¹	Model Distance (\AA) ¹	AMF _{exp} (nm) ²	Model Distance (\AA) ¹	GTP γ S _{exp} (nm) ²
WT	8.63	6.61	2.4	6.55	2.5
W131F	9.71	6.50	2.1	6.95	3.9
W211F	N/A	N/A	-0.4	N/A	-0.4
W258F	10.4	6.70	3.2	7.20	3.6

¹ Distance measured in the models from the geometric center of the indole ring in W211 to the carbon atom in the guanidinium group in R208

² Fluorescence red shifts ($\Delta\lambda_{\max}$) between GDP and AMF or GTP γ S conformations

distances greater than 8.6 Å were found for all $G_{i\alpha 1}$ proteins. In the activated AMF and GTP γ S models, however, the R208 and W211 were in the 6.5 to 7.2 Å range (Table 3).

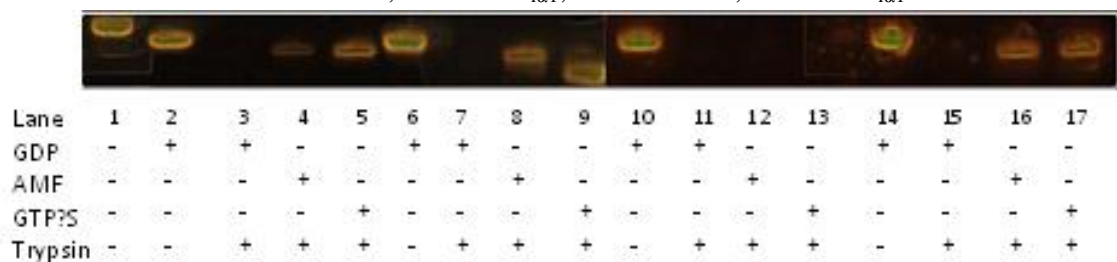
Trypsin Digestion of $G_{i\alpha 1}$ Proteins

Digestion with trypsin, a protease that cleaves at the carboxyl termini of arginines and lysines, can be used as a tool to distinguish the inactive from the other conformations (47). R208 is solvent exposed in the GDP conformation, but not in the GTP γ S or GDP•AMF conformations. SDS-PAGE was applied in conjunction with the digestion to visualize the hydrolysis. WT $G_{i\alpha 1}$ •GDP has a molecular weight of 41 kDa (Fig. 10, lane 2) and, upon trypsin addition, the band was no longer present (Fig. 10, lane 3). WT $G_{i\alpha 1}$ •AMF and GTP γ S showed bands at 40.3 kDa (Fig. 10, lanes 4 and 5, respectively) after exposure to trypsin, indicating that activated forms of WT $G_{i\alpha 1}$ do not undergo proteolytic cleavage. The same hydrolytic patterns were demonstrated for W131F and W258F $G_{i\alpha 1}$ proteins in all three conformations (Fig 10. Lanes 6-9 and 14-17, respectively). W211F•GDP displayed the same proteolytic cleavage in the GDP conformation as observed for the other three proteins (Fig. 10, lanes 10 and 11). However, that was not the case for the GDP•AMF and GTP γ S conformations of the W211F mutant; complete proteolysis was found for GDP•AMF conformation (Fig. 10, lane 12), but a light band was observed with the GTP γ S conformation suggesting incomplete hydrolysis (Fig. 10, lane 13).

Discussion

The focus of this study was to understand the contribution of each tryptophan in WT $G_{i\alpha 1}$ toward the overall intrinsic tryptophan fluorescence of the protein and to the bridge formation between R208 and W211. Single point mutations of W \rightarrow F at residues

Figure 10. Trypsin digests of wild-type and various tryptophan mutants of $G_{i\alpha 1}$. Proteins were incubated with either GDP, $GTP\gamma S$, or $AlCl_3/MgCl_2/NaF$ (AMF) and trypsin where indicated. Lane 1, marker; Lanes 2-5, WT $G_{i\alpha 1}$; Lanes 6-9, W131F $G_{i\alpha 1}$; Lanes 10-13, W211F $G_{i\alpha 1}$; Lanes 14-17, W258F $G_{i\alpha 1}$.



131, 211 and 258 were used to investigate their roles. W211 was the major determinant toward the overall change in intrinsic tryptophan fluorescence of activated $G_{i\alpha 1}$ proteins as confirmed by the absence of a fluorescence increase in W211F $G_{i\alpha 1}$ incubated with either AMF or GTP γ S (Figs. 5 and 6, trace D). However, the observed fluorescence in the emission spectra of W211F $G_{i\alpha 1}$ •GDP clearly indicates contributions from W131 and W258 (Fig. 7). Chabre and co-workers (24) also reported similar findings for the emission of W207F in G_t •AMF. The differences observed in the emission spectra of WT $G_{i\alpha 1}$ and its W mutants in the GDP conformation can be justified through the total solvent exposure of Trp residues in each respective protein as shown in table 2; column 6. W258F observed the smallest total Δ value (161), followed by W211F (187), then WT $G_{i\alpha 1}$ (210), and lastly, W131F (346). Smaller values indicate a less solvent exposed environment for the Trp residues. For the GDP form, the fluorescence intensities of the emission spectra followed the same trends as the calculated Δ values with the W258F mutant displaying the largest fluorescence followed by the W211F and WT $G_{i\alpha 1}$, and the W131F (Fig. 7). In addition, the emission spectra for the AMF and GTP γ S conformations of the $G_{i\alpha 1}$ proteins (spectra not shown) were in agreement with the calculated Δ values (Table 2, column 6). Therefore, the observation of intrinsic fluorescence is not solely dependent on the presence of W211, but W258 and W131 also contribute to the intrinsic fluorescence of $G_{i\alpha 1}$ subunits. The ranking of the contributions is W211 > W258 > W131.

Single point mutations can often have an effect on the kinetics of a protein. WT, W131F and W258F had very similar rate values for GTP γ S activation as opposed to

what was observed in AMF activation. Previous studies have found that the rate determining step for $\text{GDP} \rightarrow \text{GTP}\gamma\text{S}$ exchange in $\text{G}_{i\alpha 1}$ is the release of GDP (38, 48). Presumably, binding of $\text{GTP}\gamma\text{S}$ to GDP – free $\text{G}_{i\alpha 1}$ occurs at a rate much larger than GDP release thus explaining the monophasic nature of the curves in Fig. 6. The AMF activation curves are the sums of two exponentials. The mechanism of AMF activation may therefore involve a slower step whereby AMF binds to $\text{G}_{i\alpha 1}\cdot\text{GDP}$ followed by a fast conformational change to $\text{G}_{i\alpha 1}\cdot\text{AMF}$. The fact that the rates for the two steps involved in AMF activation do not differ as much for nucleotide exchange account for the biphasic nature of the former (Fig. 5) and the monophasic appearance of the latter (Fig. 6).

Computational data from Table 2 indicate that both W131 and W258 have finite Δ values in all conformations of the W211F mutant, thus explaining the observation of fluorescence in the emission spectra. The data in Table 2 also show that the Δ values of W131 and W258 in the W211F mutant do not change appreciably with either AMF activation (20 vs. 21 and 165 vs. 166) or GTP activation (15 vs. 21 and 165 vs. 166), which accounts for the lack of a fluorescence increase upon the AMF or $\text{GTP}\gamma\text{S}$ activation. The validity of using Δ values is supported by experimental results that were in agreement with predicted fluorescence enhancements calculated from the homology models (Table 2).

Burial of W211 is not independent from that of W131 or W258, as indicated from a comparison of the Δ values from WT with either W131F or W258F mutants (Table 2). Homology models were able to rationalize the differences in % fluorescence (Table 1). AMF activation of W131F $\text{G}_{i\alpha 1}$ displays significant contribution from W258 towards its overall fluorescence (Table 2). Examination of the W258 residue in the homology

models of W131F $G_{i\alpha 1}$ •GDP and W131F $G_{i\alpha 1}$ •AMF shows that upon activation W258 moves into a more hydrophobic environment in the mutant than in WT (-73 vs. -18, respectively). The contribution of W131 is best characterized from the activation of the W258F $G_{i\alpha 1}$ mutant and the emission spectra of W131F•GDP. Relative to the GDP conformation, the environment of W131 in W258F•AMF and GTP γ S is hydrophobic (-20 and -23, respectively), contrary to WT $G_{i\alpha 1}$ •AMF and GTP γ S, which display an increase in solvent exposure (10 and 29, respectively). Despite lacking a Trp, W258F compensates for its fluorescence by the presence of W131, resulting in increases in fluorescence intensity upon activation that are similar to WT protein (Figs. 5 and 6). W131F•GDP exhibits a substantial loss of fluorescence in comparison to WT, W211F and W258F•GDP (Fig. 7). This lack of fluorescence is due to the absence of W131, which is present in the other $G_{i\alpha 1}$ proteins. W207F•GDP in G_t reported similar intrinsic fluorescence to WT G_t •GDP in their emission spectra (24). Chabre and co-workers demonstrated that, although W207F lacked the key Trp in the GTPase domain responsible for observing the change in fluorescence upon activation with AlF_4^- , W127 like W131 in $G_{i\alpha 1}$ contributed considerably to the overall fluorescence.

ANS increases its fluorescence and is more blue shifted when exposed to increasingly polar solvents (20). Electrostatic interactions between lysines and arginines with aromatic amino acids occur when they are less than 10 Å apart (45). The presence of a red shift in the λ_{max} of the emission spectra for activated WT and W258F $G_{i\alpha 1}$ proteins was previously studied (25). Hamm and co-workers (25) reported that WT $G_{i\alpha 1}$ •GDP displayed a red shift upon addition of AlF_4^- or exchange with GTP γ S because of the formation of a bridge between R208 and W211 (25). We further investigated how the

R208 – W211 interaction compared in WT and W mutants. The electrostatic interaction was removed by deletion of W211, as seen in the W211F mutant which displayed blue shifts in both the AMF and GTP γ S conformations (Fig. 9). These observations were in accordance with previous ANS studies in which π – cation electrostatic interactions are absent (20). The blue shifts of -0.4 nm are also consistent with the shift of -0.4 observed for the R208C mutant, where the electrostatic interaction was also disrupted (25). WT and tryptophan mutants showed distinct red shifts, and to understand their relative $\Delta\lambda_{\text{max}}$ values exploration of the structural models was necessary.

Distances were measured between the C atom on the guanidinium group of R208 and the geometric center of the indole ring in the tryptophan for each protein in all conformations (Table 3). There were, however, no apparent correlations between the shifts observed for each protein in either the transition state or active conformation and the measured distances (Table 3). We suggest that the magnitude of the red shift is dependent on the interaction energies between R208 and W211 in each protein. Molecular dynamics calculations of the R208 - W211 salt bridge in WT, W131F, and W258F G_{iol} proteins indicate that both the electrostatic and Van der Waals (VdW) energies become more negative (stronger) when activating from the GDP form to the AMF or GTP γ S conformations (Table 4), with the effect being greater for the electrostatic than for VdW energies. The strongest electrostatic interaction in the AMF conformation was calculated for W258F, which also displayed the largest red shift.

Table 4. Interaction Energies between R208 and W211¹

	Elec (E)	VdW	Total	Δ_E^2
WT GDP	-0.96	-3.38	-4.34	n/a
W131F GDP	-1.12	-3.37	-4.49	n/a
W258F GDP	-0.47	-3.12	-3.59	n/a
WT AMF	-2.47	-4.33	-6.80	-2.46
W131F AMF	-2.13	-4.64	-6.77	-2.28
W258F AMF	-2.89	-4.35	-7.24	-3.65
WT GTPγS	-2.85	-4.38	-7.23	-2.89
W131F GTPγS	-2.66	-4.42	-7.08	-2.59
W258F GTPγS	-2.30	-4.47	-6.76	-3.17

¹ values are in units of kcal/mol

² Differences in the total interaction energies, between AMF or GTP γ S and GDP of the corresponding G_{10.1} protein. These values are averages of 100 (or 101) steps with standard deviations of approximately 1.0.

W131F observed the weakest interaction and subsequently the smallest red shift. The same relationship trend between the electrostatic interaction and shift in the emission spectrum was observed for WT and its W mutants in the GTP γ S form (Table 4). The exception was W131F•GTP γ S, which displayed the largest red shift, but the lowest interaction energy. This may be explained by the large standard deviation (SD) calculated for the shift in W131F•GTP γ S. All G_{ial}•GTP γ S proteins had a SD of 0.2 nm or lower, while W131F had a considerably high SD of 0.5 nm.

Digestion with trypsin was used as an indirect method to investigate the role of R208 in the bridge formation. Tryptic cleavage, which was visualized by using the SDS-PAGE, is conformation – dependent, as reported before (24). The conformational change of WT G_{ial}•GDP activation with the addition of AlF₄⁻ or exchange with GTP γ S protects the protein from cleavage (26). WT, W131F, and W258F all displayed similar characteristics in each of the respective conformations. However, W211F had some key differences in its AMF and GTP γ S conformations. Hydrolysis of the W211F•AMF form indicates that the electrostatic interaction between R208-W211 is necessary to anchor R208 into a hydrophobic pocket, where it will not be exposed to the proteolytic activity of trypsin. Trypsinization of G_{ial}•GDP proteins produced fragments of 23 Kd and 18 Kd, which are equivalent to the weights of residues 1 – 208 and 209 - 354, respectively, confirming that R208 is the site of proteolysis. To explain the experimental observations, we calculated the solvent exposure of R208 in the molecular models of WT and all three Trp mutants for all conformations. As expected, all proteins in the GDP conformation had relatively high Δ values, but in the AMF and GTP γ S conformations, WT, W131F, and W258F, R208 was more solvent exposed (Table 5; Fig. 11). Compared to the AMF

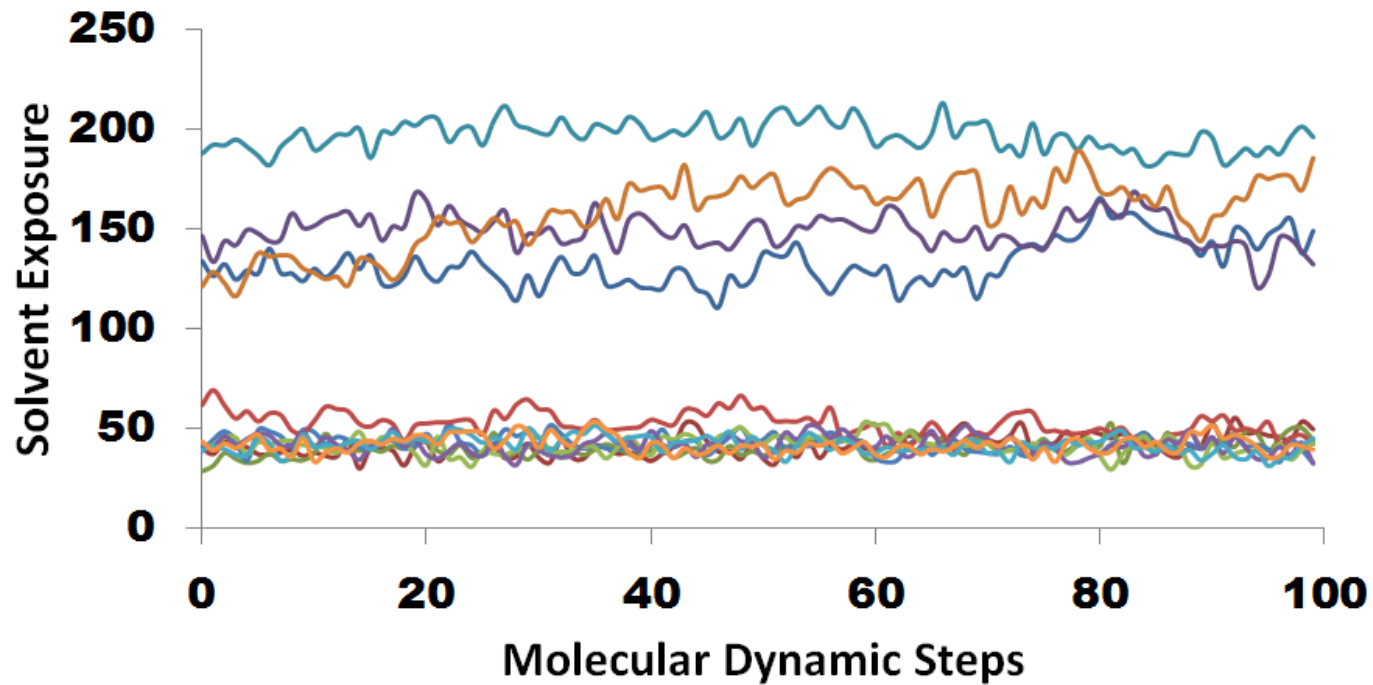
conformations of the other proteins, the solvent exposure of R208 in W211F•AMF reveals higher Δ values, which range from 72 to 52 (Fig. 11), and larger standard deviations (Table 5). These calculations support our conclusion that, without the formation of the bridge, R208 is left solvent exposed and vulnerable to tryptic cleavage. In contrast to the agreement between observed and predicted hydrolysis for W211F•AMF, the molecular dynamics calculations for W211F•GTP γ S suggested protection from hydrolysis, but partial tryptic cleavage was observed. We suggest that the molecular dynamics calculations may either not be sensitive enough or the time allowed was not sufficient to observe the effect.

Taken together, these results provide insight into the overall movement of the tryptophan residues in $G_{i\alpha 1}$ as studied from a comparison of the WT with the W131, W211, and W258 proteins, and that the R208-W211 bridge formation is a very important aspect of the protein's structural integrity.

Table 5. Computational Calculations for Solvent Exposure of R208 in the Molecular Models. Solvent exposure values and standard deviations (SD) were calculated from the last 100 steps of the molecular dynamics calculations

	Δ	SD
WT G_{iat1}•GDP	133	11.3
W131F•GDP	149	8.39
W211F•GDP	197	7.23
W258F•GDP	158	17.4
WT G_{iat1}•AMF	41.5	5.40
W131F•AMF	42.3	4.18
W211F•AMF	52.4	6.01
W258F•AMF	41.5	4.57
WT G_{iat1}•GTPγS	40.1	4.52
W131F•GTPγS	41.6	4.57
W211F•GTPγS	41.8	4.20
W258F•GTPγS	41.9	4.27

Figure 11. Molecular dynamic calculations of R208 solvent exposure in WT and its three Trp mutants in all conformations.



- WT Giα1•GDP
- W131F•GDP
- W131F•AMF
- W131F•GTPγS
- WT Giα1•AMF
- W211F•GDP
- W211F•AMF
- W211F•GTPγS
- WT Giα1•GTPγS
- W258F•GDP
- W258F•AMF
- W258F•GTPγS

CHAPTER THREE

FOLDING OF G_α SUBUNITS: CHANGES IN THE ENVIRONMENTS OF TRP AND TYR RESIDUES AND ON THE SECONDARY STRUCTURE

Introduction

G proteins are heterotrimeric membrane-bound guanine-nucleotide binding proteins that mediate transduction of extracellular signals to various intracellular effectors (1). Once a neurotransmitter or hormone binds to an extracellular receptor, it triggers the activation of the corresponding G protein. Activation is accompanied by a conformational change in which GDP bound to the α subunit exchanges for GTP and the $\beta\gamma$ dimer dissociates. $G_{i\alpha 1}$ and $G_{s\alpha}$ are the inhibitory and stimulatory, respectively, α -subunits that are responsible for the decreased or increased production of the secondary messenger adenosine-3',5'-monophosphate (cAMP) from adenosine triphosphate (ATP) (30). The activated G protein returns to its resting, GDP-bound inactive state via hydrolysis of bound GTP and release of inorganic phosphate. GTP binding impacts the structures of three flexible loop segments located near the γ -phosphate, which are named switches I, II, and III. In the GTP-bound state, these switch regions are held in place by the γ -phosphate whereas in the GDP-bound conformation they are less ordered (13). *In vitro* activation may also occur through binding of AlF_4^- to the β -phosphate of GDP, with AlF_4^- mimicking the γ -phosphate of GTP and forming a transition state (AMF) conformation. The crystal structures of WT $G_{i\alpha 1}$ •GTP (1GIA) and AMF (1GFI)

conformations depict similar folding patterns (12), which are significantly different from the WT $G_{i\alpha 1}\bullet\text{GDP}$ structure (1BOF) (13).

The structure of a protein is essential for its biological function. Thus, alteration in protein folding may cause loss of activity and denaturation, which most often leads to disease. Different types of cancers are associated with mutated G_{α} proteins. Analyses of tumors in the pituitary gland, small intestine, thyroid, and biliary tract have shown hot spot mutations of $G_{s\alpha}$ at R201 and Q227 (27). Mutations at R208 in $G_{i\alpha 1}$ may also result in carcinomas in the large intestine (27). Therefore, investigating the folding pathway of G_{α} subunits may lead to information that may be useful to the development of possible chemotherapeutic agents.

In this investigation, we used fluorescence and UV/Vis spectroscopy and circular dichroism (CD) to monitor the folding of $G_{i\alpha 1}$ and $G_{s\alpha}$ subunits. Activation of G proteins can be probed indirectly through intrinsic tryptophan fluorescence, a tool that was pioneered by Gilman and co-workers (38). As observed for other proteins (39), when tryptophan residues move into less-solvent exposed environments the fluorescence intensity increases (Figs. 12a and 12b). The polarity of the environment also affects the λ_{max} values of W residues by shifting them to lower wavelengths, i.e., λ_{max} undergoes a blue shift (20). Increases in fluorescence intensity were observed when either the active conformation was formed upon the exchange of GDP with $\text{GTP}\gamma\text{S}$ (non-hydrolyzable analog) or the transition state conformation was attained via addition of AlF_4^- to $G_{i\alpha 1}\bullet\text{GDP}$ (38). Site directed mutagenesis was performed on each tryptophan, thereby converting each residue to a phenylalanine (F). Fluorescence was used to investigate the

Figure 12. WT $G_{i\alpha 1}$ •GDP displaying its three tryptophan residues, Arg208, and Mg^{2+} (green sphere)

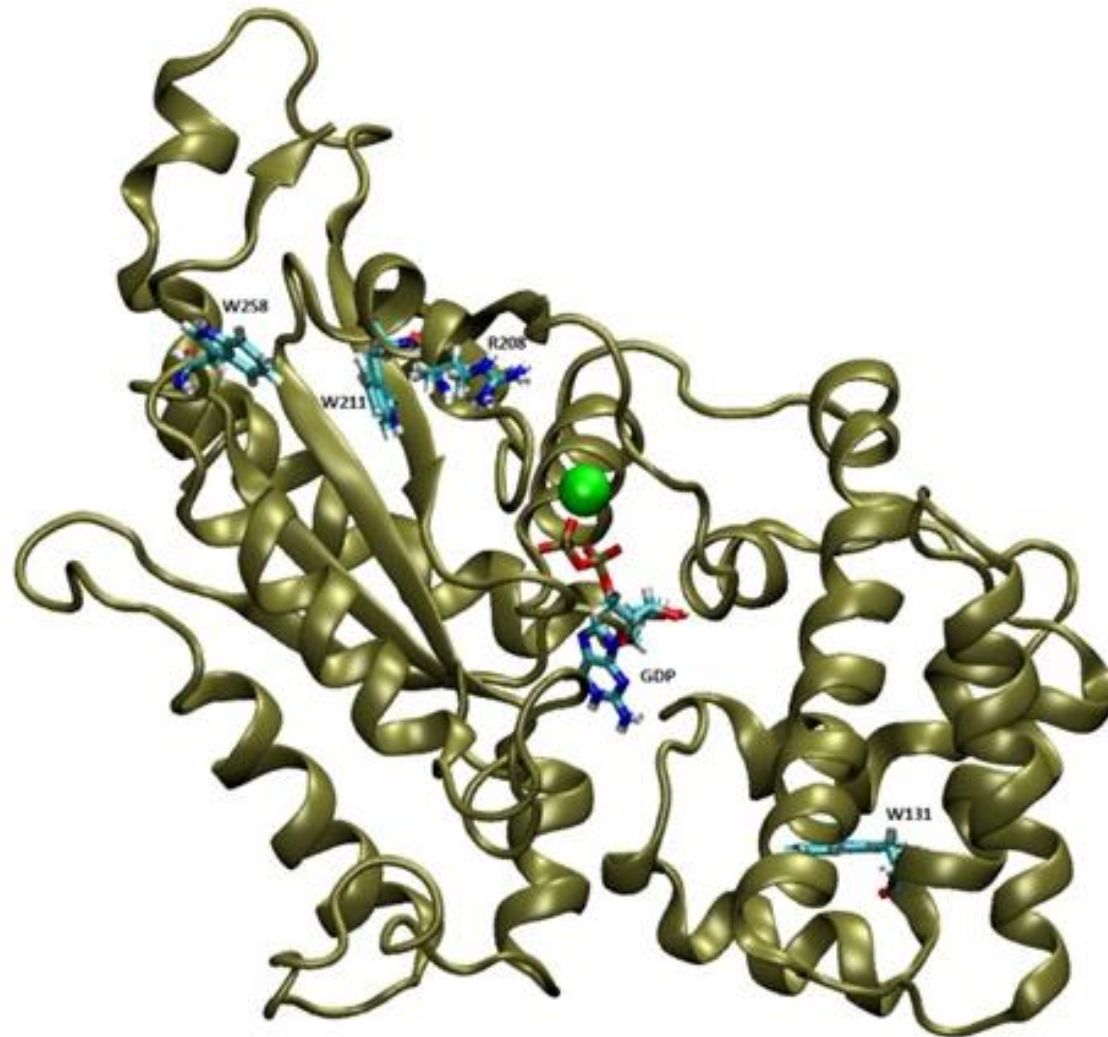
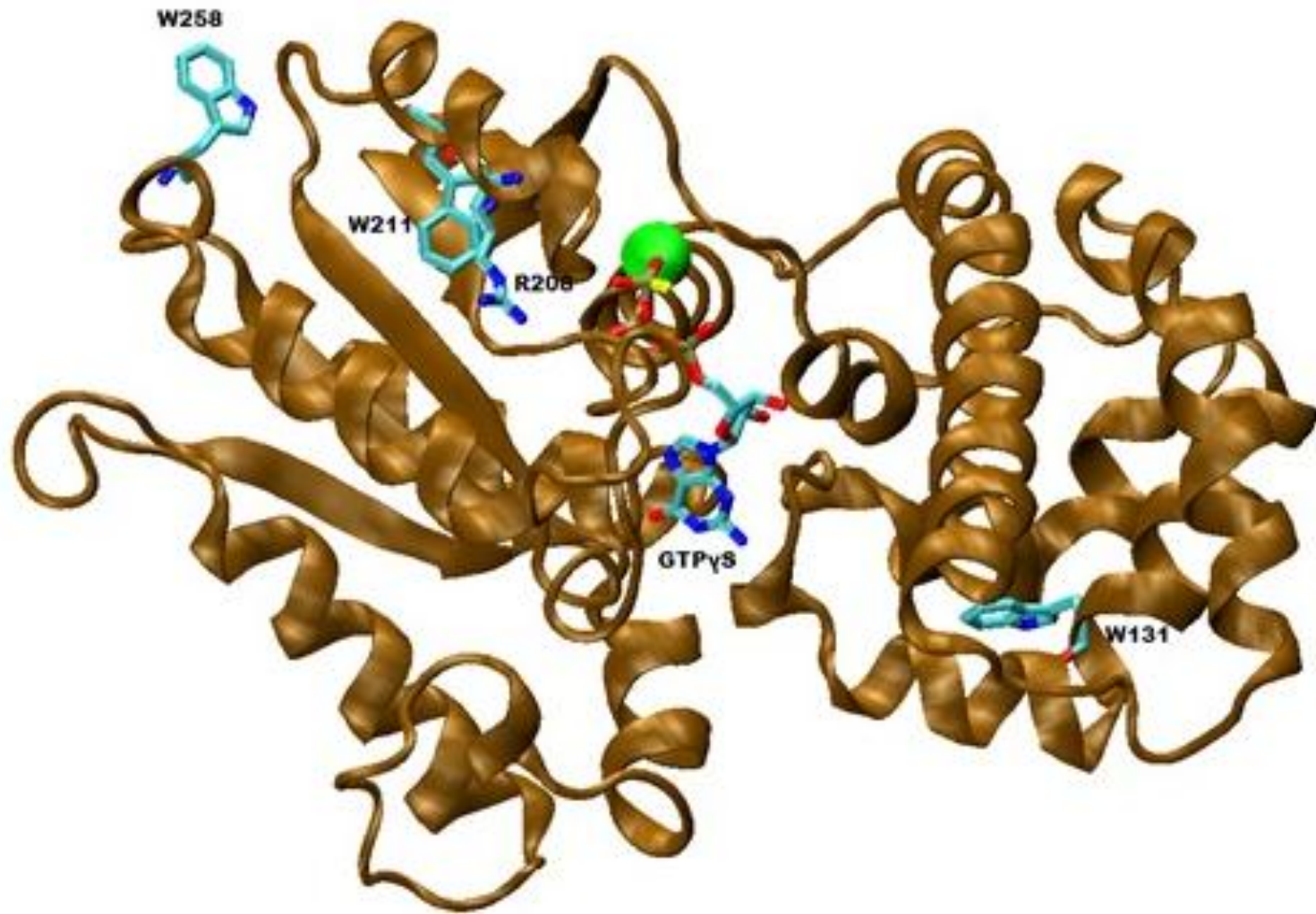


Figure 12. WT $G_{\alpha 1}$ •GTP γ S depicting the same residues at Fig. 12 except the bound nucleotide is GTP γ S



microenvironments of the three tryptophan residues in $G_{i\alpha 1}$ (W211 located in the conformational-dependent switch II region, and W131 and W258 that are located in the alpha helical and GTPase domains, respectively). The mutants obtained (W131F, W211F, and W258F) were then used to explore the environment of each tryptophan residue and its contribution to the overall protein stability. For $G_{i\alpha 1}$, the increase in fluorescence intensity upon activation depended primarily on the presence of W211, as demonstrated by a decrease in fluorescence in the W211F mutant (Najor et al., unpublished observations). Because tyrosine residues are abundant on the surface of G_{α} subunits, UV – Vis spectroscopy allowed us to monitor protein folding at the exterior of the protein. CD helped explore the unfolding of G_{α} through changes that occurred in the secondary structure.

The focus of this study was therefore to obtain a global understanding of the folding of G_{α} subunits by using complimentary spectroscopic approaches.

Materials and Methods

Expression and Protein Purification

$G_{\alpha i 1}$ and $G_{s\alpha}$ were obtained and purified as described previously (41). W131F, W211F, and W258F mutants were prepared by site directed mutagenesis using a kit provided by Stratagene (La Jolla, CA). Proteins were dialyzed overnight at 4 °C in 20 mM Tris pH 8.0 buffer containing 10% (v/v) glycerol, and 1 mM DTT and then stored at -80 °C. Protein purity was greater than 95% as estimated by SDS – PAGE. After purification on a Ni^{2+} column, activated G_{α} protein was prepared by adding stoichiometric concentrations of $GTP\gamma S$ to $G_{i\alpha 1}\bullet GDP$. Further purification on a size exclusion column was performed to separate free $GTP\gamma S$ from G_{α} bound $GTP\gamma S$.

Fluorescence Measurements

Experiments were performed with a PTI QuantaMaster fluorimeter (Photon Technologies, Inc., Mirroringham, NJ). Time-based assays were conducted with excitation and emission wavelengths set at 280 nm and 340 nm, respectively. Assays were initiated after 60 sec by addition of either AlF_4^- as a premixed solution (10 μM AlCl_3 and 10 mM NaF) or 20 μM GTP γ S to pre-incubated 500 $G_{\alpha 1}$ nM protein samples in buffer containing 10 mM HEPES, pH 7.5, 1 mM DTT and 2 mM MgSO_4 . Activation was monitored in the temperature range 4 °C \rightarrow 60 °C in samples that were incubated for 5 min at each temperature studied before addition of AlF_4^- and GTP γ S. Time-based assays were normalized to zero at 60 and 65 sec for AlF_4^- and GTP γ S activation, respectively. Upon addition of the GTP γ S nucleotide, there was a dramatic decrease in fluorescence intensity for an estimated 5 sec due to nucleotide induced quenching (48). Therefore, normalization at 65 sec indicates the time point at which GTP γ S exchanges with GDP.

Emission data was recorded over the wavelength range of 300 - 400 nm with the excitation wavelength set at 280 nm. Signal integration time was 0.2 sec with the bandpass for excitation and emission set at 5 nm. Sample preparation was the same as for time - based assays. The denaturation experiments started at a temperature of 4 °C followed by 4 °C increments and concluding at the highest temperature before aggregation occurred. There was a 2 min equilibration for each set temperature.

Tyrosine Assay

Environment of tyrosine residues in $G_{\alpha 1}$ proteins were monitored on a Hewlett Packard UV – Vis spectrophotometer. All samples contained 50 mM Tris, pH 7.5, 1

mM DTT, and 2 mM MgSO₄. Prior to initiating the experiment, samples in the transition state conformation (AMF) were incubated with 2.5 μM G_{α1}•GDP, 20 μM AlCl₃ and 10 mM NaF at room temperature for 20 min, whereas samples in the active conformation (GTPγS) were incubated with 2.5 μM G_{α1}•GTPγS and 20 μM GTPγS at room temperature for 1 hr minimum. Temperature was varied from 20 °C to 80°C, and was increased with 1 °C increments. For each temperature studied, the samples were equilibrated for 1 min and the absorbance was monitored over the wavelength range of 220 – 300 nm.

Determination of Secondary Structure

Experiments were performed using an Olis DSM 20 circular dichroism spectrophotometer. All samples were measured in a cylindrical quartz cuvette with a 1 mm pathlength, and contained either 3 μM G_{α1}•GDP or GTPγS, in 10 mM phosphate pH 7.5 buffer, 1 mM DTT, and 2 mM MgSO₄. A mixture of 50 μM AlCl₃ and 10 mM NaF was added to G_{α1}•GDP samples to form the AMF conformation, whereas an additional 20 μM GTPγS was added to G_{α1}•GTPγS samples to ensure saturation of the active conformation. Data was collected every 1 nm in the wavelength range of 190 – 260 nm. Time acquisition was determined as a function of high voltage. Temperature was varied from 20 °C to 100 °C with an incubation time of 3 min at each temperature studied. The OlisGlobalworks software was used to deconvolute the spectra and calculate percent of secondary structure and melting temperature.

Refolding of G_α Subunits

To test whether refolding of G_α proteins was reversible, fluorescence emission scans and CD were used. When results from the final temperature of an unfolding

experiment were obtained, the G_{α} sample was cooled down in 8 °C increments and incubation times remained the same as indicated above for each respective technique. Final temperatures varied depending on aggregation and ability to refold. All renaturation experiments were stopped at 4 °C and 20 °C for fluorescence and CD experiments, respectively.

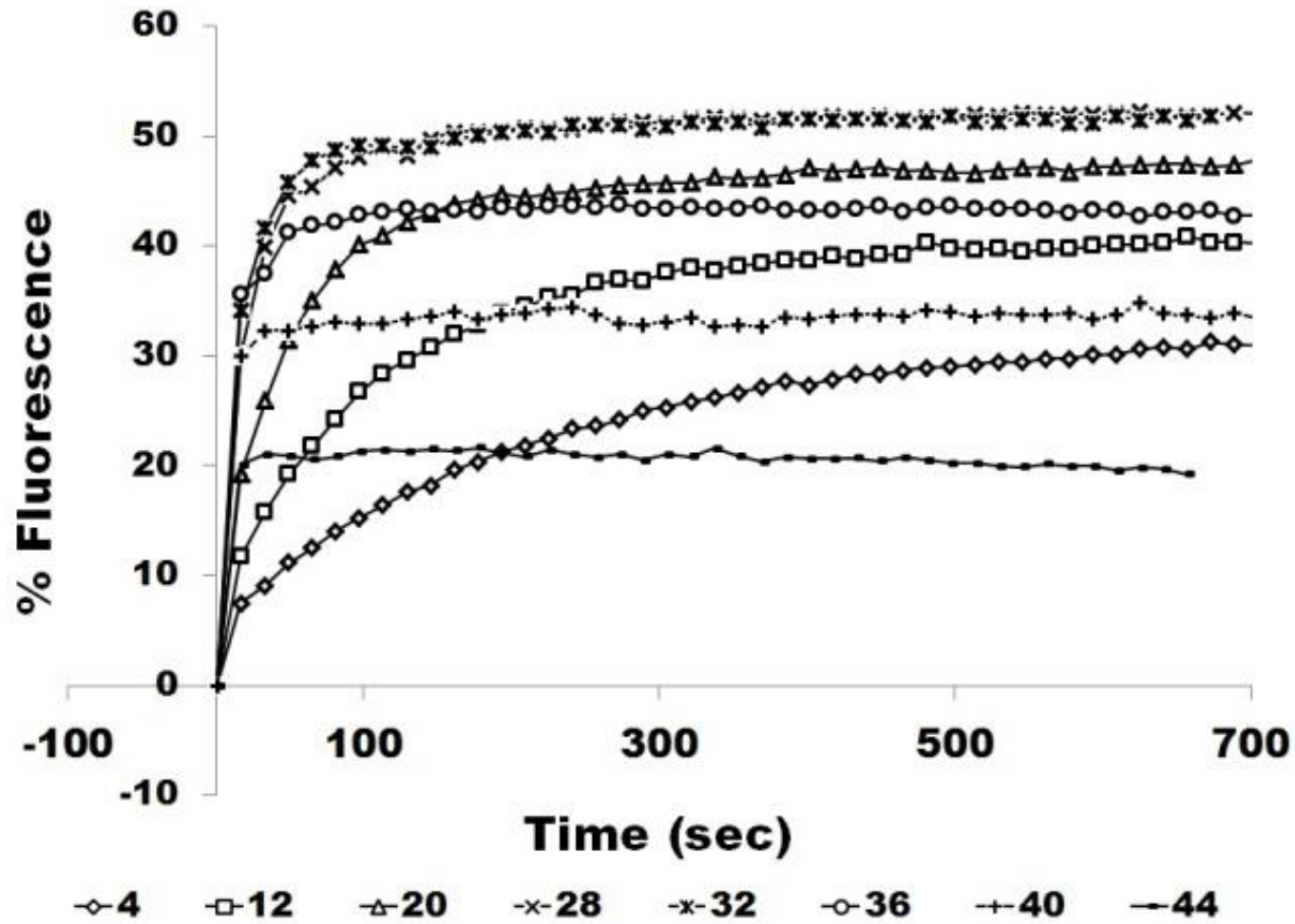
Results

AMF and GTP γ S Activation of $G_{i\alpha 1}$

Intrinsic tryptophan fluorescence is a useful technique to probe the folding of proteins. Upon the binding of AlF_4^- or exchange of GTP γ S, the G protein becomes activated and its tryptophan residues fold into more hydrophobic environments (38). We studied the ability of WT $G_{i\alpha 1}$ and its W mutants to activate as a function of temperature.

Addition of AlF_4^- to WT $G_{i\alpha 1} \cdot GDP \cdot Mg^{2+}$ causes an exponential increase in fluorescence followed by a plateau (F_{max}) (Fig. 13). We performed activation assays as a function of temperature (in the 4 °C \rightarrow 52 °C range). As the temperature was increased from 4 °C to 28 °C, there was an incremental increase in the rate and F_{max} . Temperatures above 28 °C resulted in lower F_{max} values and continued increased rates, with activation ceasing at 52 °C (data not shown). Activation that occurred after 44 °C saw a linear decay immediately after reaching its F_{max} ; the same trends were observed for AlF_4^- activation in the Trp mutants (data not shown). W211F activity could not be monitored

Figure 13. Temperature dependence of AlF_4^- activation of WT $\text{G}_{\alpha 1} \cdot \text{GDP} \cdot \text{Mg}^{2+}$



because of the absence of a change in fluorescence when going from the GDP to the AMF conformation (see chapter 2 of dissertation). The same approach was used for the exchange of GTP γ S with WT $G_{i\alpha 1}$ •GDP and its Trp mutants. It resulted in the same fluorescence trends observed earlier with the binding of AlF_4^- , but with dramatically slower rates (Fig. 14). There were a few key differences. Maximal fluorescence was achieved at a higher temperature of 40 °C as opposed to 32 °C obtained in AMF activation, and there was an absence of exchange at 60 °C vs. 52°C (data not shown).

Fluorescence Emission Spectra of G_α Proteins

The time - based assays provided useful information into the temperature dependence of the activation of $G_{i\alpha 1}$, but were not helpful in determining the folding pathway of $G_{i\alpha 1}$. However, as shown below, fluorescence emission spectra of G_α provided insight into its folding through changes in the environment of all tryptophan residues present in WT $G_{s\alpha}$, WT $G_{i\alpha 1}$ and the $G_{i\alpha 1}$ W mutants.

A decrease in intensities of the emission spectrum of WT $G_{i\alpha 1}$ •GDP is observed with an increase in temperature (Fig. 15). This pattern continues until a change in fluorescence vanishes at 96 °C. A transition midpoint of 39.0 °C was calculated for WT $G_{i\alpha 1}$ •GDP; similar T_m 's were observed for the GDP conformation of tryptophan $G_{i\alpha 1}$ mutants and of WT $G_{s\alpha}$ (Table 6). The T_m 's calculated from fluorescence emission spectra for WT $G_{i\alpha 1}$ •AMF and its tryptophan mutants, and for WT $G_{s\alpha}$ •AMF were also similar to those of their respective GDP conformations. With the exception of W211F and WT $G_{s\alpha}$, the T_m 's for WT $G_{i\alpha 1}$ and its Trp mutants in the GTP γ S conformation were ~ 18 °C higher than their respective GDP and AMF conformations.

Figure 14. Temperature dependence of GTP γ S Activation of WT $G_{i\alpha 1}\cdot\text{GDP}\cdot\text{Mg}^{2+}$

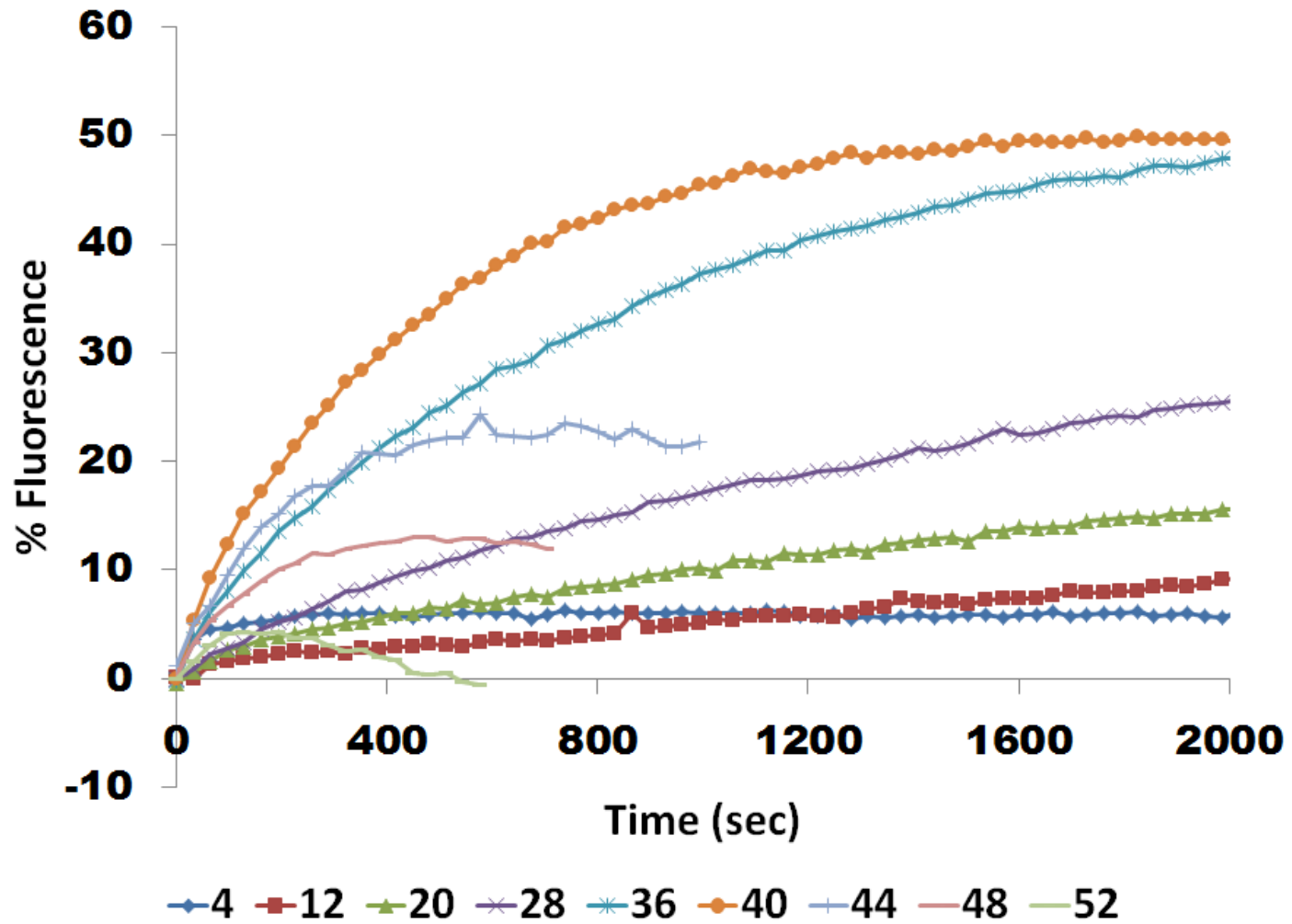


Figure 15. Fluorescence emission spectra of WT $G_{i\alpha 1} \cdot \text{GDP} \cdot \text{Mg}^{2+}$ as a function of temperature

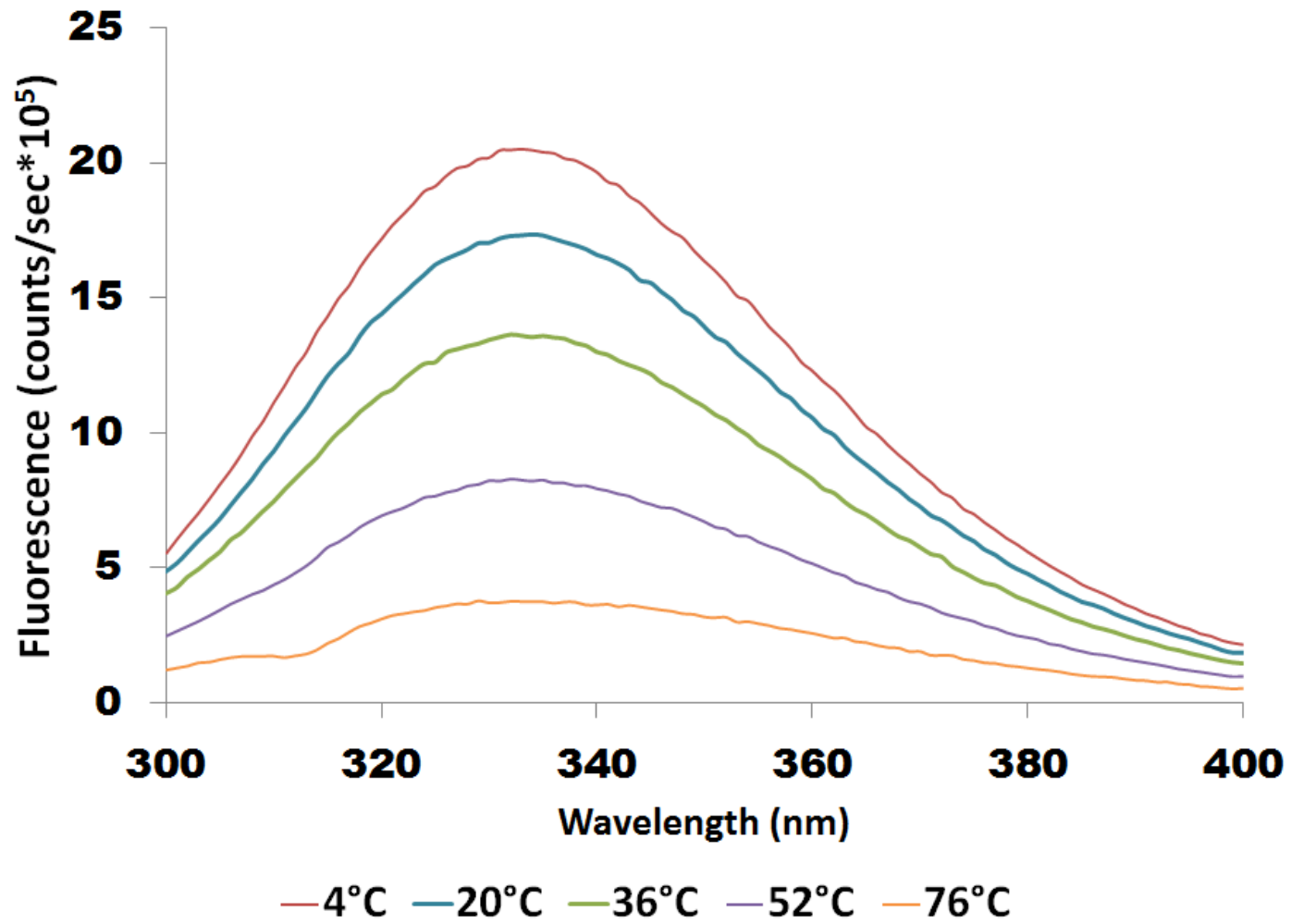


Table 6. T_m 's Estimated for all G_α Proteins Using Three Spectroscopic Methods.^{1,2}

Melting Temperatures of G_α Proteins									
	CD			UV-Vis			Fluorescence		
	GDP	AMF	GTPγS	GDP	AMF	GTPγS	GDP	AMF	GTPγS
WT $G_{i\alpha 1}$	44.2	47.5	70.9	47.6	48.6	66.5	39.0	38.3	48.7
W131F	44.0	48.8	70.7	49.9	51.9	53.9	38.1	37.9	51.7
W211F	54.3	57.0	56.5	46.8	47.4	52.3	35.3	34.1	37.2
W258F	50.2	51.9	68.1	45.8	56.1	63.1	41.6	37.8	59.2
WT $G_{s\alpha}$	42.7	56.0	56.0	³	³	³	39.6	37.6	37.6

¹S.E.M \leq 3

²All values reported in °C

³Not measured

We also investigated the ability of G_{α} subunits to refold after completion of the denaturation process. A decrease in temperature was accompanied by an increase in the fluorescence intensity of the emission spectra indicating that the tryptophan residues were re-folding back into hydrophobic environments (Fig. 16). Refolding WT $G_{i\alpha 1} \bullet \text{GDP}$ from 96 °C back to 4 °C exhibited no significant increase in fluorescence. However, upon renaturation from 48 °C, the observed increase in the fluorescence intensity indicates a refolding recovery of 21% (Fig. 17). When refolding from 32 °C, which is a temperature below its T_m , WT $G_{i\alpha 1} \bullet \text{GDP}$ exhibited the largest recovery of 72%. Unlike WT $G_{i\alpha 1} \bullet \text{GDP}$, the AMF and $\text{GTP}\gamma\text{S}$ conformations experience increases in fluorescence intensity when refolding from 96 °C. Comparison of denaturation data observed for $\text{GTP}\gamma\text{S}$ at 70 °C and 44 °C indicates more refolding than for the AMF conformation (see bars at 48 °C and 32 °C in Fig. 17). WT $G_{s\alpha} \bullet \text{AMF}$ refolded 17% of its structure after denaturation from 76 °C, whereas WT $G_{s\alpha} \bullet \text{GTP}\gamma\text{S}$ reported the most recovery by regaining 30% of its fluorescence after unfolding to 84 °C (data not shown).

Tyrosine Assays

Trp residues become buried upon activation with either AMF or $\text{GTP}\gamma\text{S}$, and thus they probe the interior of $G_{i\alpha 1}$. However, Tyr residues in $G_{i\alpha 1}$ are located at its outer surface, and therefore can be used to monitor temperature – induced changes at the exterior of $G_{i\alpha 1}$. There are 13 tyrosine (Y) residues in the amino acid sequence of $G_{i\alpha 1}$ which are located throughout the surface of both the GTPase and alpha – helical domains (Fig. 18). Tyrosine absorbs at a wavelength of 280 nm and is most commonly used to calculate protein concentration. As the temperature was increased, the changes in the

Figure 16. Refolding of WT $G_{i\alpha 1}$ •GTP γ S.
Temperatures are in ($^{\circ}$ C) and R represents refolded $G_{i\alpha 1}$

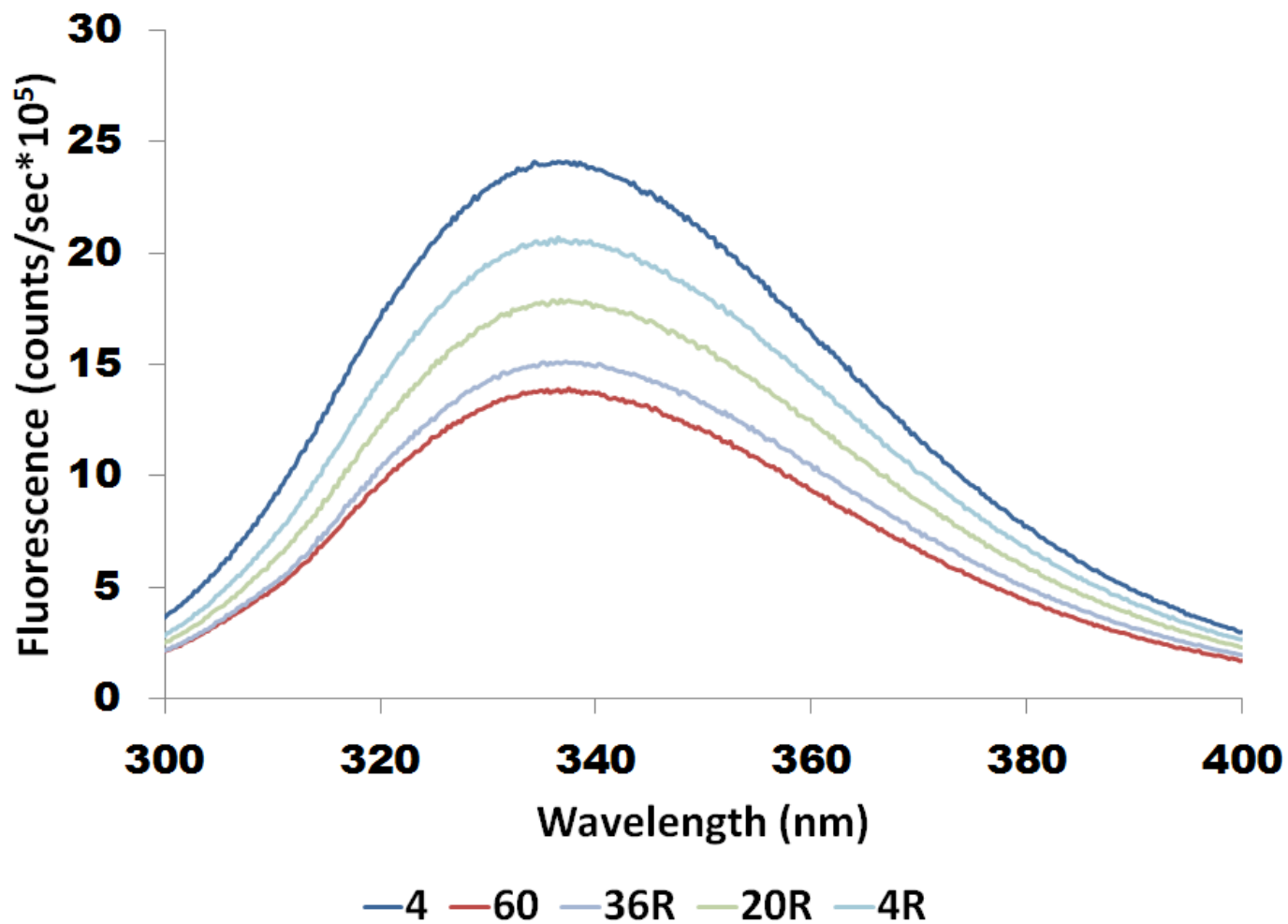


Figure 17. Refolding of WT $G_{i\alpha 1}$ in all three conformations as monitored by fluorescence. Temperatures denote the end of denaturation and beginning of renaturation process

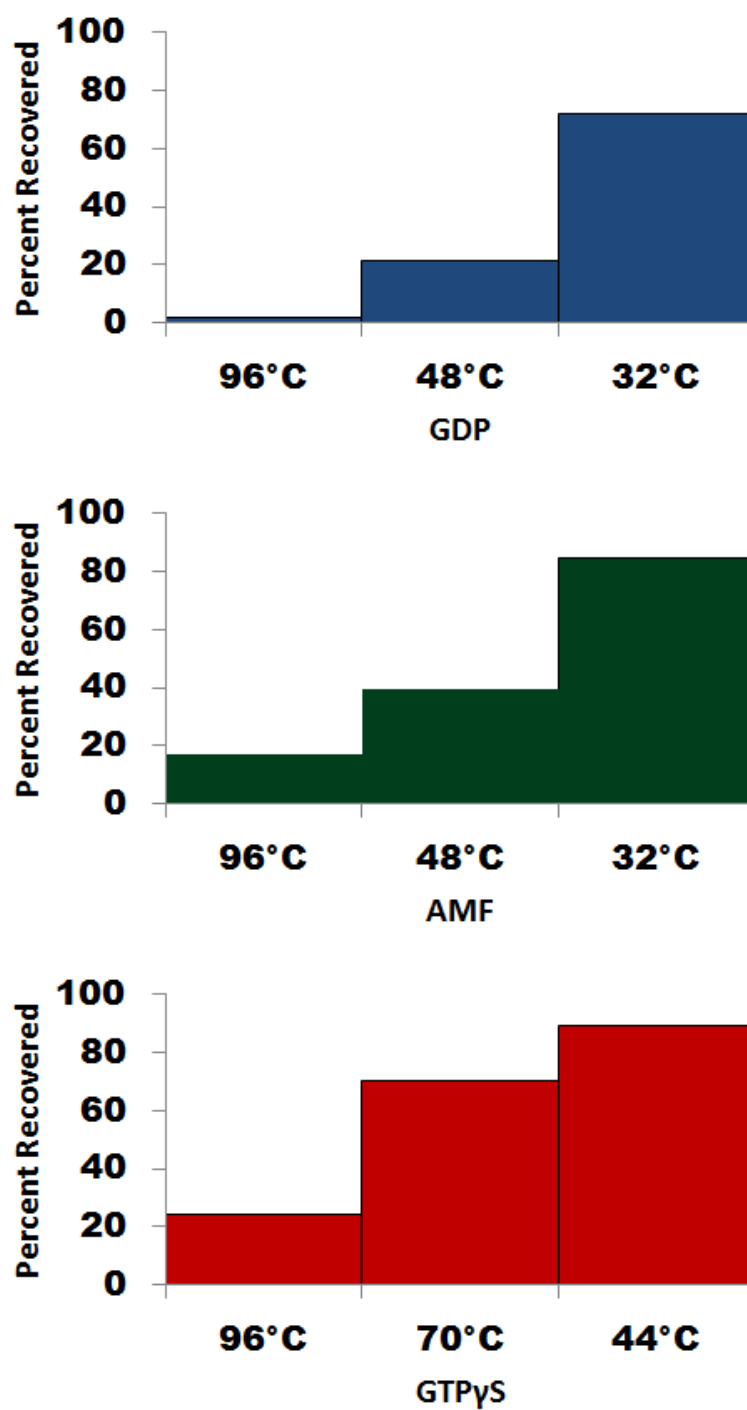
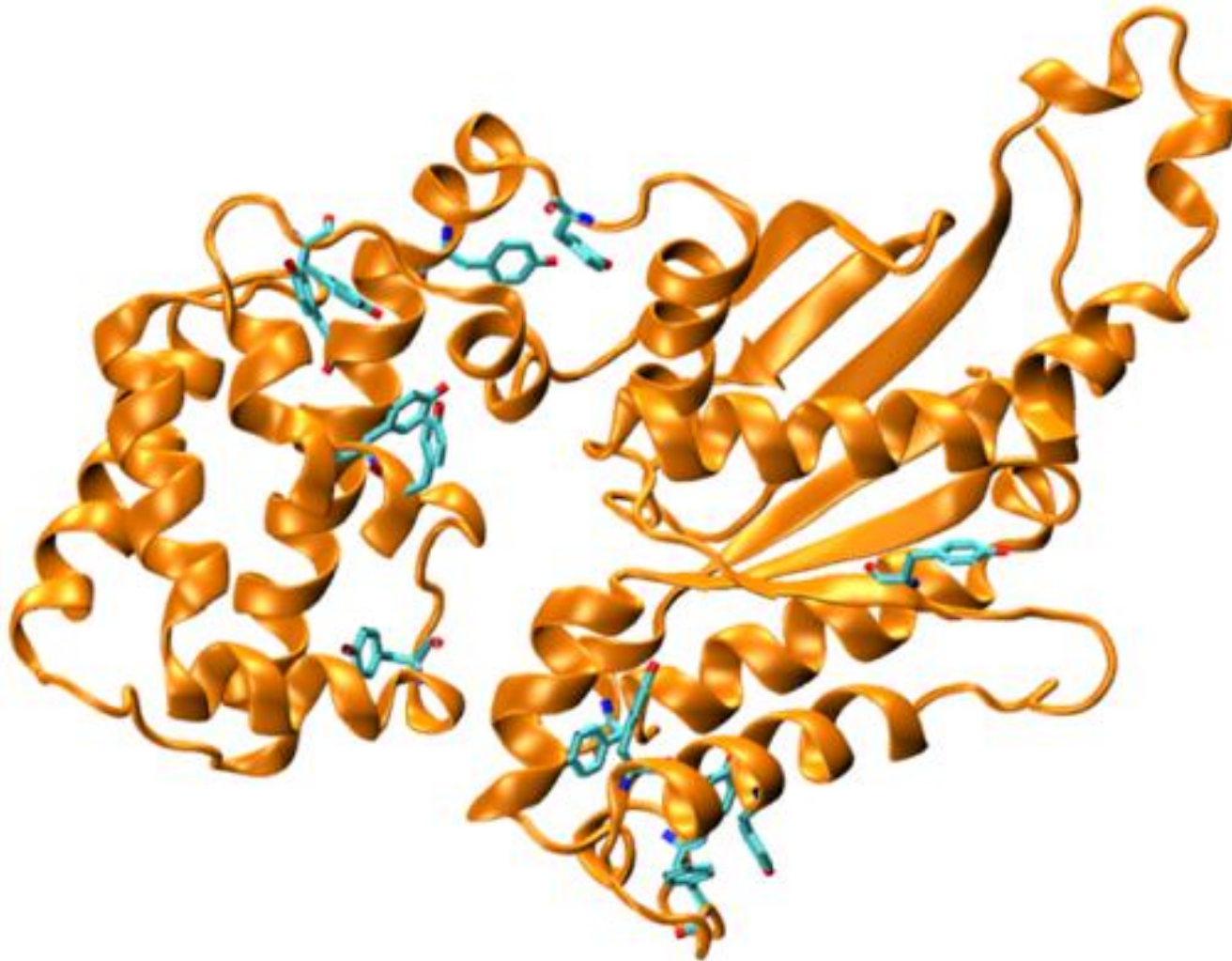


Figure 18. WT $G_{i\alpha 1}$ •GDP depicting its 13 Tyr residues



absorption spectrum of WT $G_{i\alpha 1}\bullet\text{GDP}$ were monitored; no changes in its absorption spectrum occurred from 20 °C \rightarrow 43 °C, but an increase in absorbance was observed at temperatures above 44 °C. As the protein was subjected to increasing amounts of heat, its Tyr residues became more solvent exposed causing the absorption at 280 nm to increase. The melting curves for $G_{i\alpha 1}$ in the GDP and AMF states overlapped, but the GTP γ S curve was shifted to the right indicating increased stability for this active conformation. The same trends were observed for W mutants of $G_{i\alpha 1}$ in all conformations (Fig. 19). The calculated T_m values from tyrosine assays are listed in Table 6.

Temperature-Dependence of Secondary Structure $G_{i\alpha 1}$

The crystal structure of WT $G_{i\alpha 1}\bullet\text{GDP}$ (1BOF) reports the secondary structure composition as being 47% α – helices and 12% β – sheets (13). Tanaka and co – workers (49) used CD to investigate the secondary structure of $G_{i\alpha 1}\bullet\text{GDP}$ in solution and found that its alpha helical content was consistent with the X – ray structure; using two algorithms, CCA and SELCON, respectively, they estimated it to consist of 50.6% and 55.9% α - helices with. The near UV wavelength range of the CD spectrum of $G_{i\alpha}$ proteins was used to investigate the unfolding of $G_{i\alpha}$ secondary structure as a function of temperature. A maximum at 190 nm, and minima at 205 nm and 222 nm are signatures of α – helical predominant structures, but a comparatively lower maximum at 192 nm and a minimum at 215 nm are distinctive features of β – sheets. Spectra of WT $G_{i\alpha 1}\bullet\text{GDP}$ at a temperature of 20 °C (Fig. 20) resembled that of an α – helical dominated structure with a 39.7 % α – helix composition, which is less than the reported PDB value (Table 7). The CD spectra remained unchanged in the 20 °C to 32 °C range. As the temperature

Figure 19. Unfolding of WT $G_{\alpha 1}$ as monitored through Tyr movement

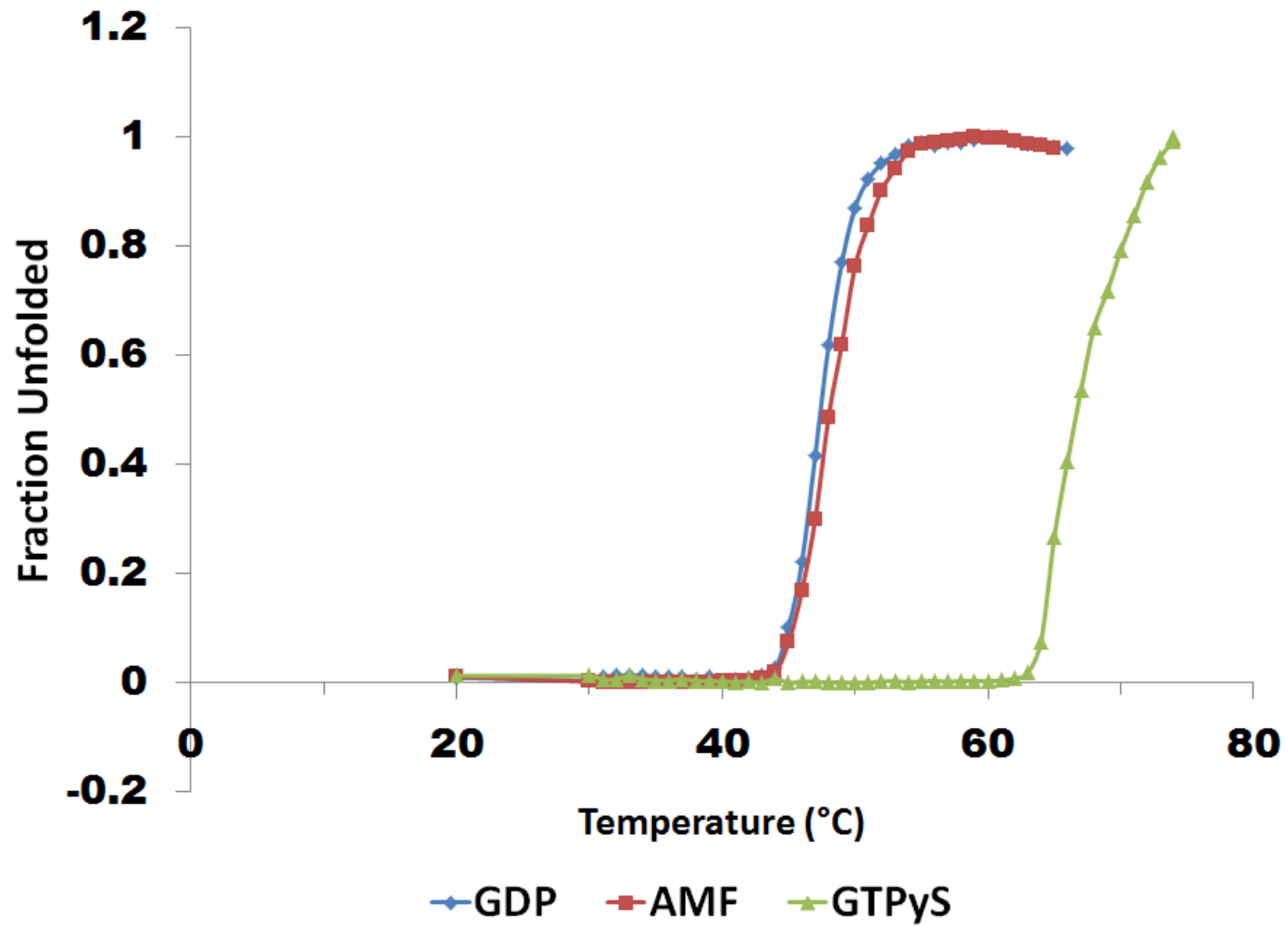


Figure 20. Unfolding of WT $G_{i\alpha 1} \cdot GDP \cdot Mg^{2+}$ secondary structure.
Temperature units are ($^{\circ}C$)

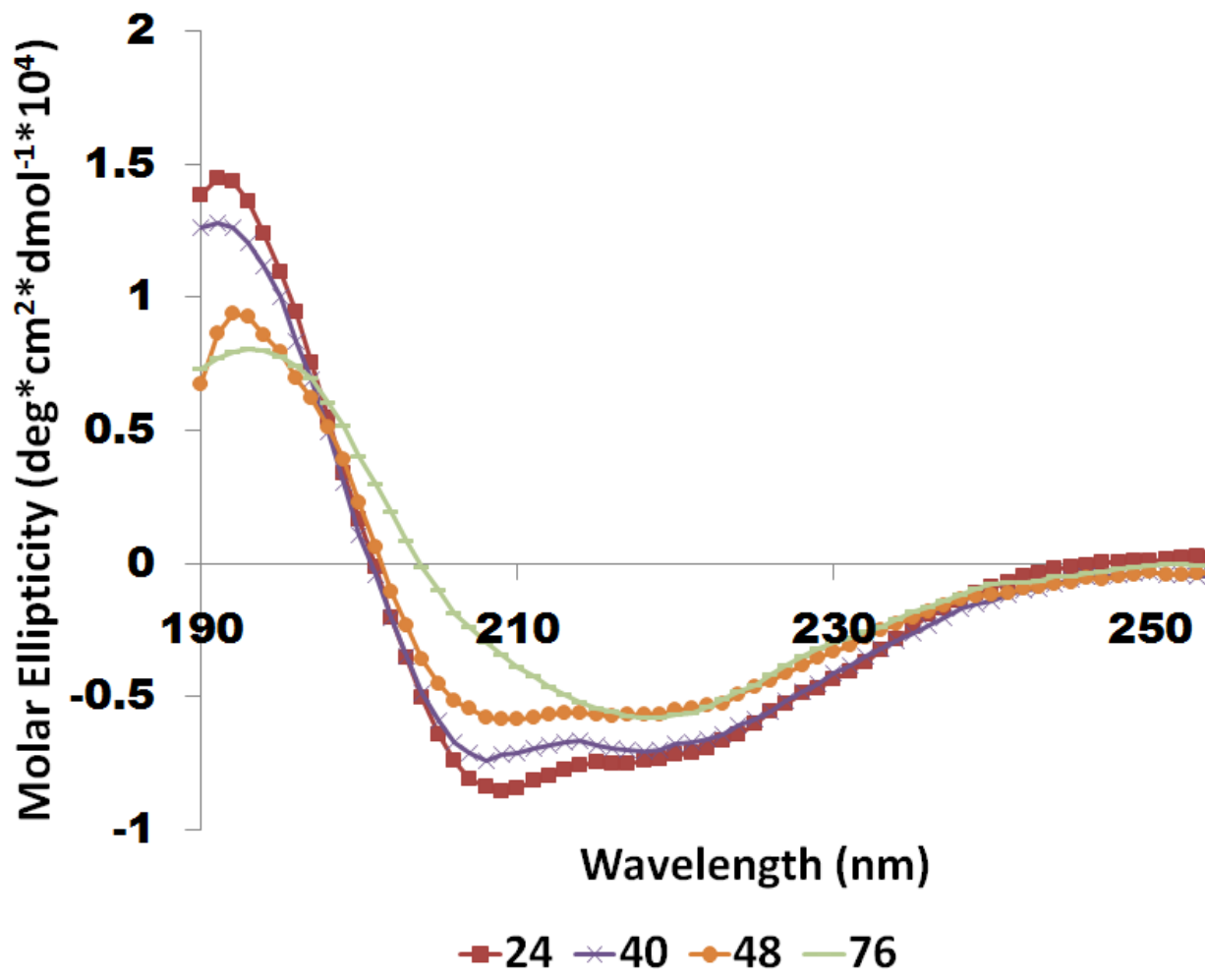


Table 7. Composition of WT $G_{i\alpha 1}$ Secondary Structure at Various Temperatures.^{1,2,3}

Secondary Structure Breakdown of WT $G_{i\alpha 1}$ Unfolding												
T (°C)	GDP				AMF				GTP γ S			
	α	β	RC ⁴	T ⁴	α	β	RC ⁴	T ⁴	α	β	RC ⁴	T ⁴
20	41.3	14.7	26.3	18.0	41.5	14.3	19.3	16.8	44.3	12.3	25.7	17.7
40	40.3	14.7	26.7	18.3	42.0	14.3	24.5	18.0	42.3	13.7	24.0	20.3
52	27.7	21.3	29.0	21.7	28.3	22.0	26.0	20.5	41.7	13.3	24.7	20.3
64	23.3	28.0	28.7	21.0	22.8	26.8	28.6	22.0	38.7	16.0	24.3	20.7
80	19.7	29.3	28.7	23.0	19.0	28.8	32.2	23.8	23.0	25.7	26.0	23.7
92³	-	-	-	-	-	-	-	-	21.5	29.0	25.5	24.5

¹S.E.M ≤ 3

²All numbers reported as percentages

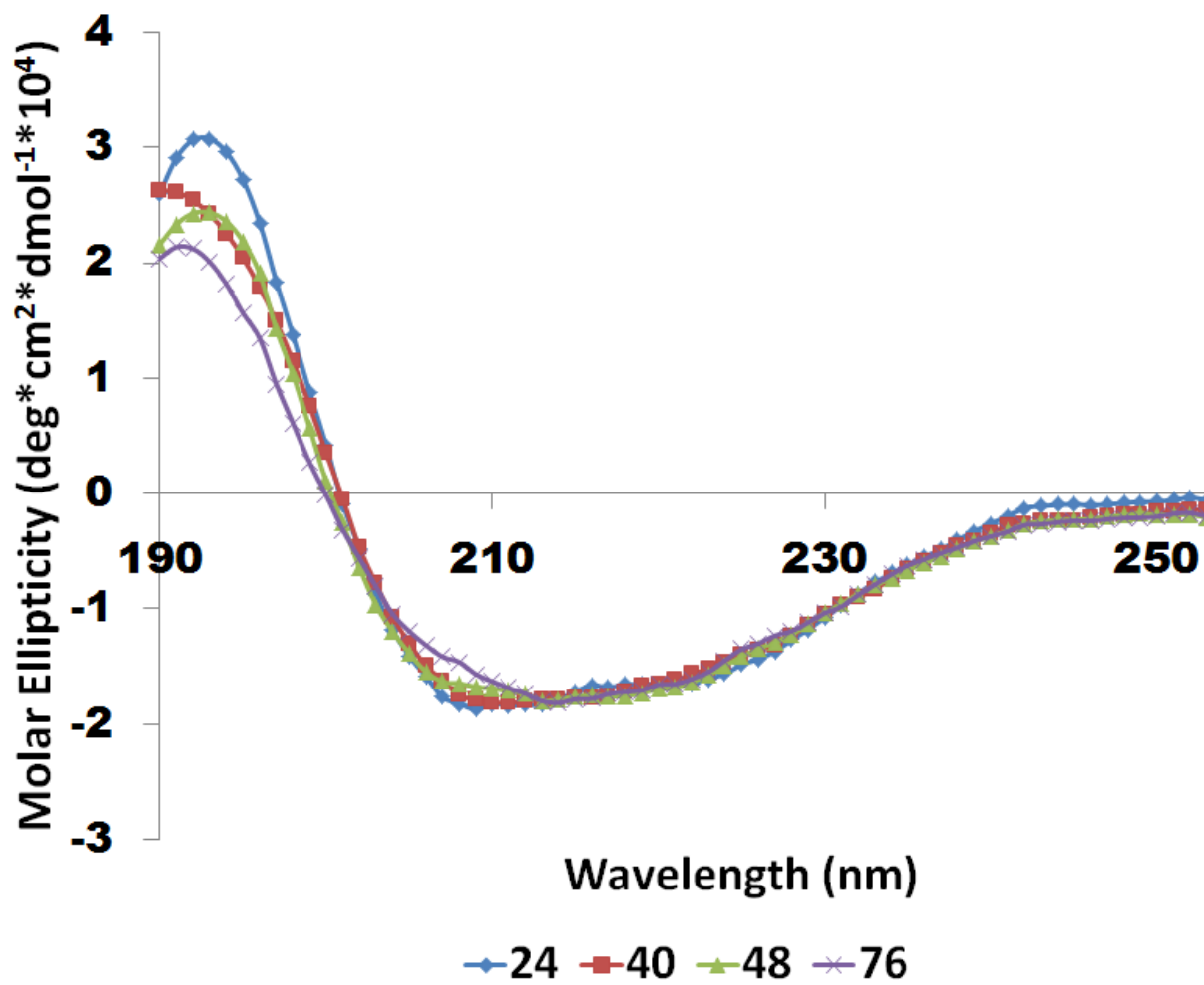
³Hyphens denote temperatures at which proteins were denatured

⁴RC and T stand for random coil and turns

increased from 36 °C → 64 °C, the CD spectra showed the most dramatic changes in secondary structure. Absorption at 190 nm decreased, while the minima at 205 nm and 222 nm increased until they converged into a new minimum at 215 nm. The once mainly α – helical protein became increasingly dominated by β – sheet (Table 7). Temperatures after 64 °C displayed little change in the spectra and the protein eventually precipitated out at 84 °C. A T_m of 44.2 °C was calculated for WT $G_{i\alpha 1}$ •GDP. The W•GDP mutants of $G_{i\alpha 1}$ observed the same spectral trends with W211F affording the highest transition midpoint (Table 6). A transition midpoint of 42.7 °C was calculated for WT $G_{s\alpha}$ •GDP. The spectra of WT $G_{s\alpha}$ •GDP displayed a similar unfolding pattern as observed with WT $G_{i\alpha 1}$ •GDP, however, the increases in the absorption at 205 nm and 222 nm as $G_{s\alpha}$ was denatured were less apparent (Fig. 21).

WT $G_{s\alpha}$, WT $G_{i\alpha 1}$ and all the W mutants observed the same trends in their AMF conformation as their GDP counterparts with higher transition midpoints calculated from the CD spectra (Table 6). Lastly, the GTP γ S conformation was explored for WT $G_{s\alpha}$, WT $G_{i\alpha 1}$ and its W mutants. Except for a few important differences, the same pattern was observed in the spectra of G_α protein solutions in the GTP γ S conformation. The $G_{i\alpha 1}$ samples were able to reach temperatures of 100 °C without aggregation and the transition midpoints were significantly higher than both the GDP and AMF conformations. At 80 °C, the secondary structure consisted of at least 4.0 % more α – helix than its GDP and AMF conformations. In contrast, WT $G_{s\alpha}$ and W211F in the GTP γ S active state displayed T_m 's closest to their AMF conformations (Table 6).

Figure 21. Unfolding of WT $G_{sd} \cdot GDP \cdot Mg^{2+}$ secondary structure.
Temperature units are ($^{\circ}C$)

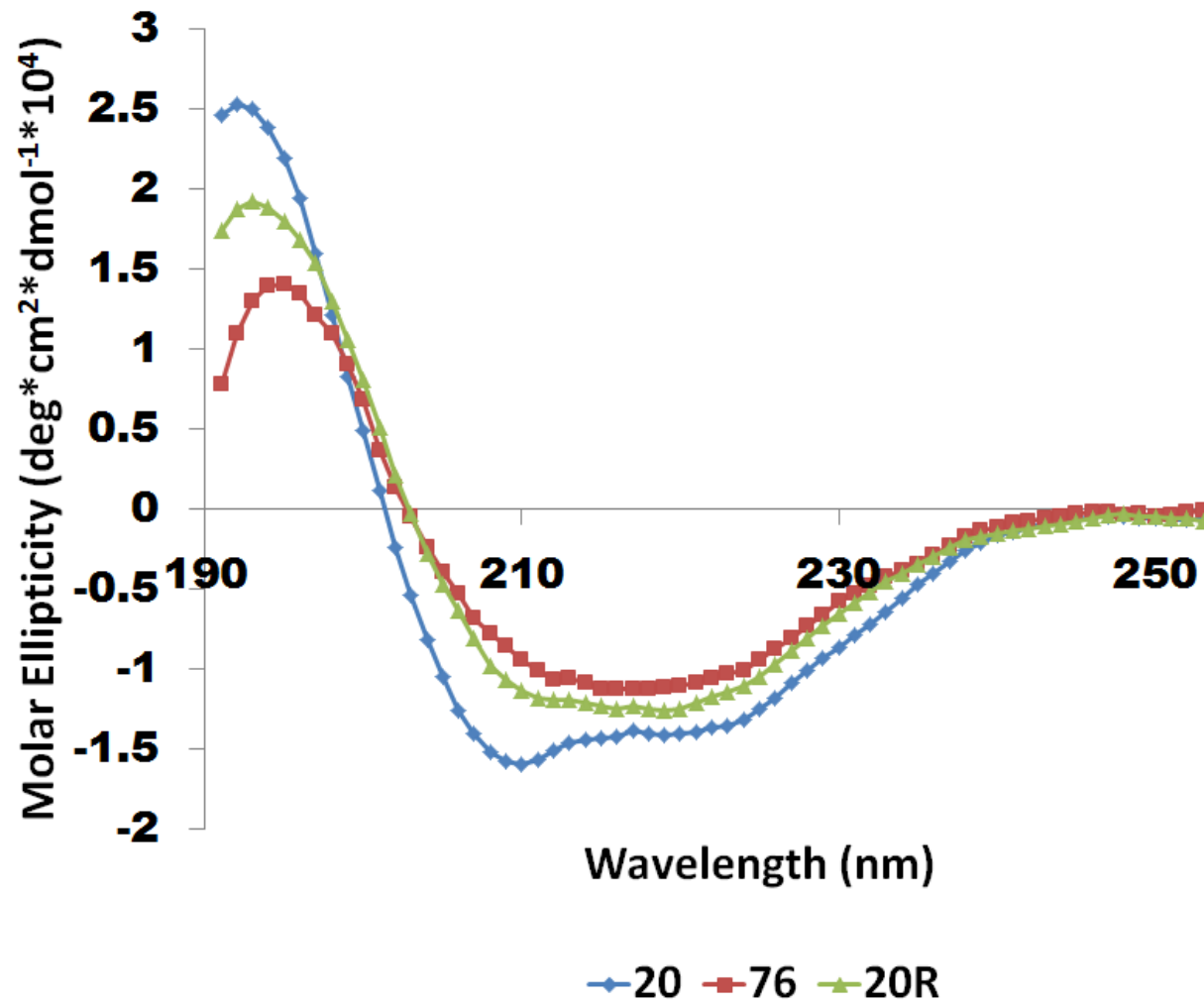


Reversibility commenced at the end of the denaturation process. As WT $G_{i\alpha 1}$ •GDP was refolded from 76 °C to 4°C there was a subsequent increase at 190 nm and a decrease at 222 nm in the CD spectra (Fig. 22). At 76 °C, $G_{i\alpha 1}$ consisted primarily of 28% β – sheets and 23% α - helices. Refolding to 20 °C increased the alpha helical content to 28% and the percent of β – sheets decreased to 21%. Stopping the denaturation process at 52 °C rather than 76 °C resulted in recovery of more α – helical structure (35%), while the β – sheet composition remained the same. At 80 °C, WT $G_{s\alpha}$ •GDP exhibited a similar denaturation pattern that was comprised of 26% β – sheets and 24% α – helices. Upon renaturation at 20 °C, the alpha helical composition increased to 29% and β – sheets decreased to 22%. The refolding of the active GTP γ S conformation was also investigated for $G_{s\alpha}$. Incubation to 80 °C resulted in predominantly β – sheet (25%) secondary structure and 19% α – helices. When refolded back to 20 °C, $G_{s\alpha}$ was able to regain 11% of its alpha helical content and its β – sheets decreased by 1%.

Discussion

Activation of WT $G_{i\alpha 1}$ with AMF and GTP γ S observed some very distinct qualities that can be attributed to its functionality. When comparing their respective rates, GTP γ S activation resulted in much slower rates than in AMF activation (Fig. 13 vs. Fig. 14). $G_{i\alpha 1}$ must first release its bound GDP before GTP γ S can bind; the release of GDP is the rate determining step (23). In contrast, AlF_4^- can immediately bind to the β phosphate of the already bound GDP (48). Thus, the difference in rates can be attributed to a two-step vs. one step process for GTP γ S and AMF activation, respectively.

Figure 22. Denaturation and refolding of WT $G_{i\alpha 1} \bullet GDP$.
Temperatures are in ($^{\circ}C$) and R represents refolded $G_{i\alpha 1}$ at $20^{\circ}C$



GTP γ S activation resulted in an F_{\max} value at 40 °C as opposed to 32 °C with the addition of AlF_4^- . It is suggested that the heat capacity of the protein in the AlF_4^- conformation is lower than in the GTP γ S form. This difference would explain why GTP γ S can still bind and induce protein folding at temperatures above 50 °C where AlF_4^- loses its ability to bind and undergo activation. In order to gain further knowledge on the folding of $G_{i\alpha 1}$ independent of the state of activation, the emission spectra of each conformation was investigated at various temperatures.

Comparison of the $G_{i\alpha 1}$ crystal structures in the GDP, AMF and GTP γ S conformations reveals that the GDP – bound structure is less compact than that of the active conformations of AMF and GTP γ S (12, 13). The crystal structure of $G_{s\alpha}\bullet\text{GTP}\gamma\text{S}$ (1AZT, (31)) displays comparable folding as observed in $G_{i\alpha 1}\bullet\text{GTP}\gamma\text{S}$. One would predict the additional folding present in AMF and GTP γ S, compared to the GDP form, would result in higher T_m 's for activated $G_{i\alpha 1}$, because the tryptophan residues are buried in hydrophobic pockets that require more heat to induce unfolding. The $G_{i\alpha 1}$ crystal structures of AMF and GTP γ S are nearly identical, thus one would expect the T_m 's to be comparable, but this was not observed for both G_{α} subunits. The GTP γ S form was significantly more stable than both the GDP and AMF conformations as indicated by a comparison of their transition midpoints (Table 6). We suggest that at a temperature near the T_m of the GDP, AlF_4^- is released from the β - phosphate of GDP and assumes the conformation of the inactive state and continues unfolding via a pathway analogous to the GDP form. The release of AlF_4^- would explain the similar transition midpoints for $G_{i\alpha 1}\bullet\text{GDP}$ and $G_{i\alpha 1}\bullet\text{AMF}$. ^{19}F NMR would provide a useful technique to detect whether the AlF_4^- becomes unbound, thus rendering the protein inactive in its GDP conformation. In

conclusion, we propose that the difference in T_m values for the active conformations may be due to a lower heat capacity of AlF_4^- vs. $GTP\gamma S$. The increased rates and maximum fluorescence observed in the time-based assays of $G_{i\alpha 1}$ for both active conformations can be accounted for by a kinetic effect taking place. As the protein absorbs heat, it can bind AlF_4^- or release GDP faster depending on the mechanism of activation.

Since structures of $G_{s\alpha}\bullet GDP$ or AMF have not been solved, it is not possible to know whether $G_{s\alpha}$ follows the same folding pattern as for $G_{i\alpha 1}$. The fact that the T_m 's for all conformations, including the $GTP\gamma S$, are not significantly different suggest that protein folding around the Trp residues in $G_{s\alpha}$ and $G_{i\alpha 1}$ is distinct. W211F• $GTP\gamma S$ mutant was the least stable of all the $G_{i\alpha 1}$ proteins and displayed similar transition midpoints in all conformations. This is contrary to what was found in the other $G_{i\alpha 1}$ proteins that showed higher melting temperatures for the $GTP\gamma S$ conformation. Previous work by Najor et al (unpublished work) and Hamm and coworkers (25) show that W211 forms an electrostatic interaction with R208 in WT $G_{i\alpha 1}\bullet AMF$ and $GTP\gamma S$. It is suggested that this bridge is playing a crucial role in the structural stability of $G_{i\alpha 1}$. The electrostatic interaction presumably acts as an anchor stabilizing the protein from unfolding.

The tyrosine absorbance assays allowed for the visualization the global unfolding of $G_{i\alpha 1}$ from another prospective. There are thirteen Tyr residues contained in $G_{i\alpha 1}$ and many of them are located at its surface. Therefore the calculated T_m 's from the tyrosine absorbance spectra probe how the overall protein unfolds as compared to glean information about the local environments of tryptophan residues from the emission spectra. The results were consistent with what was observed in the fluorescence emission denaturation experiments. With the exception of the W258F mutant, the AMF

conformation of all G_{α} proteins had similar T_m 's to those observed the GDP form, while the GTP γ S conformation was the most stable of all $G_{i\alpha 1}$ proteins (Table 6). However, the transition midpoints calculated for $G_{i\alpha 1}$ in all conformations observed in the tyrosine assay were consistently higher than the T_m 's calculated with the emission spectra. This difference may be explained through the hydrophobic interactions in $G_{i\alpha 1}$, which is a fundamental determinant of folding in all proteins. Since non-covalent interactions are the driving force in protein folding, the observed T_m values would suggest that the denaturation of $G_{i\alpha 1}$ would initiate in the vicinity of tryptophan residues and then propagate to the entire protein, including the tyrosine residues.

The secondary structure of WT $G_{i\alpha 1}$ and WT $G_{s\alpha}$ were the most stable in their GTP γ S form followed by their AMF and GDP conformations. When comparing all conformations at 20 °C, there was an increase in the α – helical content of $G_{i\alpha 1}$ upon activation with AlF_4^- or exchange with GTP γ S, but, for $G_{s\alpha}$, only the latter was true. Activation of G_{α} subunits creates a hydrophobic pocket from the folding of the switch regions into more ordered secondary structure (2), thus explaining the increased α -helices and decrease of random coil in secondary structure (Table 8). As $G_{i\alpha 1}$ proteins unfolded in their GDP and AMF conformations, precipitation at temperatures above 84 °C was observed. In contrast, $G_{s\alpha}$ exhibited aggregation in all conformations at temperatures above 80°C. At this point in the unfolding process, the G_{α} subunits were rich in β – sheet composition and their random coil was fairly unchanged from the native

Table 8. Composition of WT G_{sα} Secondary Structure at Various Temperatures.

Secondary Structure Breakdown of WT G_{sα} Unfolding												
	GDP¹²				AMF¹²				GTPγS¹²			
T (°C)	α	β	RC³	T³	α	β	RC³	T³	α	β	RC³	T³
20	34.8	17.2	31.9	12.5	33.9	18.1	31.6	12.5	36.2	16.4	31.6	12.5
40	28.8	20.5	33.2	12.5	31.1	19.9	32.7	12.5	32.2	19.2	32.8	12.5
52	27.6	22.6	33	12.5	21.4	27.2	34.4	12.5	30.3	19.1	33.5	12.5
64	26.8	23.9	33.2	12.5	21.1	27.7	34.6	12.5	24.9	23.3	34.6	12.5
80	23.8	25.8	33.7	12.5	7.2	36.4	37.6	12.5	18.6	25.1	36.2	12.5

¹S.E.M ≤ 3

²All numbers reported as percentages

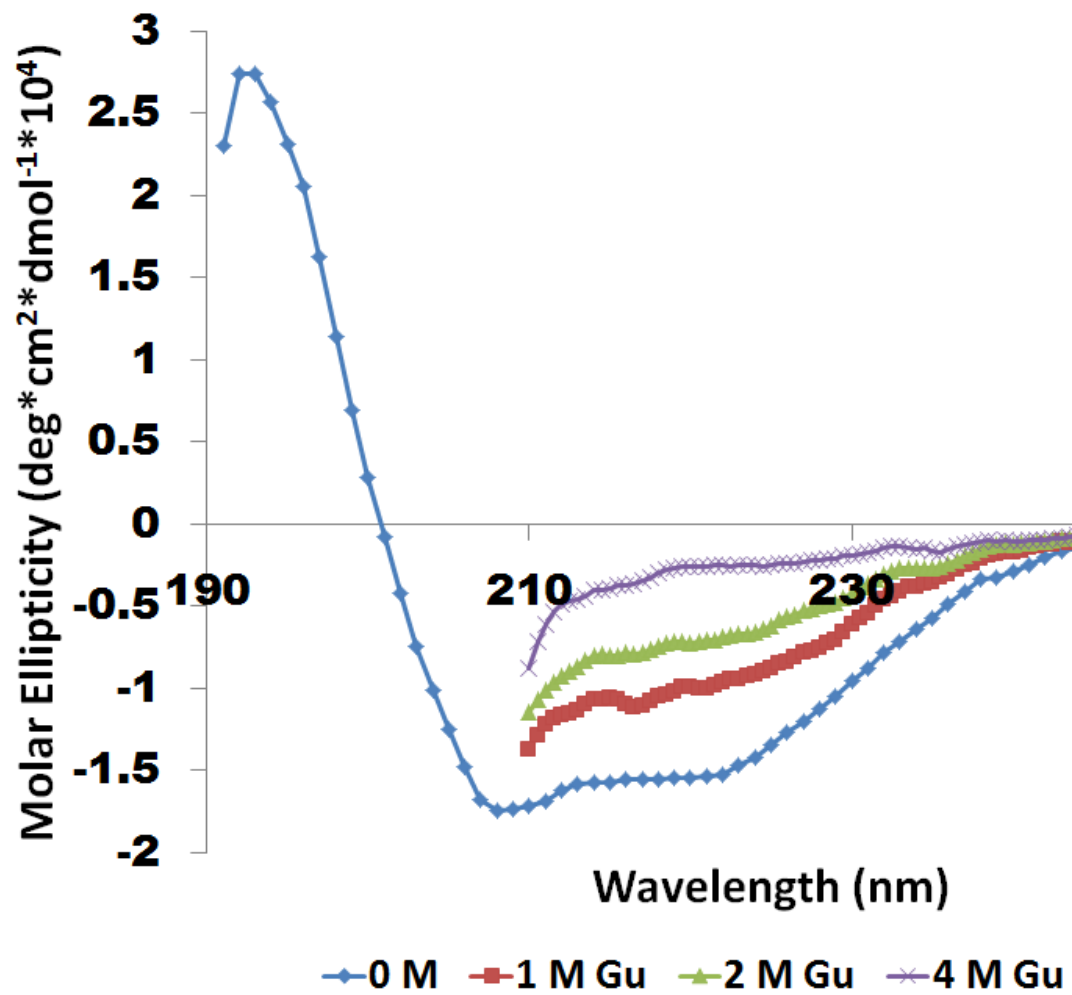
³RC and T stand for random coil and turns

form. Denaturation generally occurs when a protein is devoid of the quaternary, tertiary, and secondary structure commonly found in its native state, but this did not occur with $G_{i\alpha 1}$ or $G_{s\alpha}$. Instead, the secondary structure morphed from one high in α – helices to one rich in β – sheet at which time it proceeded to precipitate before reaching complete random coil. Addition of a detergent such as guanidinium HCl (GuHCl) was able to further unfold WT $G_{i\alpha 1}$ •GDP (Fig. 23), as demonstrated by an α – helical composition of 4% in the presence of 4 M GuHCl. At 20 °C, as expected, its random coil composition increased to 34%. However, β – sheets still represented 38% of the secondary structure.

$G_{s\alpha}$ •AMF displayed a significantly higher melting temperature, in contrast, to WT $G_{i\alpha 1}$ •AMF (Table 1). The crystal structure of $G_{s\alpha}$ •GTP γ S (31) depicts two electrostatic interactions between W231 and R234 in the GTPase domain, and W154 and R160 in the helical domain compared to one salt bridge between W211 and R208 in WT $G_{i\alpha 1}$ •GTP γ S (17). We suggest that the additional electrostatic interaction present between W154 and R160 increased the stability of $G_{s\alpha}$ •AMF compared to the other G_{α} proteins.

The stability of a protein is fundamental to its biological function, because its resistance to misfolding is greater and less likely to develop disease. Therefore, investigation into the reversibility of WT $G_{i\alpha 1}$ and WT $G_{s\alpha}$ can give insight into the probability of misfolding of G_{α} subunits. Regardless of conformation, CD spectra demonstrated that the unfolding process of G_{α} proteins was reversible when it was stopped at lower temperatures. In addition, when renaturation was initiated at temperatures below the transition midpoint of G_{α} •GDP, AMF and GTP γ S, there was a substantially higher recovery of secondary structure (Fig. 17). The ability of G_{α} subunits

Figure 23. Unfolding of WT $G_{\alpha 1}$ •GDP in the presence of guanidinium HCl



to refold is dependent on its conformation. Unlike their GDP and AMF counterparts, G_{α} •GTP γ S proteins were able to refold the most denatured protein after incubation at temperatures higher than their T_m 's (Figs. 16 and 17). Although this is true for both G_{α} proteins, $G_{i\alpha 1}$ was able to refold the most structure compared to $G_{s\alpha}$. This was indicated by the fluorescence emission spectra that displayed a 76% recovery of $G_{i\alpha 1}$ •GTP γ S after denaturation to 96 °C, whereas $G_{s\alpha}$ •GTP γ S was only able to refold 30% after denaturation to 84 °C. In addition, the $G_{s\alpha}$ •GDP exhibited precipitation at temperatures below 80 °C during renaturation.

The calculated T_m 's varied depending on the spectroscopic technique used. During the course of denaturation a protein may develop multiple intermediate conformations known as molten globule states. Common characteristics include a radius of gyration 10 – 30% larger than the native structure, a loosely packed hydrophobic core with non-polar side chains more exposed to solvent, and lack of tertiary structure, but well intact secondary structure consisting of α – helices and β – sheets (50). Overall, denaturation of G_{α} subunits showed the lowest transition midpoints with fluorescence, followed by UV – Vis and CD. It is suggested that the ranking of T_m 's can be explained through the molten globule model. The emission spectra monitored the polarity changes in the environment of the Trp residues. Oscillations centered around the non-polar side chains of tryptophan would generate low energy molten globules that would account for the lower T_m values observed by fluorescence. There is a plethora of tyrosine residues located throughout $G_{i\alpha 1}$ and only after the disruption of the non-covalent interactions, would there be molten globules lacking tertiary structure. Once the protein starts to

unfold, molten globules will morph into proteins that have less secondary structure, which explains the higher T_m 's.

$G_{i\alpha 1}$ and $G_{s\alpha}$ regulate the synthesis of the secondary messenger cyclic AMP, through their interactions with the effector adenylyl cyclase (AC). The crystal structure of a $G_{s\alpha}$ •AC complex indicates eleven points of contact between the two proteins located at $G_{s\alpha}$ residues N239, Q236, R232, R231, T284, R283, L282, W281, R280, N279, and L272 (18, 31). A $G_{i\alpha 1}$ and AC complex has not been crystallized; however, potential binding residues in $G_{i\alpha 1}$ identified through alanine scanning mutagenesis are R208, K209, I212, K312, R313, K314, K315, T316, and E318 (31). Unfolding of $G_{s\alpha}$ and $G_{i\alpha 1}$ resulted in an increased composition of β – sheets (Tables 7 and 8). Presumably, mutations at G_{α} •AC binding sites would result in a percent increase in β – sheet structure in G_{α} subunits, comparable to what was observed in the thermal denaturation of G_{α} proteins. If indeed the secondary structure at the points of contact between G_{α} subunits and AC were to change, signal transduction may be disrupted, which in turn may lead to disease. Future studies would include mutations at these residues and investigation of the temperature – dependence of the secondary structure conducted with CD.

G_{α} proteins are associated with many cancers, due in large part from hot spot mutations in the amino acid sequence of $G_{i\alpha 1}$ and $G_{s\alpha}$. Mutations at R231 in $G_{s\alpha}$ is associated with cancerous tumors in the brain and R208 in $G_{i\alpha 1}$ is related to adenocarcinomas in the large intestine. Both respective Arg residues are also involved with the binding of AC to the respective G_{α} subunit and there is a suggested relationship between the two. Presumably, mutations at R208 and R231 change the structure of G_{α} which in turn loses its ability to bind AC and may lead to the development of tumors.

The unfolding of $G_{i\alpha 1}$ and $G_{s\alpha}$ as a function of temperature lead to larger amounts of β – sheet formation. Thus, investigation of the secondary structure of the R208 mutant of $G_{i\alpha 1}$ and of the R231 mutant of $G_{s\alpha}$, is necessary to determine if there is indeed a connection between the binding of AC effector to the G_{α} subunits and cancer. The observed aggregation of $G_{s\alpha}$ and $G_{i\alpha 1}$ as it unfolds is indicative of protein misfolding, which resembles the formation of β – amyloid fibrils in Alzheimer’s disease. Proteins rich in β – sheets, such as amyloid, have been known to aggregate and cause Parkinson’s, Alzheimer’s, and Prion disease (51). In conclusion, misfolding of G_{α} subunits may lead to disruption in signal transduction cascades and ultimately lead to disease. Further investigation into the interaction of G_{α} subunits with intracellular effectors may lead to the discovery of chemo therapeutic agents.

CHAPTER FOUR

Mg²⁺ DEPENDENCE OF THE FOLDING OF G_α SUBUNITS

Introduction

G – Protein activation occurs once a hormone, chemokine, or neurotransmitter binds to an extracellular receptor and triggers the protein to release its GDP bound nucleotide and bind GTP. Upon exchange a conformational change occurs, where the α – subunit concomitantly binds GTP and dissociates from the βγ subunits. The now activated G – protein binds to an intracellular effector, such as adenylyl cyclase and affect the production of cyclic AMP from ATP. This activation process is dependent on the presence of Mg²⁺.

The crystal structures of G_α subunits in different conformations reveal critical information about the binding and functional roles of Mg²⁺. WT G_{iα1}•GDP has been crystallized in the presence and absence of Mg²⁺ (13). With the exception of Mg²⁺ bound and hexacoordinated at the active site, the apo and holo crystal structures are essentially identical (13, 17). Mg²⁺ exhibits octahedral geometry in WT G_{iα1}•GDP•Mg²⁺. The four equatorial ligands of Mg²⁺ are the sidechain hydroxyl groups of threonine (T181), located in the switch I region, and serine (S47), oxygen of the β – phosphate in GDP, and a water molecule (13). The axial ligands are two water molecules. The GDP conformation has the distinction of two unordered switch regions, switch II and switch III. Activation with GTPγS causes a conformational change that leads to rearrangement of ligands

coordinated by the Mg^{2+} ion. WT $G_{i\alpha 1} \cdot GTP\gamma S$ observes the same hexacoordinated ligands with the exception that the oxygen of the γ – phosphate at the equatorial position is replaced at the site previously occupied by the water. The active conformation observes ordering of switch II and III regions. Activation may also occur through binding of AlF_4^- to $G_{\alpha} \cdot GDP \cdot Mg^{2+}$ to form a transition state analog (AMF). AlF_4^- binds to the β – phosphate of GDP, and structurally mimics the GTP γ S conformation. However, AlF_4^- forms a square planar complex in contrast to the tetrahedral geometry observed in the γ – phosphate of GTP (12). Mg^{2+} displays similar octahedral coordination observed in WT $G_{i\alpha 1} \cdot GTP\gamma S$, except a ligand at the equatorial position is fluoride instead of the oxygen on the γ – phosphate.

Mg^{2+} is the second most common intracellular cation and the most abundant intracellular divalent cation (52). It plays a prominent role in biochemical and physiological processes, such as regulating cardiovascular function and ion channels, nucleic acid synthesis, and signal transduction. The transient receptor potential melastatin (TRPM) cation channel family has been identified as a Mg^{2+} transporter (52). TRPM7, which is found ubiquitously, has been reported to be a signaling kinase involved with vascular smooth cell growth, apoptosis, adhesion, contraction, and migration, processes that, if interrupted, can lead to hypertension and a multitude of vascular diseases. Epidemiological data along with clinical and experimental studies indicate an inverse relationship between blood pressure and dietary Mg^{2+} consumption (52). Magnesium induces vasodilation, improves blood flow, decreases vascular resistance, increases capacitance function of peripheral, coronary, renal, and cerebral arteries, attenuates agonist-induced vasoconstriction, and reduces blood pressure. In contrast, low

magnesium levels have opposite effects causing contraction, potentiation of agonist-evoked vasoconstriction, and increased vascular tone and blood pressure (52). Low Mg^{2+} levels have been implicated in other illnesses ranging from minor to severe, such as migraine headaches, traumatic brain injuries, multiple sclerosis epilepsy, and Duchenne muscular dystrophy (53).

To investigate the effect of Mg^{2+} on the structure of $G_{i\alpha 1}$, we used fluorescence and circular dichroism (CD). Intrinsic tryptophan fluorescence is a technique that monitors activation through protein folding. Protein activation typically observes aromatic residues, such as tryptophan (W), moving into less solvent accessible pockets. As the Trp residues fold into a hydrophobic pocket there is an observed increase in fluorescence intensity and a blue shift (λ_{max} shifts to lower wavelengths) in the emission spectra (20). Gilman and co-workers (38) used fluorescence to investigate indirectly the activation of G-proteins. Addition of AlF_4^- or $GTP\gamma S$ to $G_\alpha \cdot GDP \cdot Mg^{2+}$ causes an increase in fluorescence and a subsequent red shift (λ_{max} shifts to higher wavelengths) in its emission spectra (24). Hamm and co-workers (25) reported the same shift for $G_{i\alpha 1}$ and were able to determine the cause for the observed shift. A conformational change occurs upon the activation of $G_{i\alpha 1}$ and there is concomitant movement of W211 and arginine (R208) that places the residues in close proximity to one another. This creates an electrostatic interaction that causes a shift in the λ_{max} to higher wavelengths in the emission spectra, rather than a traditional blue shift. We exploited this finding to investigate the dependence of Mg^{2+} on the reported red shift in AlF_4^- and $GTP\gamma S$ activation of $G_{i\alpha 1}$ and $G_{s\alpha}$. As reported (12, 13, 17), $G_{i\alpha 1}$ exhibits ordering of its switch I,

II, and III regions upon activation with AlF_4^- or $\text{GTP}\gamma\text{S}$. By using CD, we explored how Mg^{2+} impacted the secondary structure of G_α subunits.

Using both spectroscopic methods, we found that the structures of $\text{G}_{i\alpha 1}$ and $\text{G}_{s\alpha}$ proteins were indeed dependent on the amount of Mg^{2+} present. The CD data indicated that as Mg^{2+} concentration increased in active G_α subunits the α - helical content increased. This change in secondary structure may have implications for diseases associated with abnormalities in G_α proteins.

Materials and Methods

Expression and Protein Purification

$\text{G}_{i\alpha 1}$ and $\text{G}_{s\alpha}$ were obtained and purified as described previously (41). W131F, W211F, and W258F mutants were prepared by site directed mutagenesis using a kit provided by Stratagene (La Jolla, CA). Proteins were dialyzed overnight at 4 °C in 20 mM Tris pH 8.0 buffer containing 10% (v/v) glycerol, and 1 mM DTT and then stored at -80 °C. Protein purity was greater than 95% as estimated by SDS – PAGE.

Calculation of $[\text{Mg}^{2+}]_f$ in the Presence of EDTA

The concentration of free Mg^{2+} in the presence of EDTA was calculated based on the following equation:

$$[\text{Mg}^{2+}]_t = [\text{Mg}^{2+}]_f + K [\text{Mg}^{2+}]_f [\text{EDTA}] (1 + K [\text{Mg}^{2+}]_f)^{-1}$$

$[\text{Mg}^{2+}]_t$ is the total Mg^{2+} concentration added to the sample, $[\text{Mg}^{2+}]_f$ is the free Mg^{2+} concentration in the presence of EDTA, and K is the dissociation constant of the $\text{Mg}^{2+} \cdot \text{EDTA}$ complex, which is 1 μM at pH 7.4 (54).

Fluorescence Measurements

Experiments were performed using a PTI QuantaMaster fluorimeter (Photon Technologies, Inc., Mirningham, NJ). Time-based assays were conducted with excitation and emission wavelengths set at 280 and 340 nm, respectively. Assays were initiated after 60 sec by addition of either AlF_4^- as a premixed solution (20 μM AlCl_3 and 10 mM NaF) or 20 μM GTPyS to pre-incubated 500 G_α nM protein samples in buffer containing 50 mM Tris, pH 7.5, 1 mM DTT and various concentrations of $[\text{Mg}]_f$. Time-based assays were normalized to zero at 60 sec.

W211-R208 bridge formation was probed using emission spectra recorded over a wavelength range of 300 - 400 nm with an excitation wavelength set at 280 nm. Signal integration time was 0.2 sec with an incremental step of 0.5 nm. The bandpass for excitation and emission was 5 nm. The maximum fluorescence intensity in the emission spectra was normalized to 1.0. G_α samples were incubated for a minimum of 2 hrs at room temperature with all constituents before emission assays were conducted.

Determination of Secondary Structure

Experiments were performed using an Olis DSM 20 circular dichrometer. Data was collected every 1 nm, in the wavelength range of 260 - 180 nm. Time acquisition was determined by a function of high voltage. Samples were measured in their activated forms, either AMF (20 μM AlCl_3 and 10 mM NaF) or 20 μM GTPyS. All samples were measured in a cylindrical quartz cuvette with a 1 mm pathlength and contained 3 μM WT $G_{i\alpha 1}$ or $G_{s\alpha}$, 10 mM, pH 7.5 phosphate buffer, 1 mM DTT, and various concentrations of MgSO_4 . Collected data was converted to molar extinction units. Algorithm CONTINLL

43 in the OlisGlobalworks software was used to calculate percentage of secondary structure.

Results

Effect of Mg^{2+} on the Intrinsic Fluorescence of G_{α} subunits

Time-based assays were used to monitor the effect of Mg^{2+} on the folding pathway of G_{α} subunits. AMF activation of $G_{i\alpha 1} \bullet GDP$ containing 5 mM Mg^{2+} resulted in a fluorescence intensity of 40% which is comparable to reported literature values (25, 48, 55), but the addition of AlF_4^- to $G_{i\alpha 1} \bullet GDP$ in the absence of Mg^{2+} produced a fluorescence intensity of 5% (Fig. 24). Increasing the Mg^{2+} concentration to 250 nM or greater resulted in a larger F_{max} and faster rate (Fig. 24). The F_{max} remained unchanged at Mg^{2+} concentrations above 1 mM, but the rates continued to increase until 5 mM Mg^{2+} . Similar trends were observed for WT $G_{s\alpha} \bullet AMF$, however, concentrations above 2 mM afforded the largest fluorescence intensity as compared to 1 mM in WT $G_{i\alpha 1}$, and $G_{s\alpha}$ (Fig. 25).

GTP γ S exchange of $G_{i\alpha 1}$ and $G_{s\alpha}$ was also investigated. $G_{i\alpha 1} \bullet GTP\gamma S$ in the presence of 8 mM Mg^{2+} displayed an F_{max} of 56%, whereas, in the absence of Mg^{2+} , an F_{max} of 44% and a similar initial rate was observed (Fig. 26). Exchange of GTP γ S with WT $G_{s\alpha} \bullet GDP$, containing 8 mM Mg^{2+} , exhibited an F_{max} of 33% (Fig. 27). In contrast to apo $G_{i\alpha 1} \bullet GTP\gamma S$, $G_{s\alpha} \bullet GTP\gamma S$ displayed a significantly reduced fluorescence of 3% in the absence of Mg^{2+} (Fig. 27). Activation of $G_{s\alpha}$ with GTP γ S exhibited similar F_{max} trends in the presence of increasing Mg^{2+} concentrations as compared to its AMF equivalent. Both types of G_{α} subunits resulted in slower rates for GTP γ S binding compared to their AMF conformation (Figs. 24 and 25).

Figure 24. Mg^{2+} dependence of AlF_4^- activation of WT $G_{i\alpha 1}$

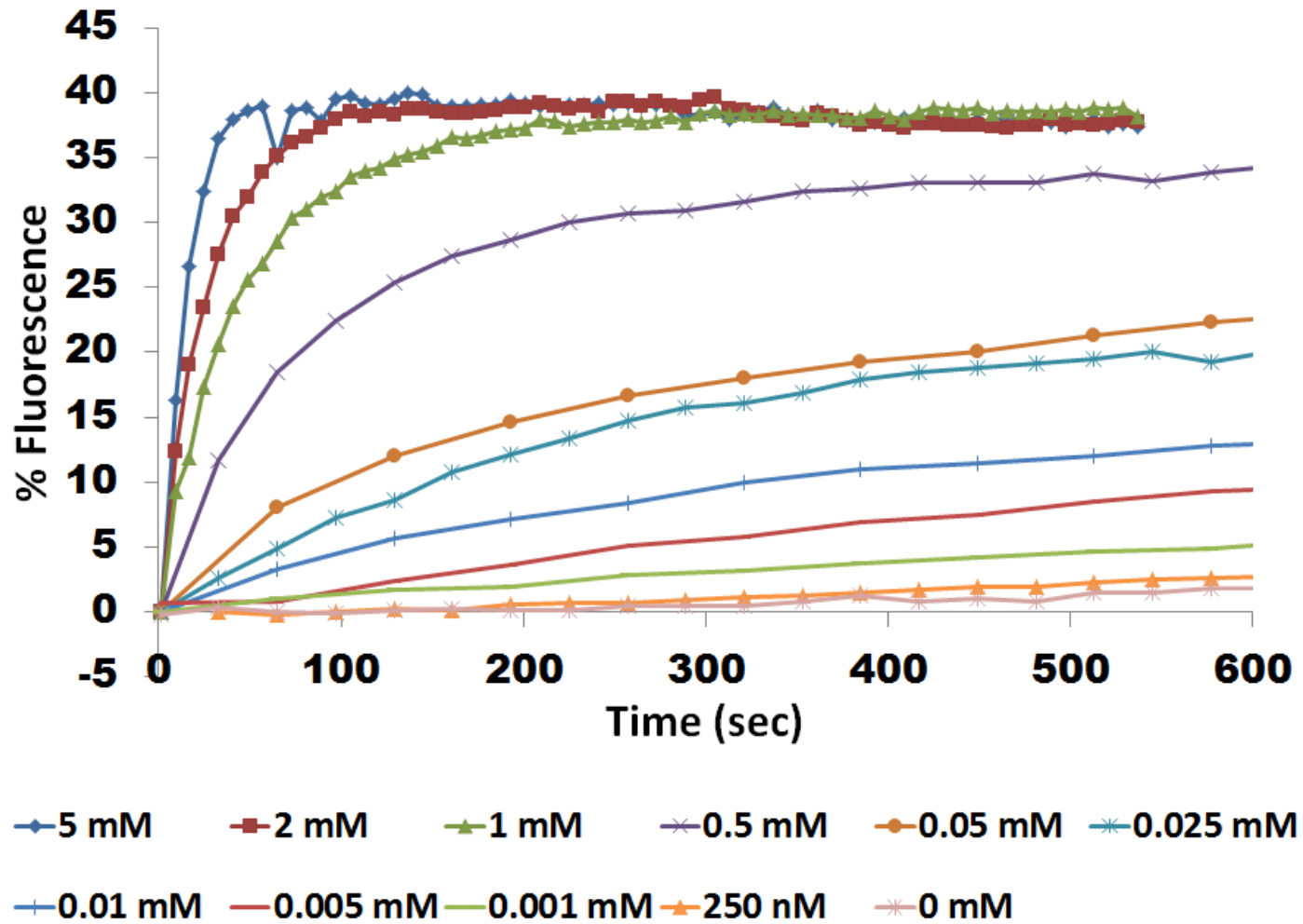


Figure 25. Mg^{2+} dependence of AlF_4^- activation of WT G_{sa}

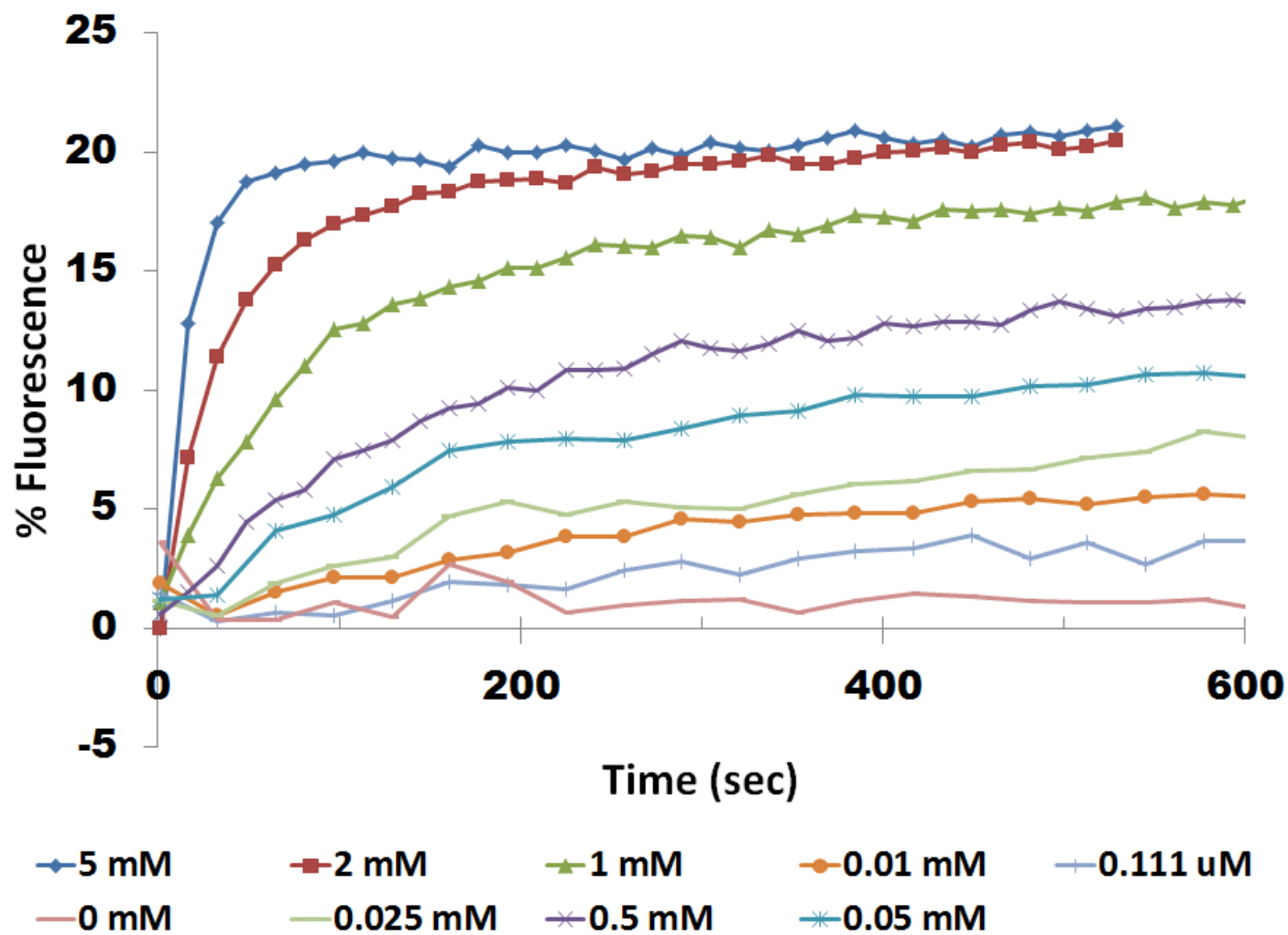


Figure 26. GTP γ S activation of WT G α_1 dependent on Mg $^{2+}$

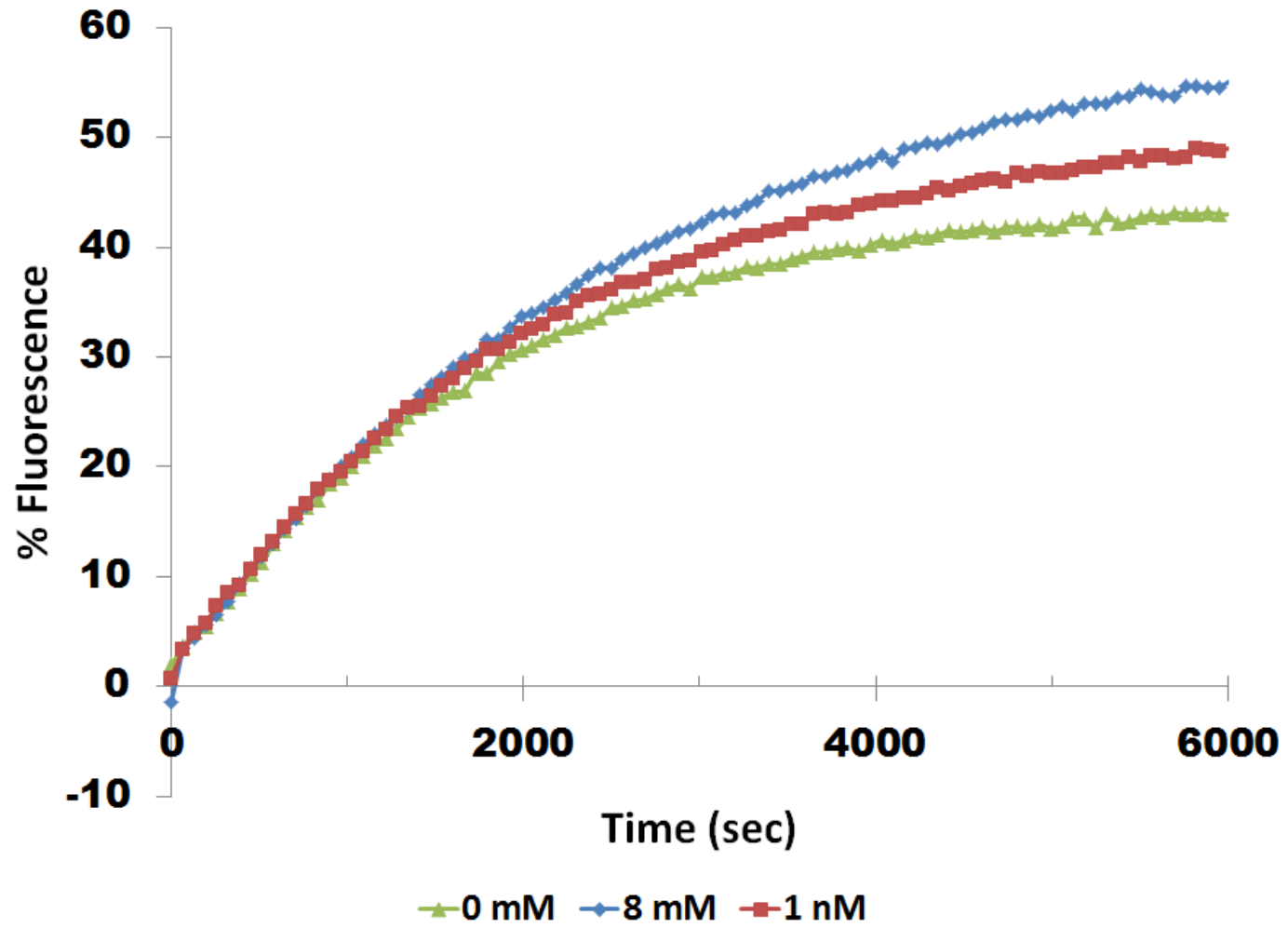
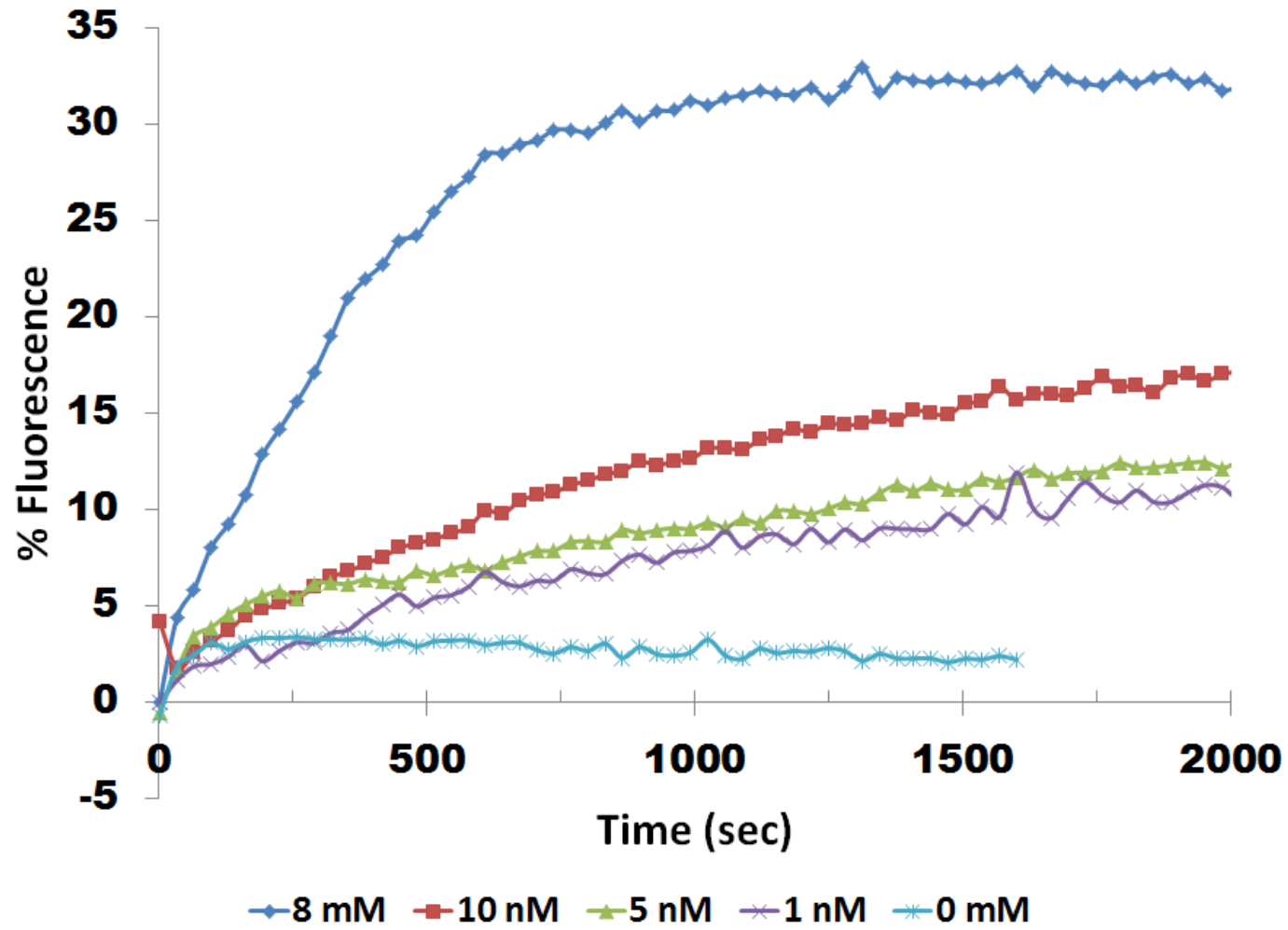


Figure 27. GTP γ S activation of WT G α dependent on Mg $^{2+}$



The emission spectra of G_{α} samples was investigated along with the activity assays. In the absence of Mg^{2+} , addition of AlF_4^- to WT $G_{i\alpha 1} \cdot GDP$ and WT $G_{s\alpha} \cdot GDP$, resulted in red shifts of 1.2 nm and 1.1 nm in the emission spectra compared to their GDP counterparts. Increasing the Mg^{2+} concentration in both G_{α} subunits resulted in incrementally larger red shifts (Fig. 28). At 5 mM Mg^{2+} , $G_{i\alpha 1}$ and $G_{s\alpha}$ completed their bridge formations and reached maximum red shifts of 3.3 nm and 2.5 nm, respectively. The shifts that occurred from activation with $GTP\gamma S$ were also explored for both G_{α} subunits. Activation with $GTP\gamma S$ in the absence of Mg^{2+} observed red shifts of 2.7 nm and 1.2 nm for $G_{i\alpha 1}$ and $G_{s\alpha}$, respectively. $G_{i\alpha 1}$ and $G_{s\alpha}$ reached their maximum shifts of 3.6 and 3.1 nm, respectively, at approximately 50 nM Mg^{2+} (Fig. 29).

Changes in the Secondary Structure of $G_{i\alpha 1}$ and $G_{s\alpha}$

Crystallization studies by Coleman and Sprang (13) discovered a conformation - dependent ordering of three switch regions in $G_{i\alpha 1}$ upon addition of Mg^{2+} to the GDP conformation. CD was used to probe the changes observed at the secondary structure level of $G_{i\alpha 1}$ and $G_{s\alpha}$. Magnesium titration of $G_{i\alpha 1} \cdot GDP$ exhibited no change in the CD spectra (data not shown). Addition of Mg^{2+} up to a concentration of 2 mM to $G_{i\alpha 1} \cdot GDP \cdot AlF_4^-$ displayed decreases in molar ellipticity at 210 nm and 220 nm of the CD spectra compared to its GDP counterpart (Fig. 30). The same trends were observed for the $GTP\gamma S$ conformations, with the exception of a slightly larger decrease at 209 nm and 220 nm (Fig. 31). $G_{s\alpha}$ observed similar findings for the AMF and $GTP\gamma S$ conformation as witnessed with $G_{i\alpha 1}$ (Figs. 32).

Figure 28. Shift resulting from AlF_4^- activation of WT $G_{i\alpha 1}$ and $G_{s\alpha}$ at various $[\text{Mg}^{2+}]_F$

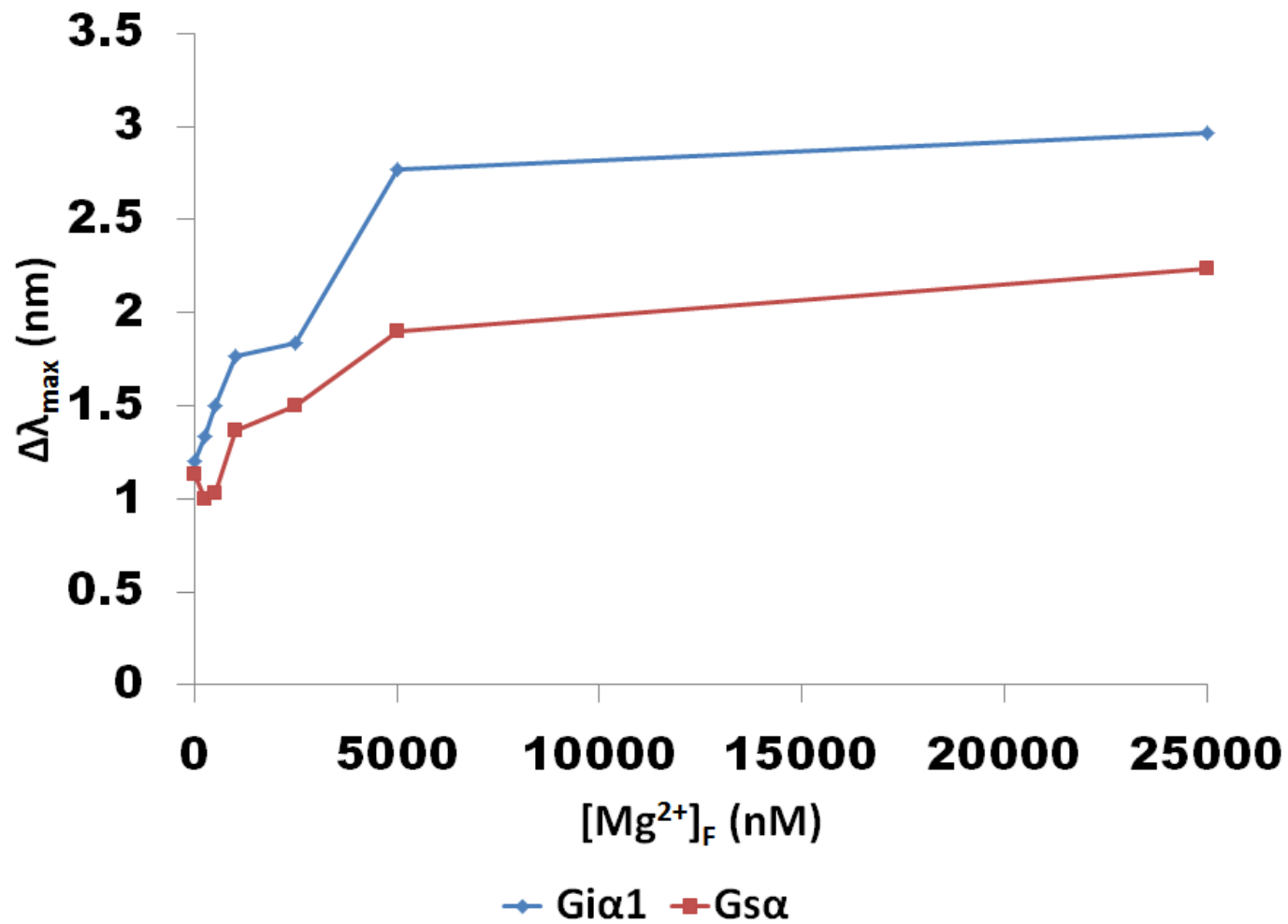


Figure 29. Shift resulting from GTP γ S activation of WT $G_{i\alpha 1}$ and $G_{s\alpha}$ at various $[Mg^{2+}]_F$

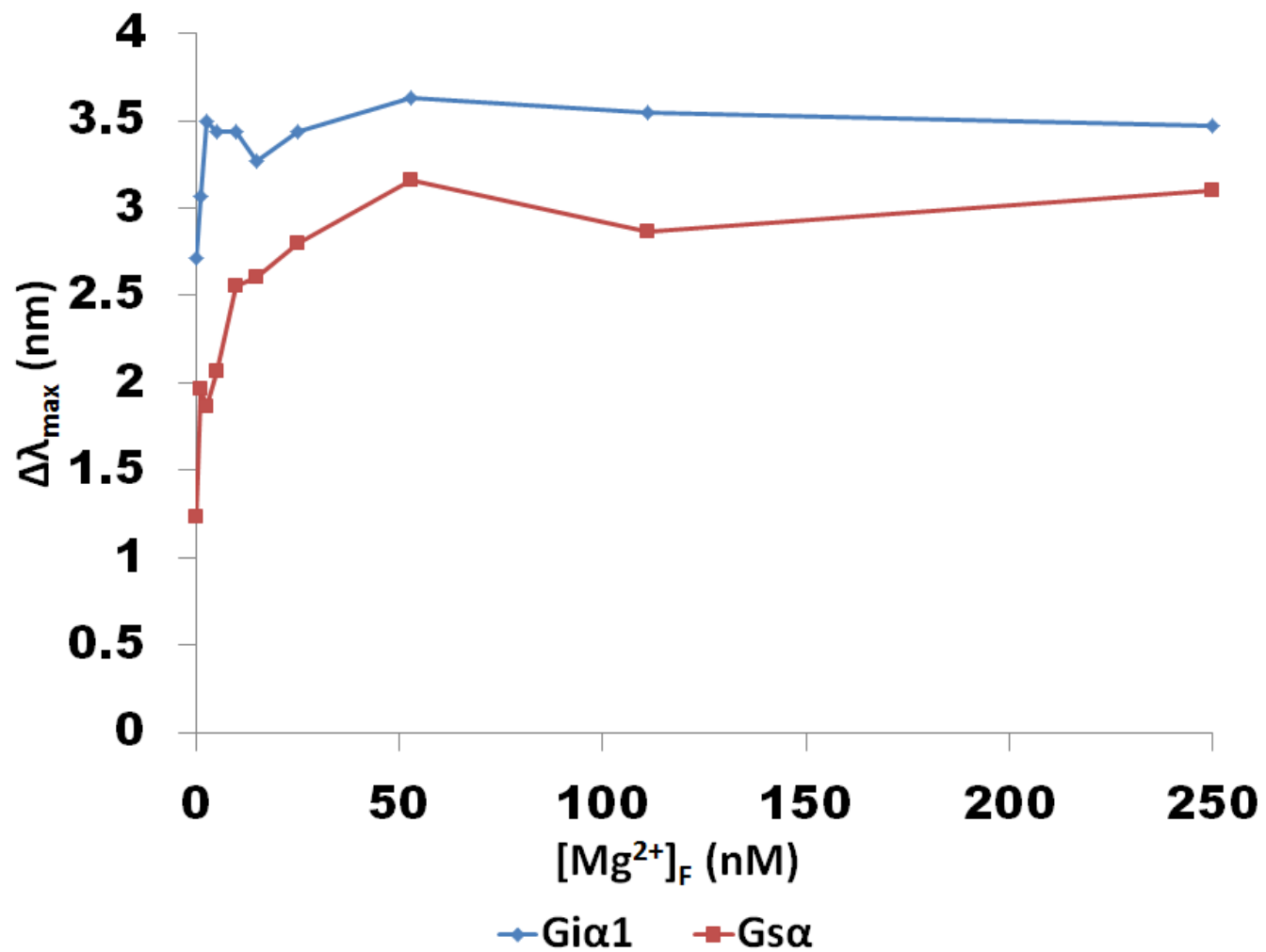


Figure 30. Secondary structure of WT $G_{i\alpha 1}$ •AMF at various Mg^{2+} concentrations

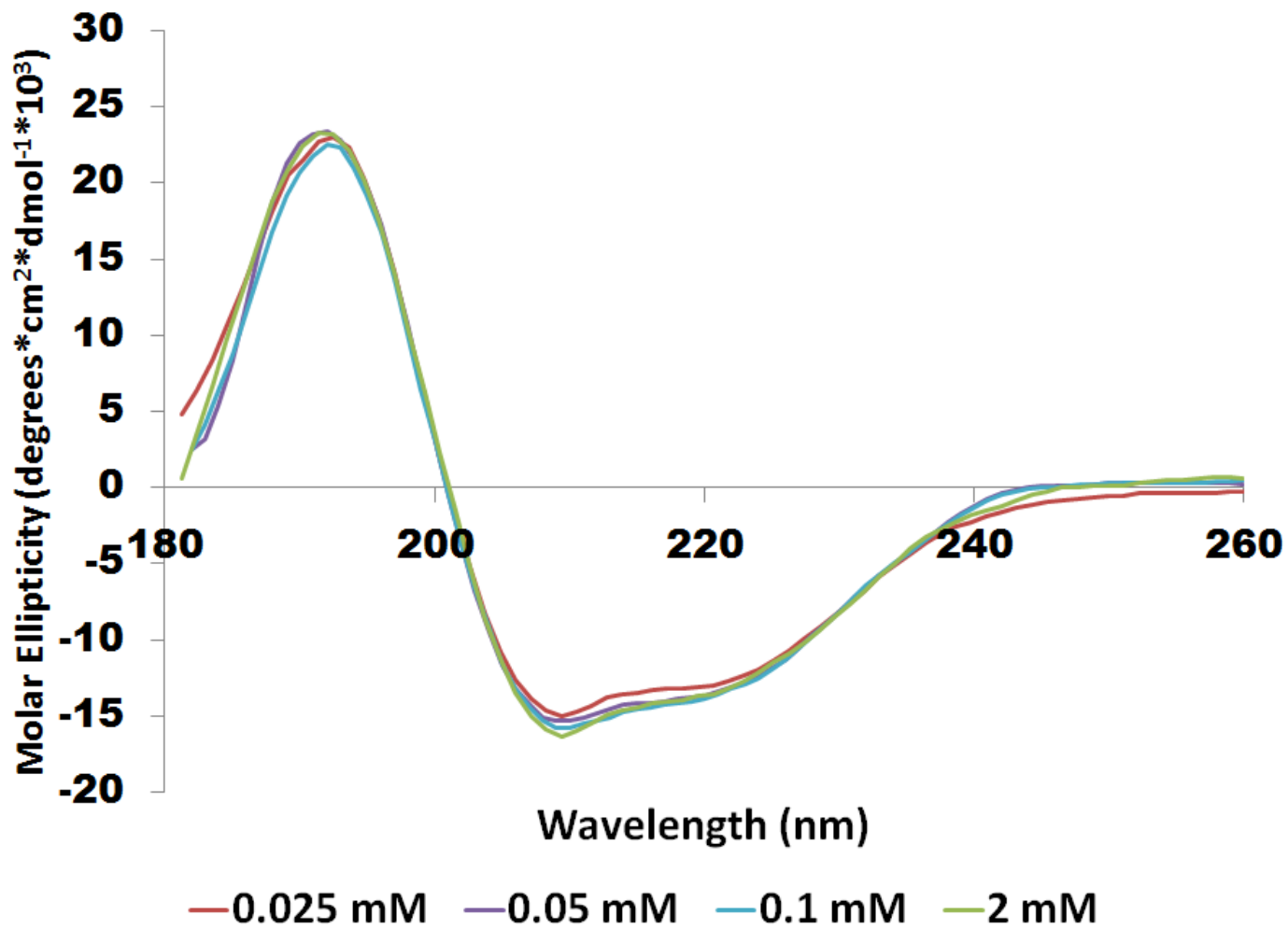


Figure 31. Mg^{2+} dependent activation of $G_{i\alpha 1}$ and $G_{s\alpha}$ with AlF_4^- or GTP γ S

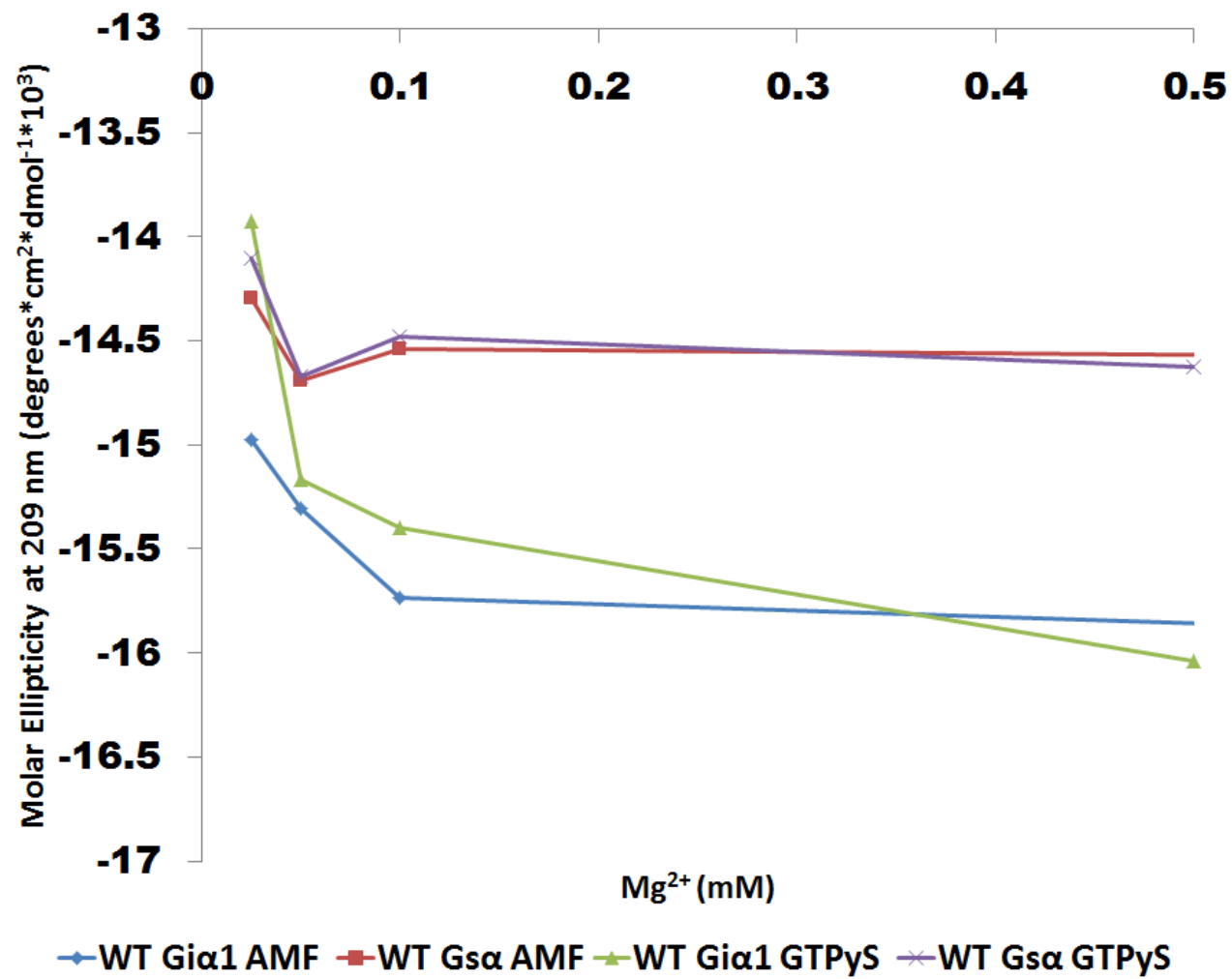
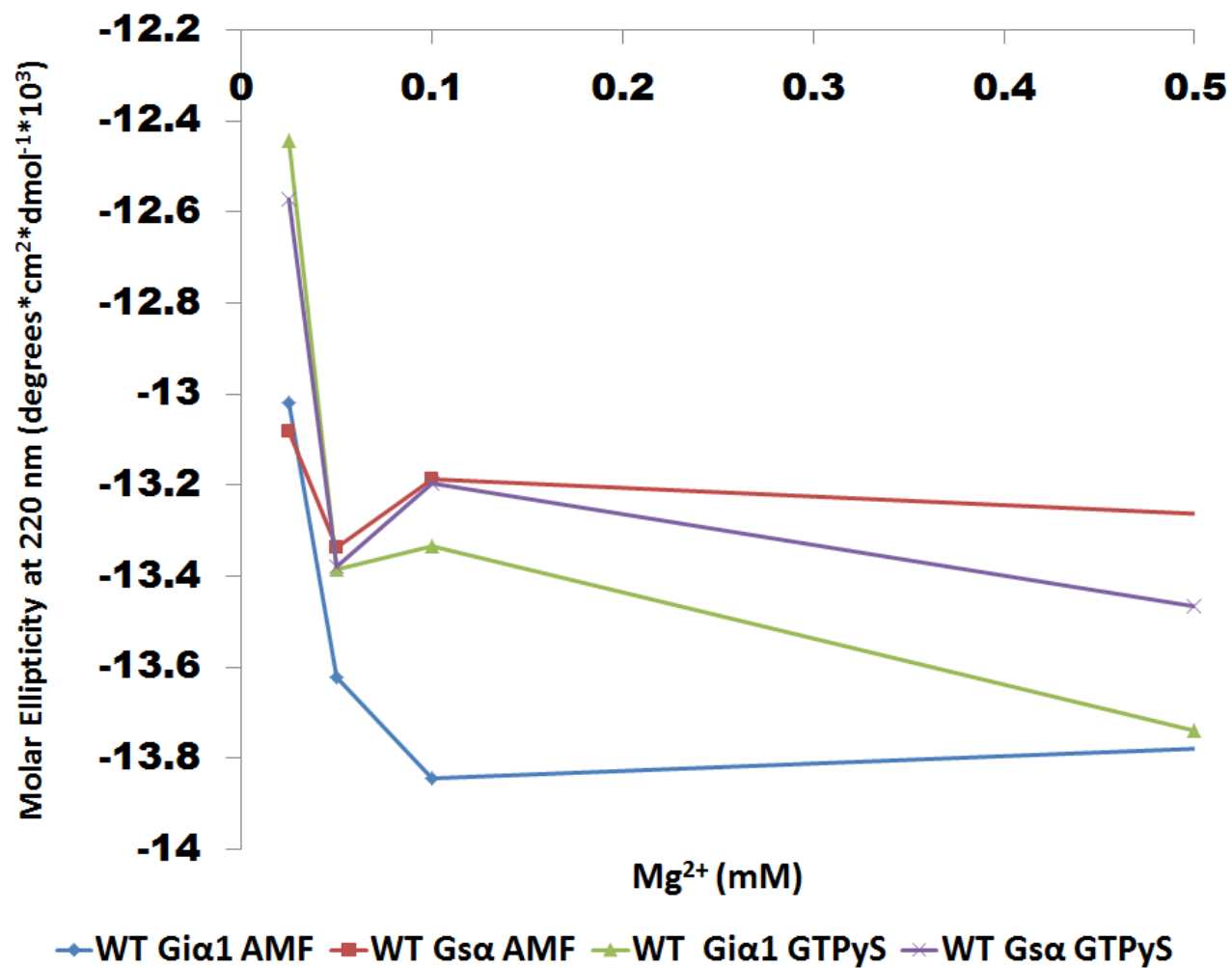


Figure 32. Mg^{2+} dependent activation of $G_{i\alpha 1}$ and $G_{s\alpha}$ with AlF_4^- or $GTP\gamma S$



Discussion

AlF_4^- may bind to GDP in apo G_α subunits and cause a small conformational change as observed for AMF activation at 0 mM Mg^{2+} (Fig. 1). The rate of formation of the AMF conformation increases in the presence of Mg^{2+} as indicated by the larger rates and F_{max} values (Fig. 1). G_{sa} was more sensitive to the presence of Mg^{2+} in AlF_4^- activation than G_{ia1} as indicated by the lower concentration needed to illicit an increase in fluorescence above the basal levels observed in the absence of Mg^{2+} . However, to complete AMF folding both G_{ia1} and G_{sa} needed Mg^{2+} concentrations in the millimolar range. Presumably, in the case of G_{sa} , relatively lower Mg^{2+} concentrations induce more folding than with G_{ia1} . One possibility is that the Mg^{2+} - Al^{3+} distance is shorter in $G_{\text{sa}} \cdot \text{AMF}$ than in $G_{\text{ia1}} \cdot \text{AMF}$. The crystal structure of $G_{\text{ia1}} \cdot \text{AMF}$ is available (17), but that of $G_{\text{sa}} \cdot \text{AMF}$ is not. Therefore, it is not possible at this time to confirm this hypothesis.

GTP γ S displayed similar increases in F_{max} at elevated concentrations of Mg^{2+} for G_α subunits as observed for the binding of AlF_4^- . However, the GTP γ S form observed slower rates than the AMF conformation. The effect of Mg^{2+} on the rate of GTP γ S activation appeared to be greater in G_{sa} than G_{ia1} . It is known that the rate determining step in GTP γ S exchange is the release of GDP from G_α subunits (54). Our results show that magnesium promotes the release of GDP as exhibited by the increased F_{max} of holo G_{ia1} and $G_{\text{sa}} \cdot \text{GTP}\gamma\text{S}$ compared to their apo equivalents, and the rate of release of GDP from G_{ia1} is faster than in G_{sa} and this step is less Mg^{2+} - dependent. It appears that, in the GTP γ S activation of G_{ia1} , the Trp residues fold in a manner that is weakly dependent on Mg^{2+} concentration. The opposite occurs with G_{sa} .

The observed red shifts and increases in fluorescence intensity for G_{α} activation with either AlF_4^- or GTP γ S are dependent on the presence of Mg^{2+} . The GTP γ S conformation is more sensitive to Mg^{2+} than the AMF form, as indicated by Mg^{2+} concentrations (in the nM range for GTP γ S binding as compared to the μ M range in AMF activation) necessary to illicit an appreciable increase in fluorescence intensities and shifts in the emission spectra. However, $G_{s\alpha} \cdot GTP\gamma S$ was significantly more dependent on Mg^{2+} than $G_{i\alpha 1} \cdot GTP\gamma S$, which is in agreement with the data from the time-based assays and the observed red shifts for both apo and holo G_{α} proteins. Apo WT $G_{i\alpha 1} \cdot GTP\gamma S$ displayed an increase of 44% in the fluorescence intensity, whereas holo WT $G_{i\alpha 1} \cdot GTP\gamma S$ observed a 56% increase in fluorescence. Apo and holo $G_{s\alpha} \cdot GTP\gamma S$ resulted in activation of 3% and 33% (Figs. 24 – 29). These findings also indicated that GDP release from G_{α} subunits is not completely dependent on Mg^{2+} , but increases the rate at which GDP may release and bind GTP γ S. In addition, the presence of Mg^{2+} is essential in trace amounts to complete the conformational change of $G_{i\alpha 1} \cdot GTP\gamma S$ and $G_{s\alpha} \cdot GTP\gamma S$.

Incremental amounts of Mg^{2+} showed increased F_{max} values and red shifts in $G_{i\alpha 1}$ and $G_{s\alpha}$ activation. We propose a direct relationship between the observed shifts and increased fluorescence intensities upon Mg^{2+} titration of G_{α} subunits. W211 and W234, in $G_{i\alpha 1}$ and $G_{s\alpha}$, respectively, are responsible for the considerable increase in fluorescence intensity witnessed upon activation and contribution to a bridge formation with R208 and R231. We suggest that incremental increases in Mg^{2+} concentrations concomitantly folded W211 and W234 into less solvent exposed regions, and into closer proximity with R208 and R231 in a stepwise fashion. Regardless of activation with AlF_4^- or GTP γ S, the larger shift observed for $G_{i\alpha 1}$ versus $G_{s\alpha}$, can be explained through the proximity of the

electrostatic interaction. Molecular modeling shows that R208 and W211 in $G_{i\alpha 1}\bullet\text{GTP}\gamma\text{S}$ has a bridge distance of 6.6 Å in comparison to R231 and W234 in $G_{s\alpha}\bullet\text{GTP}\gamma\text{S}$ which displays a distance of 7.2 Å. Computational work by Gallivan and Dougherty (45) found that electrostatic interactions between Trp residues and Arg residues to be considerably stronger when less than 6 Å as opposed to greater than 6 Å apart. The maximum red shifts incurred by $G_{i\alpha 1}$ and $G_{s\alpha}$ in the $\text{GTP}\gamma\text{S}$ conformation are 3.5 nm and 2.8 nm, respectively. If the length of the R231 – W234 bridge in $G_{s\alpha}\bullet\text{GTP}\gamma\text{S}$ were to result in a weak interaction then one would expect a much smaller shift than observed. However, this may be explained through a second electrostatic interaction occurring in the α – helical domain of $G_{s\alpha}\bullet\text{GTP}\gamma\text{S}$ between W154 and R160, which displays a distance of 4.3 Å. This bridge would indicate a significantly stronger interaction and be contributing to the overall shift displayed in the activation of $G_{s\alpha}$.

The crystal structures of $G_{i\alpha 1}$ depict unordered segments in its GDP conformation. These regions known as switch II and III become ordered when activated with $\text{GTP}\gamma\text{S}$ or AMF (13). When titrated with Mg^{2+} , $G_{i\alpha 1}\bullet\text{GDP}$ did not undergo any changes in its secondary structure. Deconvolution of $G_{i\alpha 1}\bullet\text{GDP}$ and $G_{s\alpha}\bullet\text{GDP}$ samples found the secondary structure to be 40% α – helical, 15% β – sheets, 18% turns and 27% random coil (RC) and 38% α – helical, 15% β – sheets, 20% turns, and 28% RC, respectively. Upon addition of AlF_4^- or $\text{GTP}\gamma\text{S}$, a 2% increase in α - helical content and subsequent 1% decrease in random coil and β – sheet was calculated for both G_{α} subunits. This suggests that upon activation a fraction of the β – sheets and RC are refolding their structure into α – helices. In addition, since the switch II and III regions are unordered in the crystal structure of $G_{i\alpha 1}\bullet\text{GDP}$ ($G_{s\alpha}\bullet\text{GDP}$ is unavailable) it may be plausible that the effects in the

secondary structure may be occurring in these protein segments. In conclusion, the CD data confirm that the secondary structure of $G_{i\alpha 1}$ and $G_{s\alpha}$ in their activated forms is dependent on Mg^{2+} . Understanding the role of Mg^{2+} in G_{α} activation may lead to possible therapeutic targets in G_{α} protein associated illnesses, such as bipolar disorder and cancer (27, 56). Future studies would include crystallization of $G_{s\alpha}\cdot GDP$ and $G_{s\alpha}\cdot AMF$ to investigate the conformational dependent switch regions and to probe the electrostatic interaction of R231 and W234.

APPENDIX A
EFFECT OF DTT ON WT G_{id1} ACTIVATION

The amino acid cysteine contains a thiol group that is capable of disulfide bridge formation via oxidation of cysteine side chains to form cystines. A polypeptide chain can form cystines either through intramolecular interactions of two thiol groups within the chain or through intermolecular interactions of thiol groups between two subunits. A classic example of cystine formation within a subunit is Christian Anfinsen's work with bovine ribonuclease (57). Native ribonuclease contains multiple cystines bonded intramolecularly that are required for stability and function. In the presence of a reducing agent, β – mercaptoethanol, and 8 M urea the non – covalent bonds were disrupted and ribonuclease formed a completely reduced random coil conformation. When dialyzed against buffer, in the absence of urea and β – mercaptoethanol , it spontaneously renatured and retained most of its enzymatic activity. However, when 8 M urea remained and the reducing agent was absent, ribonuclease refolded and had less than 1 % enzymatic activity, because the disulfide bridges that formed were between the wrong pairs of cysteine residues. Properly folded protein typically demonstrates a specific biological function. Mis-folding or denaturation of the protein can lead to altered biological function, which in turn often leads to disease.

Disulfide bridge formation can also occur intramolecularly as demonstrated by insulin (58, 59). Frederick Sanger and co – workers (60, 61) pioneered the technique of sequencing in proteins, RNA, and DNA. Sanger's foundational work was with insulin, the first protein ever sequenced. Insulin consists of two polypeptide chains bonded through two cystine residues. There is also an intramolecular bond between cysteine residues at positions 6 and 7 within chain A, in human insulin (62). Crystallographic studies of G_{α} suggest that oligomerization occurs between multiple α subunits (17).

Thus, we investigated the polymerization of WT $G_{i\alpha 1}$ based on the hypothesis that that disulfide linkage between G_{α} subunits occurred.

A method to express and purify high yields of G_{α} subunits has been well researched and documented by Lee and co – workers (41). Expression of hexahistidine tagged WT $G_{i\alpha 1}$ typically leads to yields of 40 mg/ 1 L. After purification with Ni^{2+} and size exclusion columns, the protein is usually greater than 95% in purity and is typically stored in 20 mM β – mercaptoethanol or 2 mM dithiothreitol (DTT) (41, 63, 64). An indirect method to determine functionality of newly purified G_{α} protein is through intrinsic tryptophan fluorescence (38, 48). Using this purification method that includes DTT, activation with the addition of AlF_4^- or exchange with $GTP\gamma S$ typically produces fluorescence of 40% or greater (25, 65).

WT $G_{i\alpha 1}$ expression and purification was obtained as described (41). The only difference was the protein was stored and activated in the absence of the reducing agents β – mercaptoethanol and DTT. Activation of WT $G_{i\alpha 1}\cdot GDP\cdot Mg^{2+}$ with AlF_4^- resulted in a fluorescence intensity of 34% (Fig. 33). In the presence of increasing concentrations of DTT, the fluorescence intensity increased with AlF_4^- activation and, in the presence of 5 mM DTT, it reached a maximum fluorescence of 55%.

Oligomerization of WT $G_{i\alpha 1}\cdot GDP$ was also investigated through SDS – PAGE in the presence and absence of β – mercaptoethanol. WT $G_{i\alpha 1}\cdot GDP$ in the absence of β – mercaptoethanol displays bands at 41, 82, and 123 kDa (Fig. 34, lanes 2 and 3). In the

Figure 33. WT $G_{i\alpha 1} \cdot \text{GDP} \cdot \text{Mg}^{2+}$ activation with AlF_4^- at various DTT concentrations

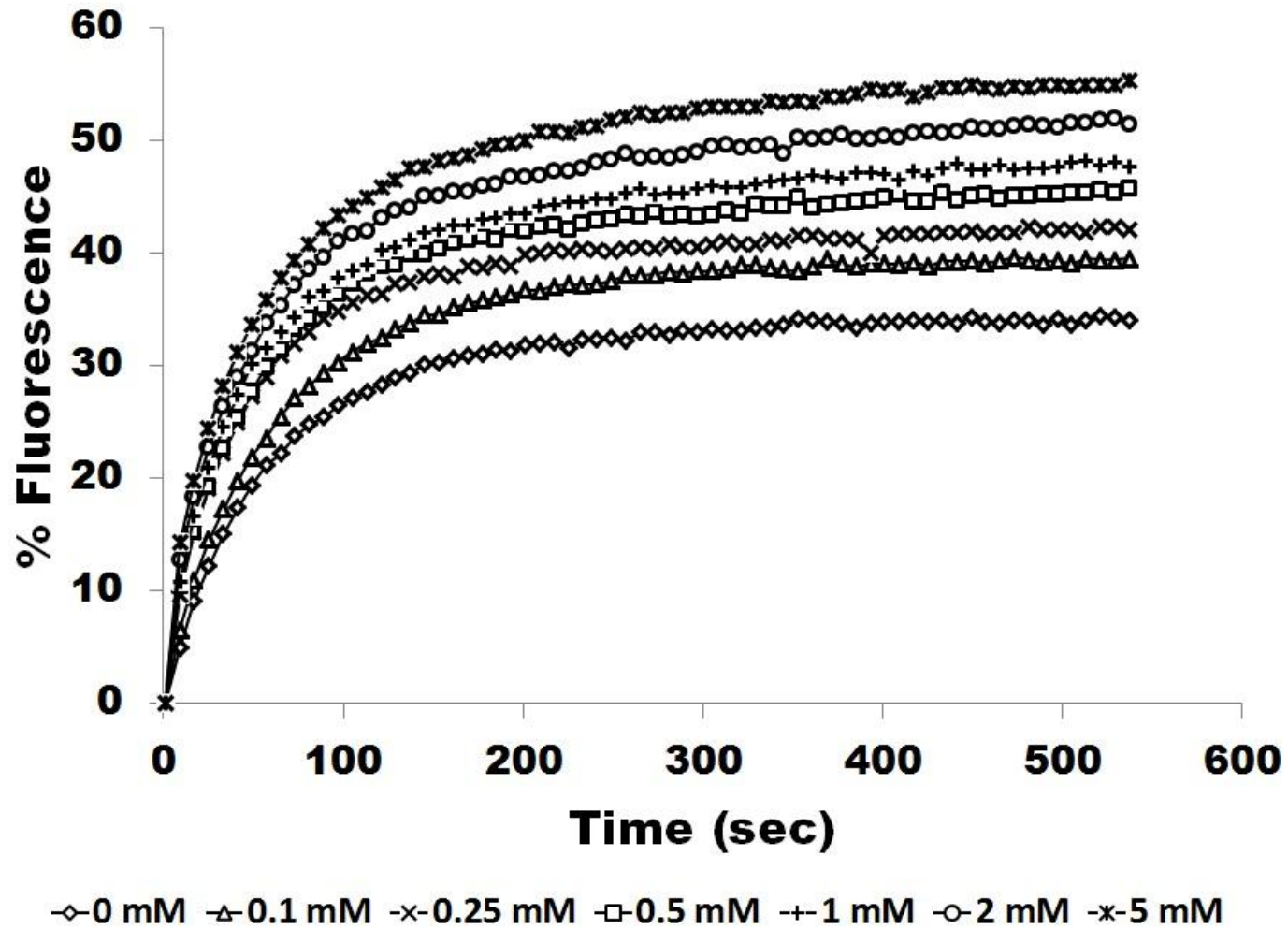
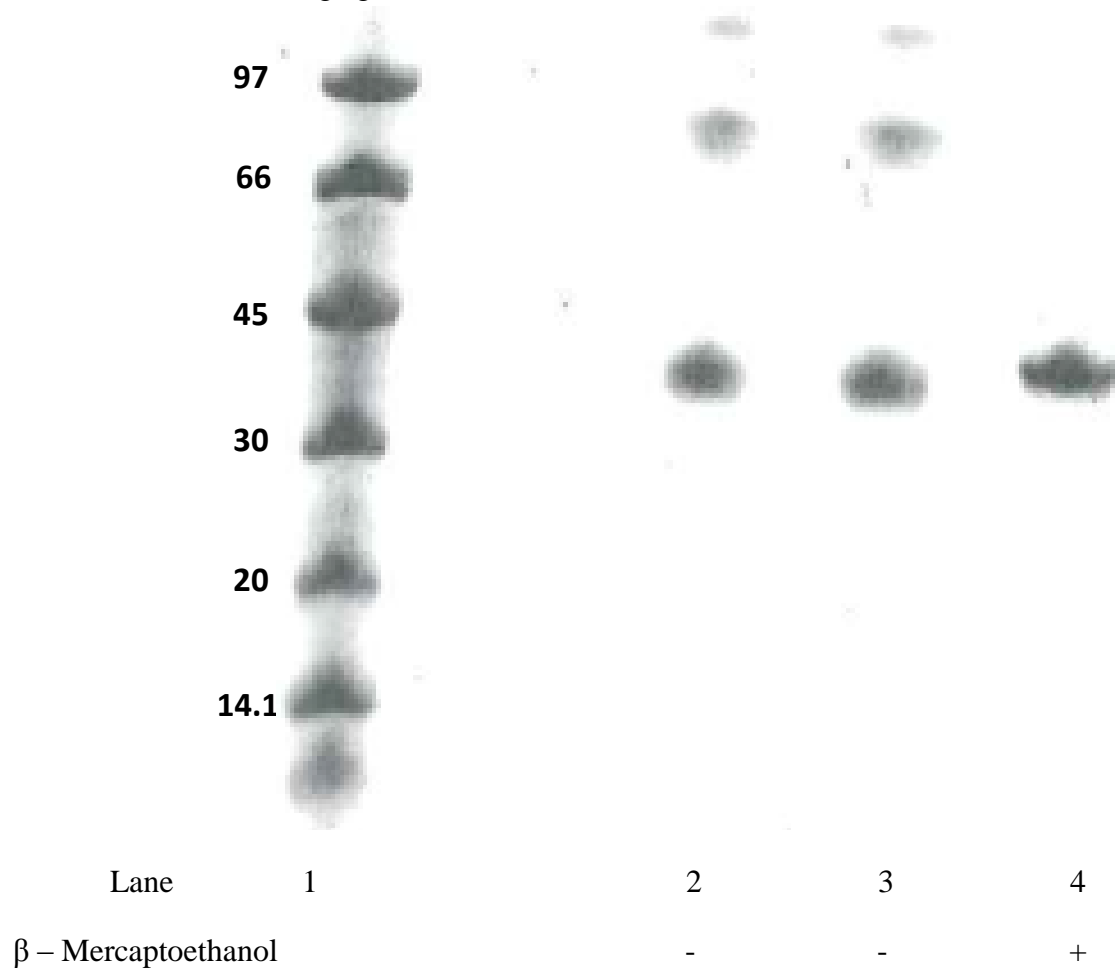


Figure 34. Visualization of WT $G_{i\alpha 1}$ •GDP polymerization with SDS – PAGE. Lane 1, Molecular weight markers; Lanes 2 and 3 depict gels of WT $G_{i\alpha 1}$ •GDP samples in the absence (-) of β – mercaptoethanol, and lane 4 is for a similar protein sample in the presence (+) of the reducing agent.



presence of 0.7 M β – mercaptoethanol, a single band at 41 kDa is observed for WT $G_{i\alpha 1}$ •GDP (Fig. 34, lane 3).

As discussed earlier, fully functional WT $G_{i\alpha 1}$ typically displays values greater than 40%. This agrees well with the results observed where the amount of DTT is greater than 0.1 mM. It is suggested that the presence of a reducing agent is necessary in order to obtain fully functional, monomeric WT $G_{i\alpha 1}$. There are ten cysteine residues in WT $G_{i\alpha 1}$ and four of them are located at the protein's surface. It is therefore possible that, without a reducing agent present, WT $G_{i\alpha 1}$ polymerizes through bonding of its monomers. A disulfide bridge is formed through linkage of solvent – exposed cysteine residues between two α subunits. Increasing amounts of the reducing agent resulted in increased activity due to the reduction of these polymers. As the protein was reduced its flexibility and movement was enhanced. SDS – PAGE confirmed the suggested expectations of $G_{i\alpha}$ polymerization. The use of β – mercaptoethanol, completely reduced the dimer and trimer bands to a single monomer band.

We therefore recommend that investigation of WT $G_{i\alpha 1}$ through functional assays or structure determination should be conducted in the presence of a reducing agent to ensure reliable information on the unpolymerized α - subunit. To better understand the effects of DTT on $G_{i\alpha}$ subunits, future studies could make use of other reducing and oxidizing agents, for example (*tris*(2-carboxyethyl)phosphine) and glutathione. Determination of specific intramolecular cystine formation could also be explained through Mass Spectrometry and X – ray crystallography. It will also be interesting to see if disulfide bridges are present in the active $GTP\gamma S$ conformation of $G_{i\alpha 1}$, and in both forms of $G_{s\alpha}$.

APPENDIX B

Li⁺ INHIBITION OF GTP_γS BINDING AND GTP HYDROLYSIS

Bipolar disease is a severe mental illness in which the person experiences clinical episodes of depression and mania or hypomania, or mixed states (66). The most identifiable symptom is that of a person experiencing extreme changes in behavior ranging from tremendous aggressiveness to complete and utter depression.

Approximately 2.5% of the population over the age of 18 in the United States suffers from bipolar disorder (67). It is a debilitating illness that can result in tremendous loss in productivity, and has been known to occasionally contribute to patient suicide. There are many drugs in the market today that are used to stabilize mood swings associated with bipolar disorder, such as anticonvulsants, antipsychotics, and benzodiazepines (68, 69). However, the most common and effective for treatment is the use of lithium salts. Li^+ treatment doses are between 0.5-1.2 mM just short of the lethal doses that occur at approximately 2.0 mM. Because the toxic levels can easily be reached during treatment, patients must have continuous renal screenings to ensure safe plasma levels at all times (70). Despite these shortcomings, Li^+ is still the preferred treatment for bipolar disorder. The study of the Li^+ mechanism of action can lead to a better understanding of bipolar disorder and to the development of a better drug for its treatment (71).

Li^+ inhibits several Mg^{2+} dependent activated enzymes that are involved in signal transduction, such as inositol monophosphatase in the phosphoinositide cascade, adenylyl cyclase, glycogen synthase kinase – 3 beta ($\text{GSK} - 3\beta$), and G – proteins (72).

Overabundance and hyperactivity of guanine nucleotide binding (G) proteins have been linked to patients suffering from bipolar disease (71). In rat cortex membranes, Li^+ , at therapeutic concentrations, inhibits α subunits of both the G_i and G_s , thus lessening the

manic and depressive states that the disease causes (73). During mania, there are increased levels of dopamine neurotransmission (74). Post synaptic actions of dopamine are mediated via G – protein coupled receptors. An increase in receptor and G - protein coupling have been found in post mortem subjects, and studies in animal models showed lower levels of dopamine when treated with lithium (74). Furthermore, it has been reported that specific subunits of G – proteins are associated with higher dopamine levels in bipolar patients and lithium controls the equilibrium of nucleotide activation and not the levels of G – proteins (74).

Li^+ and Mg^{2+} exhibit similar physiochemical properties due to their fairly similar hydrated ionic radii (0.60 Å for Li^+ and 0.65 Å for Mg^{2+}). They exhibit a “diagonal relationship” in the periodic table, with lithium being the first element in Group IA and magnesium the second element in Group IIA. These chemical similarities of Li^+ and Mg^{2+} occur in their stable oxidation states in aqueous solution. However, their different ionic charges, and preferred coordination numbers (4 vs. 6) and ligand geometries (tetrahedral vs. octahedral) lead them to have unique properties (72). Because of all these properties it is plausible that Li^+ may compete with Mg^{2+} at its binding sites. Ral, a member of the GTPase ras family, depicts two Mg^{2+} binding sites in its crystal structure (75). The crystal structures of $\text{G}_{i\alpha 1}$ (12, 13) and $\text{G}_{s\alpha}$ (31) display only one Mg^{2+} binding site, however crystallization was performed under high concentrations of LiCl and Li^+ could be out competing Mg^{2+} at another possible binding site. Dr. Guoyan Wang and Dr. Chris Malarkey, past graduate students of the de Freitas group, investigated the possibility of two Mg^{2+} binding sites in $\text{G}_{i\alpha 1}$ and $\text{G}_{s\alpha}$ through the use of the Mg^{2+} specific,

fluorescence probe, furaptra (76). Their studies found evidence for two Mg^{2+} binding sites, one with a high affinity and the second with a lower affinity for Mg^{2+} . These data suggest that Li^+ may out compete Mg^{2+} at the lower affinity site. These findings provided the motivation to explore the effect of Li^+ on the activity of G – proteins.

We used radiolabeled isotopes to investigate whether Li^+ inhibited Guanosine – 5' – triphosphate (GTP) binding to G_{α} subunits and the nucleotide hydrolysis. To investigate nucleotide binding a non – hydrolysable analog of GTP, $GTP\gamma S^{35}$, was used. Exploration of the hydrolysis of GTP was monitored through GTP^{32} . WT $G_{s\alpha}$ was able to reach maximum exchange of $GTP\gamma S$ with GDP and hydrolysis of GTP in the presence of 0.1 mM Mg^{2+} and in the absence of Li^+ (Fig. 35). Increasing the concentration of Li^+ to 1 mM reduced the binding of $GTP\gamma S$ by 70% compared to the observed binding in the absence of Li^+ . Maximum Li^+ inhibition of $GTP\gamma S$ binding was reached at 20 mM Li^+ with an IC_{50} of 0.6 mM. The effect on hydrolysis of GTP was also investigated (Fig. 36). GTP hydrolysis was reduced by 15% in the presence of 1 mM Li^+ . Maximum inhibition of GTP hydrolysis was observed at 10 mM Li^+ and had a calculated IC_{50} of 2.0 mM.

WT $G_{s\alpha}$ observed significant inhibition of $GTP\gamma S$ binding and GTP hydrolysis in the presence of Li^+ at concentrations within the therapeutic range. Li^+ had a larger effect on the binding of $GTP\gamma S$ than in the hydrolysis of GTP. Therefore, the conditions used for the two experiments enable us to differentiate the two steps - nucleotide exchange and hydrolysis - in the cyclic function of G – proteins. The data suggest that Li^+ has a direct effect on nucleotide binding to $G_{s\alpha}$, and that the effect on hydrolysis is secondary and propagated by the inhibition observed in the exchange. We propose that

Figure 35. Effect of Li^+ on GTP γ S binding to WT G_{sa} .

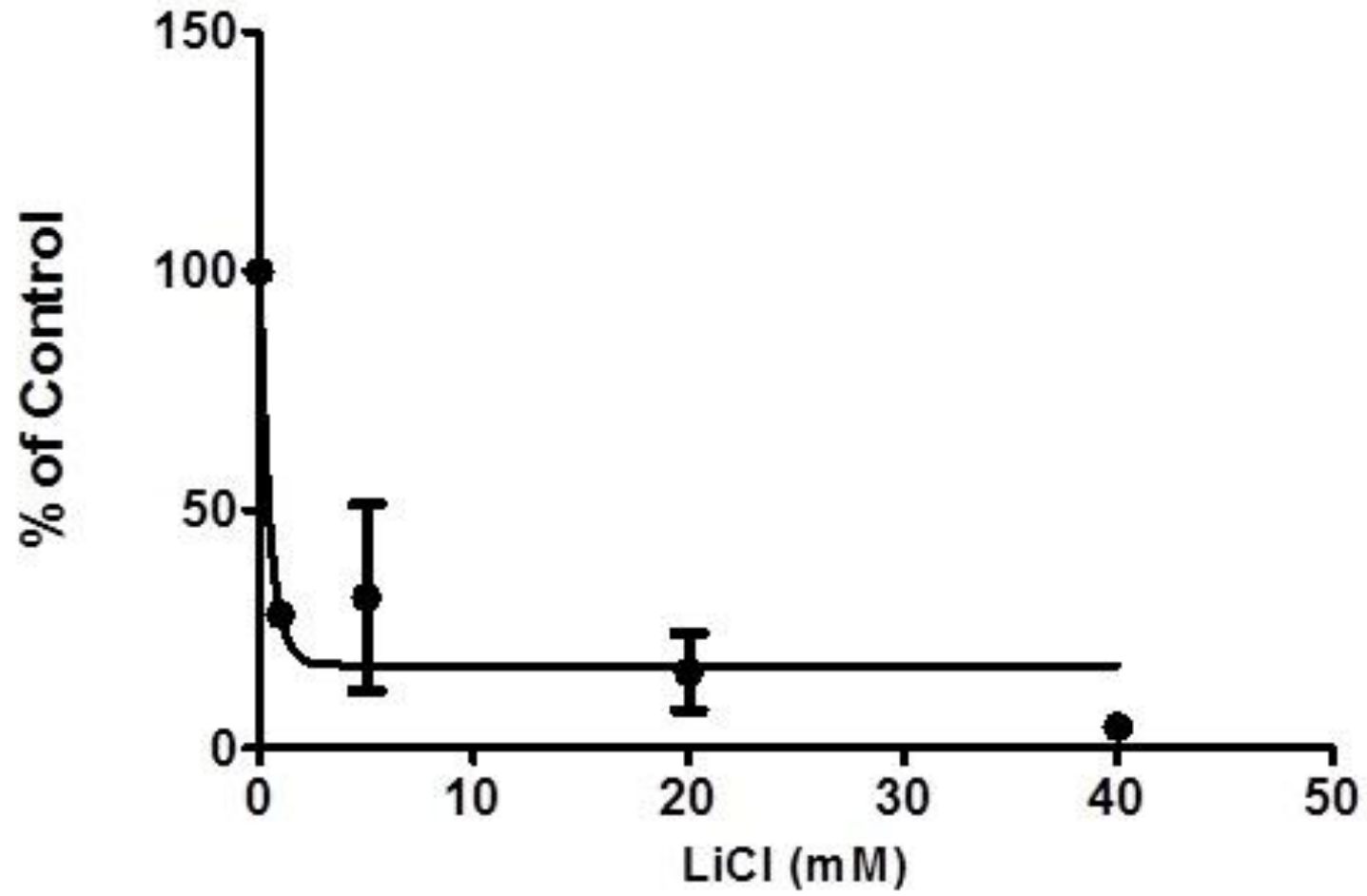
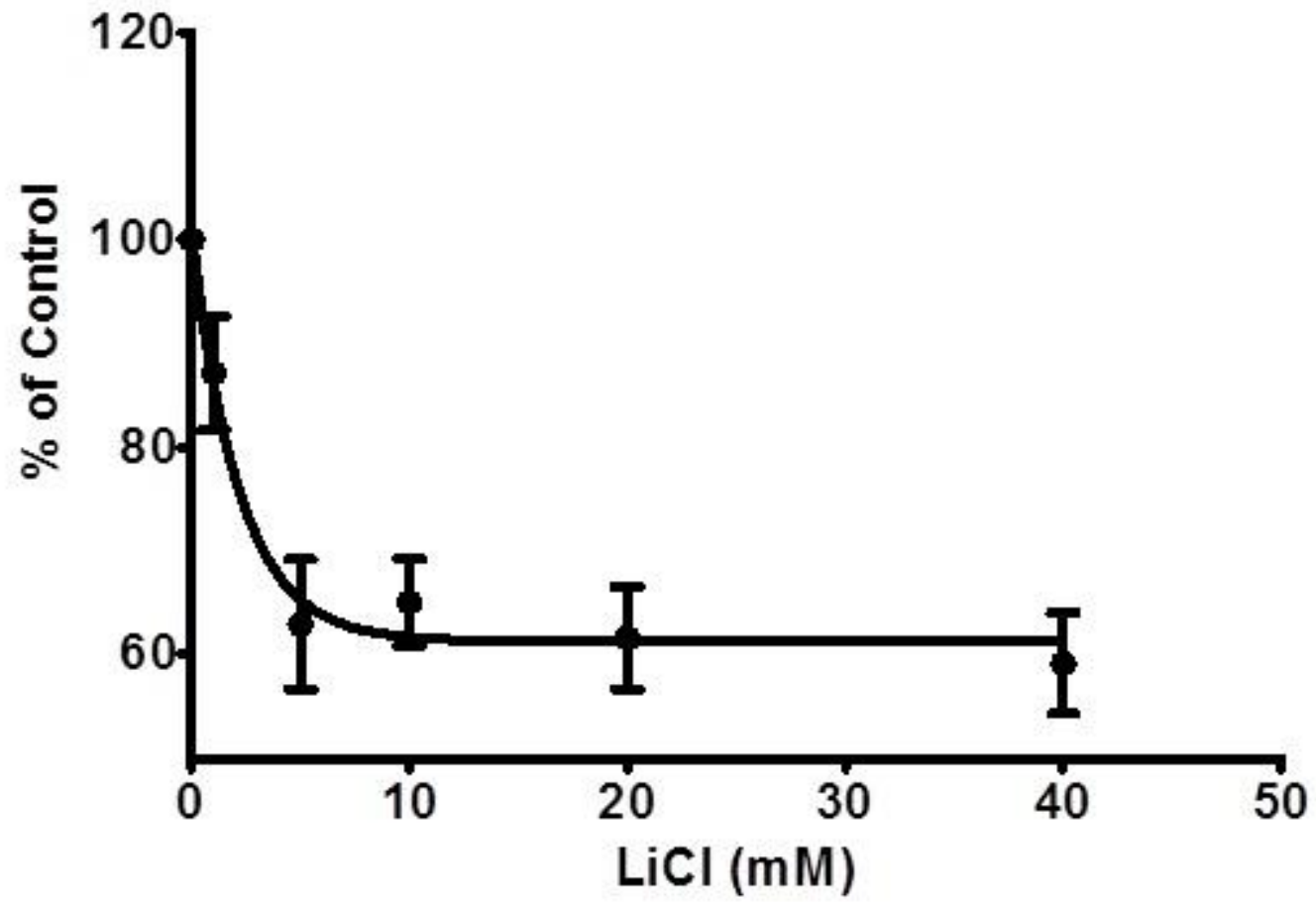


Figure 36. Effect of Li^+ on GTP Hydrolysis of WT G_{sa}



Li^+ is out competing Mg^{2+} , at a second low affinity Mg^{2+} binding site that may regulate binding at the high affinity site, which, in turn, impacts nucleotide exchange. Li^+ binding may cause a conformational change at the second site which may account for the regulation of the Mg^{2+} dependent exchange. The limiting factor in nucleotide exchange is the release of GDP (23). Therefore, it is necessary to further investigate whether Li^+ is inhibiting the release of GDP or slowing the rate of binding of $\text{GTP}\gamma\text{S}$.

Future experiments to be conducted would be possible crystallization of WT $\text{G}_{i\alpha 1}$ and $\text{G}_{s\alpha}$ in the absence of LiCl to determine if there are two Mg^{2+} binding sites. Also, the use of radiolabeled $\alpha - \text{GTP}^{32}$ to investigate whether Li^+ inhibition of GDP release occurs.

Li^+ inhibition of nucleotide exchange and of hydrolysis was also studied with $\text{G}_{i\alpha 1}$. No evidence of Li^+ inhibition of $\text{G}_{i\alpha 1}$ activity was found (data not shown). The different behavior of $\text{G}_{s\alpha}$ and $\text{G}_{i\alpha 1}$ may correlate with the reported effects of Li^+ on G_s , but not in $\text{G}_{i\alpha 1}$, in post – mortem cortex membranes, peripheral blood elements, and mononuclear leukocytes (71, 77). When Li^+ inhibition of $\text{GSK} - 3\beta$ was studied, it was found that 2.5 mM of Li^+ , which is a toxic level, was required to induce a 50% decrease in activity (78). However, in our studies, 1.0 mM of Li^+ , a concentration within the therapeutic range, caused 50% inhibition of nucleotide exchange in $\text{G}_{s\alpha}$. Although there is strong support for the role that $\text{GSK} - 3\beta$ plays in bipolar disorder, it may not be the complete story and targeting Li^+ interactions with G – proteins is imperative.

REFERENCES

1. McCudden C, Hains M, Kimple R, Siderovski D, Willard F. G-protein signaling: Back to the future. *Cell Mol Life Sci.* 2005;62:551-77.
2. Baltoumas FA, Theodoropoulou MC, Hamodrakas SJ. Interactions of the α -subunits of heterotrimeric G-proteins with GPCRs, effectors and RGS proteins: A critical review and analysis of interacting surfaces, conformational shifts, structural diversity and electrostatic potentials. *J Struct Biol.* 2013;182:209-18.
3. Oldham WM, Hamm HE. Structural basis of function in heterotrimeric G proteins. *Q Rev Biophys.* 2006;39:117-66.
4. Cabrera-Vera T, Vanhauwe J, Thomas T, Medkova M, Preininger A, Mazzoni M, et al. Insights into G protein structure, function, and regulation. *Endocr Rev.* 2003;24:765-81.
5. Hescheler J, Rosenthal W, Trautwein W, Schultz G. The GTP-binding protein, go, regulates neuronal calcium channels. *Nature.* 1987;325:445-7.
6. Offermanns S. G-proteins as transducers in transmembrane signalling. *Prog Biophys Mol Biol.* 2003;83:101-30.
7. Ho M, Wong Y. G(z) signaling: Emerging divergence from G(i) signaling. *Oncogene.* 2001;20:1615-25.
8. Harden TK, Waldo GL, Hicks SN, Sondek J. Mechanism of activation and inactivation of Gq/phospholipase C-beta signaling nodes. *Chem Rev.* 2011;111:6120-9.
9. Little PJ. GPCR responses in vascular smooth muscle can occur predominantly through dual transactivation of kinase receptors and not classical Gq protein signalling pathways. *Life Sci.* 2013;92:951-6.
10. Dhanasekaran N, Dermott J. Signaling by the G(12) class of G proteins. *Cell Signal.* 1996;8:235-45.
11. Kozasa T, Hajicek N, Chow CR, Suzuki N. Signalling mechanisms of RhoGTPase regulation by the heterotrimeric G proteins G12 and G13. *J Biochem.* 2011;150:357-69.

12. Coleman D, Berghuis A, Lee E, Linder M, Gilman A, Sprang S. Structures of active conformations of G(i-alpha-1) and the mechanism of GTP hydrolysis. *Science*. 1994;265:1405-12.
13. Coleman D, Sprang S. Crystal structures of the G protein G(i alpha 1) complexed with GDP and Mg²⁺: A crystallographic titration experiment. *Biochemistry*. 1998;37:14376-85.
14. Liu W, Clark W, Sharma P, Northup J. Mechanism of allosteric regulation of the rod cGMP phosphodiesterase activity by the helical domain of transducin alpha subunit. *J Biol Chem*. 1998;273:34284-92.
15. Lambright D, Sondek J, Bohm A, Skiba N, Hamm H, Sigler P. The 2.0 angstrom crystal structure of a heterotrimeric G protein. *Nature*. 1996;379:311-9.
16. Wall M, Coleman D, Lee E, Iniguezlluhi J, Posner B, Gilman A, et al. The structure of the G-protein heterotrimer G(i-alpha-1)beta(1)gamma(2). *Cell*. 1995;83:1047-58.
17. Mixon M, Lee E, Coleman D, Berghuis A, Gilman A, Sprang S. Tertiary and quaternary structural-changes in G(i-alpha-1) induced by GTP hydrolysis. *Science*. 1995;270:954-60.
18. Tesmer J, Sunahara R, Gilman A, Sprang S. Crystal structure of the catalytic domains of adenylyl cyclase in a complex with G(s alpha).GTP gamma S. *Science*. 1997;278:1907-16.
19. Santiveri CM, Jiménez MA. Tryptophan residues: Scarce in proteins but strong stabilizers of β -hairpin peptides. *Biopolymers*. 2010;94:779-90.
20. Stryer L. Fluorescence spectroscopy of proteins. *Science*. 1968;162:526-33.
21. Weber G, Laurence DJ. Fluorescent indicators of adsorption in aqueous solution and on the solid phase. *Biochem J*. 1954;56.
22. Stryer L. The interaction of a naphthalene dye with apomyoglobin and apohemoglobin. A fluorescent probe of non-polar binding sites. *J Mol Biol*. 1965;13:482-95.
23. Ferguson KM, Higashijima T, Smigel MD, Gilman AG. The influence of bound GDP on the kinetics of guanine nucleotide binding to G proteins. *J Biol Chem*. 1986;261:7393-9.
24. Faurobert E, Ottobruc A, Chardin P, Chabre M. Tryptophan-W207 in transducin T-alpha is the fluorescence sensor of the G-protein activation switch and is involved in the effector-binding. *EMBO J*. 1993;12:4191-8.

25. Hamm HE, Meier SM, Liao G, Preininger AM. Trp fluorescence reveals an activation-dependent cation- π interaction in the switch II region of G α (i) proteins. *Protein Sci.* 2009;18:2326-35.
26. Kleuss C, Raw A, Lee E, Sprang S, Gilman A. Mechanism of GTP hydrolysis by G-protein α -subunits. *Proc Natl Acad Sci U S A.* 1994;91:9828-31.
27. O'Hayre M, Vazquez-Prado J, Kufareva I, Stawiski EW, Handel TM, Seshagiri S, et al. The emerging mutational landscape of G proteins and G-protein-coupled receptors in cancer. *Nat Rev Cancer.* 2013;13:412-24.
28. Sipe J. Amyloidosis. *Annu Rev Biochem.* 1992;61:947-75.
29. Sprang S. G protein mechanisms: Insights from structural analysis. *Annu Rev Biochem.* 1997;66:639-78.
30. Taussig R, Iniguezlluhi J, Gilman A. Inhibition of adenylyl-cyclase by G(i- α). *Science.* 1993;261:218-21.
31. Sunahara R, Tesmer J, Gilman A, Sprang S. Crystal structure of the adenylyl cyclase activator G(S α). *Science.* 1997;278:1943-7.
32. Noel JP, Hamm HE, Sigler PB. The 2.2-angstrom crystal-structure of transducin- α complexed with gtp- γ -S. *Nature.* 1993;366:654-63.
33. Lambright D, Noel J, Hamm H, Sigler P. Structural determinants for activation of the α -subunit of a heterotrimeric G-protein. *Nature.* 1994;369:621-8.
34. Sondek J, Lambright D, Noel J, Hamm H, Sigler P. Gtpase mechanism of gproteins from the 1.7-angstrom crystal-structure of transducin α -center-dot-gdp-center-dot-Alf4(-). *Nature.* 1994;372:276-9.
35. Bokoch GM, Katada T, Northup JK, Ui M, Gilman AG. Purification and properties of the inhibitory guanine nucleotide-binding regulatory component of adenylate cyclase. *J Biol Chem.* 1984;259:3560-7.
36. Medkova M, Preininger A, Yu N, Hubbell W, Hamm H. Conformational changes in the amino-terminal helix of the G protein α (i1) following dissociation from G γ subunit and activation. *Biochemistry.* 2002;41:9962-72.
37. Van Eps N, Preininger AM, Alexander N, Kaya AI, Meier S, Meiler J, et al. Interaction of a G protein with an activated receptor opens the interdomain interface in the α subunit. *Proc Natl Acad Sci U S A.* 2011;108:9420-4.

38. Higashijima T, Ferguson KM, Sternweis PC, Ross EM, Smigel MD, Gilman AG. The effect of activating ligands on the intrinsic fluorescence of guanine nucleotide-binding regulatory proteins. *J Biol Chem.* 1987;262:752-6.
39. Teale FW. The ultraviolet fluorescence of proteins in neutral solution. *Biochem J.* 1960;76:381-8.
40. Abdulaev NG, Mao X, Ramon E, Ngo T, Mysliwy J, Marino JP, et al. Designing point mutants to detect structural coupling in a heterotrimeric G protein alpha-subunit by NMR spectroscopy. *Photochem Photobiol.* 2009;85:431-6.
41. Lee E, Linder M, Gilman A. Expression of G-protein alpha-subunits in escherichia-coli. *Methods Enzymol.* 1994;237:146-64.
42. Berman HM, Westbrook J, Feng Z, Gilliland G, Bhat TN, Weissig H, et al. The protein data bank. *Nucleic Acids Res.* 2000;28:235-42.
43. Vivian J, Callis P. Mechanisms of tryptophan fluorescence shifts in proteins. *Biophys J.* 2001;80:2093-109.
44. Noel JP, Hamm HE, Sigler PB. The 2.2-angstrom crystal-structure of transducin-alpha complexed with gtp-gamma-S. *Nature.* 1993;366:654-63.
45. Gallivan JP, Dougherty DA. Cation-pi interactions in structural biology. *Proc Natl Acad Sci U S A.* 1999;96:9459-64.
46. Burley SK, Petsko GA. Amino-aromatic interactions in proteins. *FEBS Lett.* 1986;203:139-43.
47. Fung BK, Nash CR. Characterization of transducin from bovine retinal rod outer segments. II. evidence for distinct binding sites and conformational changes revealed by limited proteolysis with trypsin. *J Biol Chem.* 1983;258:10503-10.
48. Higashijima T, Ferguson KM, Smigel MD, Gilman AG. The effect of GTP and Mg²⁺ on the GTPase activity and the fluorescent properties of go. *J Biol Chem.* 1987;262:757-61.
49. Tanaka T, Kohno T, Kinoshita S, Mukai H, Itoh H, Ohya M, et al. Alpha helix content of G protein or subunit is decreased upon activation by receptor mimetics. *J Biol Chem.* 1998;273:3247-52.
50. Lajtha A, Banik NL, editors. *Handbook of neurochemistry and molecular neurobiology.* . . ; 2007.

51. Robbins, Stanley L., Kumar, Vinay,, Cotran,Ramzi S.,,. Robbins and cotran pathologic basis of disease. ; 2010.
52. Touyz RM. Transient receptor potential melastatin 6 and 7 channels, magnesium transport, and vascular biology: Implications in hypertension. *American Journal of Physiology-Heart and Circulatory Physiology*. 2008;294:H1103-18.
53. Mota de Freitas D, Dorus D. Techniques for measuring magnesium in tissues from hypertensive, psychiatric, and neurological patients. In: Nicholas J. Birch, editor. *Magnesium and the Cell*. ; 1993. p. 51,52-79.
54. Higashijima T, Ferguson KM, Sternweis PC, Smigel MD, Gilman AG. Effects of Mg²⁺ and the beta gamma-subunit complex on the interactions of guanine nucleotides with G proteins. *J Biol Chem*. 1987;262:762-6.
55. Huang P, Yeh H, Yi H, Lin C, Yang C. Fluorescence-based assay probing regulator of G protein signaling partner proteins. *Anal Biochem*. 2012;423:133-40.
56. Catapano LA, Manji HK. G protein-coupled receptors in major psychiatric disorders. *Biochimica Et Biophysica Acta-Biomembranes*. 2007;1768:976-93.
57. Anfinsen CB. Principles that govern the folding of protein chains. *Science*. 1973;181:223-30.
58. Sanger F. Sequences, sequences, and sequences. *Annu Rev Biochem*. 1988;57:1-28.
59. Stretton A. The first sequence: Fred sanger and insulin. *Genetics*. 2002;162:527-32.
60. Ryle AP, Sanger F. Disulphide interchange reactions. *Biochem J*. 1955;60:535-40.
61. Ryle AP, Sanger F, Smith LF, Kitai R. The disulphide bonds of insulin. *Biochem J*. 1955;60:541-56.
62. Hua Q, Gozani S, Chance R, Frank J, Weiss M. Structure of a protein in a kinetic trap. *Nat Struct Biol*. 1995;2:129-38.
63. Smrcka AV. *G protein signaling : Methods and protocols*. Totowa, NJ: Humana Press; 2004.
64. Manning DR. *G proteins : Techniques of analysis*. Boca Raton: CRC Press; 1999.
65. Huang P, Yeh H, Yi H, Lin C, Yang C. Fluorescence-based assay probing regulator of G protein signaling partner proteins. *Anal Biochem*. 2012;423:133-40.

66. Freeman M, Freeman S. Lithium: Clinical considerations in internal medicine. *Am J Med.* 2006;119:478-81.
67. Kessler R, Chiu W, Demler O, Merikangas K, Walters E. Prevalence, severity, and comorbidity of 12-month DSM-IV disorders in the national comorbidity survey replication. *Arch Gen Psychiatry.* 2005;62:709.
68. Keck P, McElroy S, Strakowski S. Anticonvulsants and antipsychotics in the treatment of bipolar disorder. *J Clin Psychiatry.* 1998;59:74-81.
69. Leclerc E, Mansur RB, Brietzke E. Determinants of adherence to treatment in bipolar disorder: A comprehensive review. *J Affect Disord.* 2013;149:247-52.
70. Licht RW. Lithium: Still a major option in the management of bipolar disorder. *CNS Neurosci Ther.* 2012;18:219-26.
71. Avissar S, Schreiber G. The involvement of G proteins and regulators of receptor-G protein coupling in the pathophysiology, diagnosis and treatment of mood disorders. *Clin Chim Acta.* 2006;366:37-47.
72. Mota de Freitas D, Castro MMCA, Geraldés CFGC. Is competition between Li^+ and Mg^{2+} the underlying theme in the proposed mechanisms for the pharmacological action of lithium salts in bipolar disorder? *Acc Chem Res.* 2006;39:283-91.
73. Avissar S, Schreiber G, Danon A, Belmaker RH. Lithium inhibits adrenergic and cholinergic increases in GTP binding in rat cortex. *Nature.* 1988;331:440-2.
74. Malhi G, Tanious M, Das P, Coulston C, Berk M. Potential mechanisms of action of lithium in bipolar disorder. *CNS Drugs.* 2013;27:135-53.
75. Nicely N, Kosak J, de Serrano V, Mattos C. Crystal structures of ral-GppNHp and ral-GDP reveal two binding sites that are also present in ras and rap. *Structure.* 2004;12:2025-36.
76. Malarkey CS, Wang G, Ballicora MA, de Freitas DEM. Evidence for two distinct Mg^{2+} binding sites in G(s)alpha and G(i)alpha(1) proteins. *Biochem Biophys Res Commun.* 2008;372:866-9.
77. Avissar S, Schreiber G. Toward molecular diagnostics of mood disorders in psychiatry. *Trends Mol Med.* 2002;8:294-300.
78. Ryves WJ, Harwood AJ. Lithium inhibits glycogen synthase kinase-3 by competition for magnesium. *Biochem Biophys Res Commun.* 2001;280:720-5.

VITA

The author, Matthew Najor, was born August 10, 1985 in Detroit, MI. In August 2003, he started his undergraduate studies at Loyola University Chicago. He played division II collegiate rugby for Loyola University Chicago. In May 2007, he received a Bachelor of Science degree in chemistry.

In August of 2007, he was admitted to the Ph.D. program in chemistry at Loyola University Chicago. He was awarded a graduate fellowship from August 2007 to December 2013. In April 2010, he was awarded first prize at the Frontiers in Life Sciences at Loyola University Chicago. The author received the chemistry department for best teaching assistant in 2010.

